ATMOSPHERIC EFFECTS ON GEODETIC SPACE MEASUREMENTS

Edited by
F.K. BRUNNER

MONOGRAPH 12

SCHOOL OF SURVEYING

THE UNIVERSITY OF NEW SOUTH WALES KENSINGTON, NSW AUSTRALIA 2033

MONOGRAPH 12

ATMOSPHERIC EFFECTS ON GEODETIC SPACE MEASUREMENTS

Edited by

F. K. Brunner

Contributors: I. Bauersima, G. Beutler, F.K. Brunner, A. Geiger, W. Gurtner, D.C. Hogg, K. Kaniuth, R. Leitinger, G. Petit, E. Putz, M. Rothacher, T. Schildknecht, P. Shi, J.B. Snider.

SCHOOL OF SURVEYING
UNIVERSITY OF NEW SOUTH WALES
P.O. BOX 1
KENSINGTON N.S.W. 2033
AUSTRALIA

Published by
The School of Surveying
University of New South Wales
P.O. Box 1
Kensington
N.S.W., 2033
AUSTRALIA

Published 1988

National Library of Australia
Card Number and I. S. B. N.
0 85839 048 5

PREFACE

A scientific meeting dedicated to discussions of the atmospheric propagation effects on geodetic observations was held in Vancouver during the General Assembly of IAG, 17 August, 1987. The meeting "Refraction Effects in Geodesy" was structured around two major topics: Geodetic refraction effects on terrestrial measurements; and on space observations. The meeting was convened by Professor H. Kahmen and myself.

The effects of the propagation medium cause major accuracy limitations in geodetic space measurements. Therefore, those papers which deal with atmospheric effects on geodetic space measurements were selected from the above scientific meeting to form this monograph. An additional motivation for this monograph, was to present research work relevant to the IAG Special Study Groups: SSG 2.84 "Atmospheric effects on geodetic space measurements" and SSG 4.93 "Wave propagation in refractive media".

This monograph represents significant recent advances in several aspects of refraction effects on space measurements. It begins with an introduction to the problem area and a report giving the main achievements of the abovementioned IAG Special Study Groups. The papers report on the estimation of atmospheric bias terms in GPS results, modelling of atmospheric effects on GPS observations including local models for the wet path delay, recent advances in water vapour radiometry, the investigation of second order ionospheric refraction errors, and a study of ionospheric effects on VLBI results. These papers represent vigorous research activities and point to new problems in geodetic refraction studies.

I would like to thank all authors for contributing to this monograph.

Sydney
September 1988

Fritz K. Brunner

CONTENTS

CONTRIBUTORS

BAUERSIMA, Ivo, Astronomical Institute, University of Berne, Sidlerstrasse 5, CH-3012 Berne, Switzerland.

BEUTLER, Gerhard, Astronomical Institute, University of Berne, Sidlerstrasse 5, CH-3012 Berne, Switzerland.

BRUNNER, Fritz K., School of Surveying, University of New South Wales, P.O. Box 1, Kensington, N.S.W., 2033, Australia.

GEIGER, Alain, Institute for Geodesy and Photogrammetry, ETH Zurich CH-8093, Zurich Switzerland.

GURTNER, Werner, Astronomical Institute, University of Berne, Sidlerstrasse 5, CH-3012 Berne, Switzerland.

HOGG, David C., Cooperative Institute for Research in Environmental Science, University of Colorado, Boulder, CO, 80309, USA.

KANIUTH, Klaus, Deutsches Geodätisches Forschungsinstitut (DGFI), Abteilung I, Marstallplatz 8, 8000 München 22, FRG.

LEITINGER, Reinhart, Institut für Meteorologie und Geophysik, Universität Graz, Halbärthgasse 1, A - 8010 Graz, Austria.

PETIT, Gerard, Institut Géographique National , 2, Avenue Pasteur 94160 Saint-Mandé, France.

PUTZ, Erich, Institut für Meteorologie und Geophysik, Universität Graz, Halbärthgasse 1, A - 8010 Graz, Austria.

ROTHACHER, Markus, Astronomical Institute, University of Berne, Sidlerstrasse 5, CH-3012 Berne, Switzerland.

SCHILDKNECHT, Thomas, Astronomical Institute, University of Berne, Sidlerstrasse 5, CH-3012 Berne, Switzerland.

SHI, Pinhao, Department of Geodesy, Wuhan Technical University of Surveying & Mapping, 39 Luoyu Load, Wuhan, Hubei, 430070, PRC.

SNIDER, J.B., NOAA, ERL, Wave Propagation Laboratory, Boulder, CO, 80303, USA.

ATMOSPHERIC EFFECTS ON GEODETIC SPACE MEASUREMENTS: A PROGRESS REPORT

F.K. Brunner

Abstract:

Major limitations in accuracy of geodetic space measurements are caused by the propagation medium. For microwaves, the propagation medium consists of two distinctly different regions: the ionosphere and the neutral atmosphere. The selection of topics was prompted by the recent accuracy improvements of VLBI and GPS measurements. In this report the following aspects are covered: geodetic space refraction effects, atmospheric effects on microwaves propagating through the earth's neutral atmosphere and ionosphere. Each section consists of a brief outline of the principles followed by a progress report of achievements during the past five years.

In Brunner, F.K. (Ed.), 1988, "Atmospheric Effects on Geodetic Space Measurements", *Monograph 12, School of Surveying, University of New South Wales, pp. 1-13.*

1. INTRODUCTION

It has been recognised that one of the major limitations to further improvements in the accuracy of geodetic space measurements is the effect of the propagation medium. The term geodetic space measurements encompasses satellite microwave ranging and its rate of change, satellite laser ranging, VLBI, baseline measurements using GPS, satellite-to-satellite ranging, and satellite altimetry. The propagation medium consists of two different regions, the ionosphere and the neutral atmosphere. The propagation effects in these two regions depend on the frequencies of the electromagnetic waves. Therefore, microwaves behave differently to light waves in the two regions. Furthermore, it is of importance to distinguish between the single path situation and the differential effect on two adjacent paths propagating through the atmosphere.

The International Association of Geodesy (IAG) has considered "Geodetic Refraction" a very important topic for research and has established a series of special study groups to carry out dedicated investigations. Two special study groups SSG 2.84 "Atmospheric effects on geodetic space measurements" and SSG 4.93 "Wave propagation in refractive media" were established during the XVIII General Assembly of IAG in Hamburg in 1983.

In general, the task of SSG 2.84 was identified to study the nature of the atmospheric effects on various geodetic space measurements, to develop remote sensing techniques and accurate models for these effects, and include statements about the range of applicability and their inherent limitations. The following topics were considered to be of foremost interest: (a) models and limitations; (b) GPS baseline measurements; (c) residual ionospheric effects; (d) water vapour delay; and (e) spatial variation of meteorological parameters. The scientific program of SSG 4.93 was defined to concentrate on the following research topics: (a) the physical causes of refraction; (b) large scale refraction of radio waves; (c) statistical description of irregularities in the troposphere and the ionosphere; and (d) effect of the refractive media on geodetic measurements.

This paper gives a brief overview of the atmospheric effects on geodetic space measurements combined with a report giving the main achievements of both groups during the period 1983-1987, including a representative list of selected publications. Special attention is given to the progress made in the following areas: studies of geodetic space refraction effects in a brief review (section 2), the atmospheric effects on microwaves propagating through the earth's neutral atmosphere (section 3) and ionosphere (section 4). This selection of topics is prompted by the tremendous improvements of the accuracy of

recent VLBI and GPS results. Again, propagation effects were identified as the ultimate limiting factor in accuracy.

2. REVIEW OF GEODETIC SPACE REFRACTION STUDIES.

The monograph "Geodetic Refraction" (Brunner, 1984a) contains nine state-of-the-art reviews about the instrumental determination of the refraction effect and the modelling of atmospheric effects. The Proceedings of the "Workshop on Refraction Determination in the Optical and Radio Astrometry" which was held in Leningrad in 1985 consist of a great wealth of papers mainly about astronomical refraction effects (Teleki, 1987). A review of the determination of astronomical refraction effects was given by Teleki (1986) which also contains a summary of the abovementioned Workshop.

Grafarend (1984) derived from first principles a special form of Maxwell's equations for electromagnetic wave propagation in a refractive medium corotating with the earth. Dodson (1986) reviewed the effects of the ionosphere and troposphere on both optical and microwave observations, and discussed both the instrumental and modelling approaches to the determination of the propagation delay, giving examples of the solution adopted for geodetic and navigation satellite observations. The refraction effects on radio-astronomical observations were reviewed by Spoelstra (1987a). He discussed the contributions of the smooth and irregular components of the atmosphere in some detail. The application of the procedures was described for single dish instruments, connected element interferometers and very long baseline interferometry.

The proper modelling of atmospheric effects on geodetic measurements was reviewed by Brunner (1984b). In this paper modelling principles were proposed which have wider applicability than expressed by the title of the paper. Brunner (1984b) developed an indicator (skill) for the testing of the effectiveness of a model.

Naito and Sugawa (1984) showed that the variation of the astronomical refraction effect is correlated with the dominant time scale of the atmospheric variations in the nocturnal boundary layer. The residual refraction error is of the order of 0.01".

Progress in modelling of the astronomical refraction effect was reviewed by Teleki (1984, 1986). The derivation of the three-dimensional ray equations was based on the fundamental work by Harzer in an investigation by Yatsenko and Teleki (1985).

3. NEUTRAL ATMOSPHERIC EFFECT

3.1 General Remarks

For microwave propagation studies it is convenient to define the refractivity N in terms of the refractive index, n , by:

$$N \equiv (n - 1)\ 10^6 \tag{1}$$

For the atmospheric correction of VLBI or GPS observations it is required to calculate the appropriate propagation delay τ along the wave path. The propagation delay is given as:

$$\tau = 10^{-6} \int_o^s N\, ds + B \tag{2}$$

where the integral of the refractivity is taken along the wave path, and B expresses the curvature correction. B is negligible except for the path with very low elevation angles. The magnitude of the delay in the zenith direction is about 2.5 m for normal atmospheric conditions.

The refractivity can be expressed as a function of the meteorological parameters which describe the physical condition of air. The most commonly used formula was given by Smith and Weintraub (1953) as:

$$N = 77.6\ \frac{P}{T} + 3.53 \times 10^5\ \frac{e}{T^2} \tag{3}$$

where P is the total pressure of air (mb), T is the temperature (K), and e is the water vapour pressure (mb). An improved formula was proposed by Thayer (1974). However, there are unresolved problems between theory and experiments (Hill et al., 1982) in determining the accurate numerical coefficient of equation (3). The refractive index of microwaves does not show any appreciable dependency on the frequency (dispersion) in the neutral atmosphere, thus the group and phase velocities are identical.

The first term in equation (3) is often called the "dry term", as the water vapour pressure e does not enter this term explicitly. However, recognising that the total air pressure P is the main parameter it is preferred to use the name "hydrostatic term", N_h . The second term is

the "wet term", N_v . It is convenient to express N as the sum of both terms:

$$N = N_h + N_v \qquad (4)$$

Similarly, it is useful to investigate the propagation delays separately as related to the integration of N_h and N_v .

3.2 Hydrostatic Delay

The hydrostatic zenith delay τ_h^o (the integral of N_h with height) can be scaled to other elevation angles, β , using:

$$\tau_h^\beta = m_h(\beta)\ \tau_h^o \qquad (5)$$

where $m(\beta)$ is the mapping function for the hydrostatic delay. The value of τ_h^o is about 2.3 m and shows rather small variations. The critical meteorological parameter for the calculation of τ_h^o is the total atmospheric pressure P, which is not difficult to measure to the required accuracy of about 0.5 mb. If measurements are not available, P needs to be modelled as a function of altitude. Formulae for the calculation of the hydrostatic zenith delay for microwaves were developed by Davis et al. (1985), Davis (1986), and Askne and Nordius (1987).

New mapping functions for the elevation angle dependence of the propagation delay were developed independently by Davis et al. (1985) and Lanyi (1984). The mapping function as formulated by Davis et al. (1985) appears to have computational advantages.

3.3 Water Vapour Delay

The water vapour delay in the zenith, τ_v^o, (the integral of N_v with height) can be scaled to other elevation angles, β , using:

$$\tau_v^\beta = m_v\ (\beta)\ \tau_v^o \qquad (6)$$

where $m_v(\beta)$ is the mapping function for the water vapour delay. The value of τ_v^o ranges from a minimum of 0.01 m to a maximum of about 0.40 m, and is highly variable with location and weather condition. Known investigations indicate the validity of the assumption that $m_v(\beta)$ equals $m_h(\beta)$, see Davis (1986). The zenith water vapour delay τ_v^o can be expressed as a function of the total precipitable water vapour in the atmosphere, V. Unfortunately, surface measurements of water vapour pressure are poor indicators for V. Askne and Nordius (1987) derived a closed formula for τ_v^o using meteorological surface parameters.

The major accuracy limitation for geodetic space measurements is the insufficient knowledge about the propagation delay caused by the water vapour distribution at the time of the measurement. The most promising technique uses passive microwave radiometer observations. These measurements can be designed in such a way that they estimate the water vapour delay in the direction of the satellite or radio source and thus τ_v^β directly without the application of a mapping function. Resch (1984a) presented a thorough review of the theoretical background (Resch 1984c), instrumental design principles (Resch 1984b) and attainable accuracies of water vapour radiometry (Resch 1984d). These references describe mainly the research and development efforts at the Jet Propulsion Laboratory, Pasadena.

Important contributions to water vapour radiometry have been made at the Environmental Research Laboratories, Boulder. The development of techniques and implementation of microwave instrumentation for measuring integrated tropospheric water vapour was reviewed by Hogg et al. (1983a). The most relevant instrument is a mobile dual-channel radiometer with coaxial steerable beams of equal angular width operating at wavelengths of about 1 and 1.4 cm. This instrument provides accurate measurement of water vapour induced path delay even in the presence of non-precipitating clouds (Hogg 1983b). Exhaustive calibration of these instruments with radiosondes and numerous successful intercomparisons between radiometers have been made. Temporal variations in excess radio path delay have been measured and their spectra determined (Hogg, 1985). Use of these instruments in support of the Global Positioning System has led to much improved accuracy in baseline measurements (Ware et al. 1985, 1986).

A Swedish group reported its extensive research into water vapour radiometry, Elgered et al. (1985). They estimated the ultimate

precision of the water vapour radiometer measurements with 9 mm (rms).

Stochastic modelling of the wet tropospheric delay requires information about the behaviour of the water vapour fluctuations. The structure function of the water vapour fluctuations was investigated by Treuhaft and Lanyi (1987) and Davis (1986).

3.4 Tropospheric Delay

It appears convenient to describe models for the total delay (the sum of the dry and wet term) by the name 'tropospheric delay'. The closed form for the tropospheric delay as derived by Askne and Nordius (1987) may be used if only meteorological surface values are available. This closed form is of general applicability. The local model for the tropospheric delay as derived by Kaniuth (1986) requires meteorological data at the tracking site over several years in order to become representative.

Black and Eisner (1984) developed a simple geometrical model which includes one estimated parameter for the tropospheric effect (wet and dry component) on satellite Doppler data at microwave frequencies. The effect of the measuring error of the meteorological data for the correction of Doppler positioning results was studied by Chen (1983). The tropospheric range error of geodetic measuring systems was reviewed by Hartmann and Leitinger (1983, 1984).

4. IONOSPHERIC EFFECTS

4.1 General Remarks

The free electrons in the ionosphere cause the refractive index of microwaves to become frequency dependent. The refractive index can be expressed with sufficient accuracy (for this present overview) by:

$$n = 1 \pm AN_e/f^2 \qquad (7)$$

where A is a constant, N_e is the free electron density, and f is the frequency. The appropriate sign in (7) needs to be used for the group (+) or phase (-) refractive index.

The ionospheric zenith delay τ_I^o for a microwave propagating between a satellite and an earth station can be expressed as:

$$\tau_I^o = \frac{A}{f^2} \text{ (TEC)} \qquad (8)$$

where TEC is the Total Electron Content. TEC is the (zenith) value of the integral of the N_e distribution with height. TEC is highly variable and depends mainly on time, latitude and solar activity. Typical values for the ionospheric delay are about 10 m for 1.2 GHz, which is the L2 carrier frequency of the GPS signals. It is necessary to relate the ionospheric zenith delay, τ_I^o, to the slant wave path using a suitable mapping function.

The dispersion effect can be used to remove the first order ionospheric delay effect by measuring at two frequencies, see equation (8). This method is successfully used for the ionospheric correction of phase and range measurements (GPS, VLBI) and Doppler frequencies (TRANSIT). However, for single frequency observations, e.g. GPS receivers using the L1 carrier frequency only, models for TEC need to be developed.

4.2 Recent Investigations

The ionospheric propagation errors on geodetic range measurements were investigated by Leitinger and Hartmann (1983) and Hartmann and Leitinger (1984). Precise formulae were derived for the second order refraction error in the case of a spherically layered ionosphere. Four quantities derived from the height profile of the electron density are needed in the formulae for error correction: the electron content, the slab thickness, the height of the layer, and a shape factor (Leitinger, 1987). Prilepin (1987) proposed the use of dual frequency GPS signals to calculate both the ionospheric delay and the refraction effect using simultaneous measurements of the group and phase velocities.

The accuracy of single frequency GPS results is degraded by the ionospheric propagation effects. An algorithm was developed by Klobuchar (1986) to compute this effect using a simple diurnal model of the total electron content (TEC). Another approach to predicting TEC uses the data from two Doppler receivers (Leitinger et al, 1984). This investigation aims both at finding details of the long-term behaviour and at studies of geophysical events. For application purposes the long-term behaviour is needed to refine ionization models. The case studies give information about deviation from mean or typical behaviour and

reveal gradients (both spatial and temporal) which the average models necessarily ignore.

Large and small scale inhomogeneities in the ionosphere cause distortions in radio signals passing through it. The nature of these effects was reviewed by Lyon et al (1983) and Spoelstra (1987b). The influence of ionospheric refraction on radio interferometry was investigated by Spoelstra (1983) and Spoelstra and Kelder (1984). Phase and amplitude scintillations of radio signals which are caused by the ionosphere were investigated by Spoelstra (1985). Medium scale travelling ionospheric disturbances were studied by Kelder and Spoelstra (1984, 1987a, 1987b) using a combination of radio interferometry and the differential Doppler technique.

REFERENCES

Askne J and Nordius H (1987) Estimation of tropospheric delay for microwaves from surface weather data. Radio Science 22:379-386

Black H D and Eisner A (1984) Correcting Satellite Doppler Data for Tropospheric Effects. J Geophys Res 89:2616-2626

Brunner F K (1984a) (Editor) Geodetic Refraction. Springer Verlag 213 pp

Brunner F K (1984b) Modelling of Atmospheric Effects on Terrestrial Geodetic Measurements. In Brunner F K (Ed) Geodetic Refraction. Springer Verlag: 143-162

Chen J Y (1983) On the Effect of the Measuring Errors of Meteorological Parameters on the Results of Doppler Positioning. Zeitschrift für Vermessungswesen 108:75-82

Davis J L (1986) Atmospheric Propagation Effects on Radio Interferometry. Air Force Geophysics Laboratory. Techn. Report 86-0243, 276 pp

Davis J L, Herring T A, Shapiro I I, Rogers AEE, and Elgered G (1985) Geodesy by radio interferometry: Effects of atmospheric modeling errors on estimates of baseline length. Radio Science 20:1593-1607

Dodson A H (1986) Refraction and propagation delays in space geodesy. Int J Remote Sensing 7:515-524

Elgered G, Rönnäng B, Winberg E, and Askne J (1985) Satellite-Earth Range Measurements. I. Correction of the Excess Path Length due to Atmospheric Water Vapour by Ground Based Microwave Radiometry. Report 147, Onsala Space Observatory, Chalmers University of Technology, Sweden

Grafarend E W (1984) The Equations of Electromagnetic Wave Propagation in a Refractive Medium Corotating with the Earth. In Brunner F K (Ed) Geodetic Refraction. Springer Verlag: 189-208

Hartmann G K and Leitinger R (1983) Entfernungsfehler bei geodätischen Messystemen aufgrund von Atmosphäreneinflüssen bei Signalfrequenzen grösser als 100 MHz. Teil I: Einfluss der Troposphäre. Kleinheubacher Berichte 26:125-128

Hartmann G K and Leitinger R (1984) Range errors due to ionospheric and tropospheric effects for signal frequencies above 100 MHz. Bull. Geod. 58:109-136

Hill R J, Lawrence R S, and Priestley J T (1982) Theoretical and calculational aspects of the radio refractive index of water vapour. Radio Science 17: 1251 - 1257

Hogg D C (1985) Measurement of movement of the earth's crust - the role of microwave remote sensing. IEEE/Geosci Remote Sens.Soc Newsletter 9:5-6

Hogg D C, Guiraud F O, Snider J B, Decker, M T, and Westwater E R (1983a) Microwave radiometry for measurement of water vapour. Reviews of Infrared and Millimeter Waves. In Button K J (Ed) Plenum Press, New York, 113-154

Hogg D C , Guiraud G O, Snider J B, Decker M T, and Westwater E R (1983b) A steerable dual-channel microwave radiometer for measurement of water vapor and liquid in the troposphere. J Appl Meteorol 22:789-806

Kaniuth K (1986) A Local Model for Estimating the Tropospheric Path Delay at Microwave Frequencies. Proc 4th Int Geodetic Symp on Sat Positioning, Austin: 589-601

Kelder H and Spoelstra T A T (1984) Multi-technique study of medium scale TIDs Kleinheubacher Berichte 27:575-584

Kelder H and Spoelstra T A T (1987a) Medium scale TIDs observed by radio interferometry and differential Doppler techniques. J Atmos Terr Phys 49:7-17

Kelder H and Spoelstra T A T (1987b) Multi-technique observations of medium scale TIDs: Evidence for their generation by atmospheric tides. In Tauriainen A (Ed). Proc Int Symp "Radio beacon contribution to the study of ionization and dynamics of the ionosphere and to corrections to geodesy", Oulu

Klobuchar J A (1986) Design and Characteristics of the GPS Ionospheric Time Delay, Algorithm for Single Frequency Users. Proc Position Location and Navigation Symposium, Las Vegas, 280-286

Lanyi G (1984) Tropospheric Delay Effects in Radio Interferometry. TDA Progress Report, JPL, 42-78: 152-159

Leitinger R and Hartmann G K (1983) Entfernungsfehler bei geodätischen Messystemen aufgrund von Atmosphäreneinflüssen bei Signalfrequenzen grösser als 100 MHz. Tel II: Einfluss der Ionosphäre. Kleinheubacher Berichte 26:129-137

Leitinger R, Hartmann G K, Lohmar F J and Putz E (1984) Electron content measurements with geodetic Doppler receivers. Radio Science 19:789-897

Leitinger R (1987) Ionosphärische Ausbreitungsfehler und ionosphärische Messgrössen. Kleinheubacher Berichte 30:127-136

Lyon G F, Fulford J A and Forsyth P A (1983) Ionospheric Effects on Space Application Systems. Canadian Aeronautics and Space J 29:315–326

Naito N and Sugawa C (1984) Atmospheric Refraction Effects in Time and Latitude Observations Using Classical Techniques. In Brunner F K (Ed) Geodetic Refraction. Springer Verlag: 181-187

Prilepin M T (1986) Determination of Ionospheric Correction by Group and Phase Velocity. Proc 4th Int Geodetic Symp on Sat Positioning, Austin: 615-629

Resch G M (1984a) Water Vapor Radiometry in Geodetic Applications. In Brunner F K (Ed) Geodetic Refraction. Springer Verlag: 53-84

Resch G M (1984b) Another Look at the Optimum Frequencies for a Water Vapor Radiometer. TDA Progress Report, JPL, 42-76: 1-11

Resch G M (1984c) Inversion Algorithms for Water Vapor Radiometers Operating at 20.7 and 31.4 GHz.TDA Progress Report, JPL, 42-76: 12-26

Resch G M (1984d) Radiometric Correction of Atmospheric Path Length Fluctuations in Interferometric Experiments. Radio Science 19: 411-422

Smith E K and Weintraub S (1953) The constants in the equation for atmospheric refractive index at radio frequencies. Proc. Inst. Radio Engrs, 41, 1035

Spoelstra TAT (1983) The influence of ionospheric refraction on radio astronomy interferometry. Astron. Astrophys 120:313-321

Spoelstra TAT (1985) Effects of amplitude and phase scintillations on decimeter wavelength observations at mid-latitudes. Astron. Astrophys. 148: 21-28

Spoelstra TAT (1987) Correcting refraction in radio astronomy. In Teleki G (Ed) Proc Workshop on Refraction Determination in the Optical and Radio Astrometry. Publ Astron. Obs. 35: 213-241

Spoelstra TAT (1987b) Correcting ionospheric effects in radio astronomy and satellite geodesy. In Tauriainen A (Ed) Proc Int Symp "Radio beacon contribution to the study of ionization and dynamics of the ionosphere and to corrections to geodesy", Oulu

Spoelstra TAT and Kelder H (1984) Effects produced by the ionosphere on radio interferometry. Radio Science 19:779-788

Teleki G (1984) Progress Report on the Astronomical Refraction. Bull Obs Astron Belgrade, 134: 39-47

Teleki G (1986) Present-Day Potentialities of Refraction Influences Determination and Perspective Developments. Bull Obs Astron Belgrade, 136: 61-72

Teleki G (1987) (Editor) Workshop on Refraction Determination in the Optical and Radio Astrometry, Leningrad. Publ of the Astronomical Observatory, Belgrade, No. 35, 350 pp

Thayer G D (1974) An improved equation for the radio refractive index of air, Radio Science 9, 803- 807

Treuhaft R N and Lanyi G E (1987) The effect of the dynamic wet troposphere on radio interferometric measurements. Radio Science 22:251-265

Ware R H, Rocken C, and Snider J B (1985) Experimental Verification of Improved GPS-Measured Baseline Repeatability Using Water-Vapor Radiometer Corrections. IEEE Trans Geosc and Rem Sens GE-23:467-473

Ware R H, Rocken C, and Hurst K J (1986) A Global Positioning System Baseline Determination including Bias Fixing and Water Vapor Radiometer Corrections. J Geophys Res 91:9183-9192

Yatsenko A Yu and Teleki G (1985) Harzer's Works on Astronomical Refraction Viewed from Today's Standpoint. Bull Obs Astron Belgrade, 135: 1-15.

ATMOSPHERIC REFRACTION AND OTHER IMPORTANT BIASES IN GPS CARRIER PHASE OBSERVATIONS

G. Beutler, I. Bauersima, W. Gurtner, M. Rothacher, T. Schildknecht, and A. Geiger

Abstract

Tropospheric and ionospheric refraction are very important accuracy limiting factors when processing GPS carrier phase observations. Here these effects are discussed as members of two different classes of biases: One class producing height errors, the other producing scale errors. Simple rules are given to estimate the height and scale errors caused by not (correctly) modeling the refraction effects. We then show that, with the same tools developed to estimate the influence of the atmosphere, it is also possible to estimate the influence of biases in the GM-value, in the coordinates of fixed stations, and of orbit errors. In the summary we will give a realistic error budget for GPS observations.

In Brunner, F.K. (Ed.), 1988, "Atmospheric Effects on Geodetic Space Measurements", *Monograph 12, School of Surveying, University of New South Wales, pp. 15-43.*

1. TWO BIAS CLASSES AND THEIR INFLUENCE ON BASELINE ESTIMATES

The geodesist uses the GPS in the relative mode. The basic observable is the so called single difference, which is the difference of two one-way phases (Bock et al., 1984) recorded by two different receivers at locations P_1 and P_2. Somewhat simplified (light travel times neglected, ideal receiver clocks assumed) the single difference may be interpreted as the distance difference of a satellite S from the two receivers at P_1, P_2 at observation time t (see Figure 1). This basic observable may be biased by an integer (but originally unknown) number of cycles of the observed carrier. Here we assume that ambiguity resolution was successful, i.e. that we are dealing with the plain distance difference as observable.

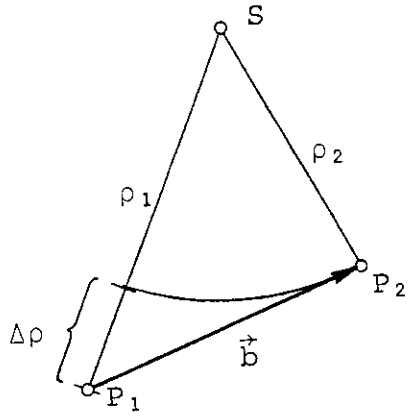

Figure 1: The single difference observable

Legend:

S:	Satellite at observation time t
$P_i, i=1,2$:	Receiver locations at observation time t
$\rho_i, i=1,2$:	Distance from satellite S to receiver at P_i
$\Delta\rho := \rho_1 - \rho_2$:	Single difference observable
b:	Baseline to be estimated

In order to study the influence of a bias ε on the baseline $\vec{b}$, we make the following simplifying assumptions:

Assumption 1: For each observation $\Delta\rho$ of a satellite S made at zenith distance z and azimuth a there exists an observation $\Delta\rho^*$ of a satellite S^* made at the same zenith distance z but at the azimuth a+180°. S and S^* may be identical or not. (Approximately we have $\Delta\rho^* = -\Delta\rho$.)

Assumption 2: Receivers at P_1 and P_2 are lying in a horizontal plane, or, the height difference between the two receiver locations is small compared to the baseline length.

Assumption 3: The baseline length $\ell = |\vec{b}|$ is small compared to the distances ρ_i:

$$\ell \ll \rho_i \quad , \quad i=1,2 \tag{1}$$

Let $\Delta\tilde{\rho}$, $\Delta\tilde{\rho}^*$ stand for the biased observations of $\Delta\rho$, $\Delta\rho^*$. (2)

Let us furthermore define two classes of biases:

Bias class 1: Observations $\Delta\rho$ and $\Delta\rho^*$ are biased by the same value ε:

$$\Delta\tilde{\rho} := \Delta\rho + \varepsilon\,(z,a) \tag{3}$$

$$\Delta\tilde{\rho}^* := \Delta\rho^* + \varepsilon(z,180^\circ+a)$$

where $\varepsilon(z,180^\circ+a) = \varepsilon(z,a)$

and where the bias ε, as indicated in eqns. (3), may depend on zenith distance z and azimuth a.

Bias class 2: Observations $\Delta\rho$ and $\Delta\rho^*$ are biased by $+\varepsilon$ and $-\varepsilon$ respectively:

$$\Delta\tilde{\rho} := \Delta\rho + \varepsilon(z,a) \tag{4}$$

$$\Delta\tilde{\rho}^* := \Delta\rho^* + \varepsilon(z,180^\circ+a)$$

where $\varepsilon(z,180^\circ+a) = -\varepsilon(z,a)$.

It is our goal now to show that the main effect of a bias of class 1 is a height error (of receiver at P_2 with respect to receiver at P_1), whereas the main effect of a bias of class 2 is an error in baseline length. In order to demonstrate that, we use a very simple geometrical method: Observation $\Delta\rho$ tells us that P_2 has to lie in a plane E_1 perpendicular to the line P_1S at a distance $\Delta\rho$ from P_1 (assumption 3). In an analogous way we may conclude that P_2 has to lie in a plane E_2 perpendicular to P_1S^* at a distance $\Delta\rho^*$ from P_1. (Observe that E_1 and E_2 have to lie on different sides of P_1). Obviously P_2 has to lie on the intersection line of E_1 and E_2. Now, if we are working with biased observations, we have to introduce planes $\tilde{E}_1$, $\tilde{E}_2$ parallel to E_1, E_2 at distances of $\pm\varepsilon$, from E_1, E_2 and the effect of the bias introduced by observations $\Delta\rho$, $\Delta\rho^*$ may be studied immediately by comparing the intersection line of $\tilde{E}_1$, $\tilde{E}_2$ with that of E_1 and E_2. Figure 2 shows the influence of a class 1 bias of absolute value ε, Figure 3 that of a class 2 bias of absolute value ε. Both Figures show the plane defined by P_1, S and S^*. This means that we can see "only" the normal projection P_2' of P_2 onto this plane. The projection of the baseline consequently will be of length $\ell\cdot\cos(a-a_o)$, where a is the azimuth of satellite S, a_o that of the baseline b in point P_1, and ℓ is the length of baseline b.
Figures 2 reveals clearly that a bias ε of class 1 induces a height error

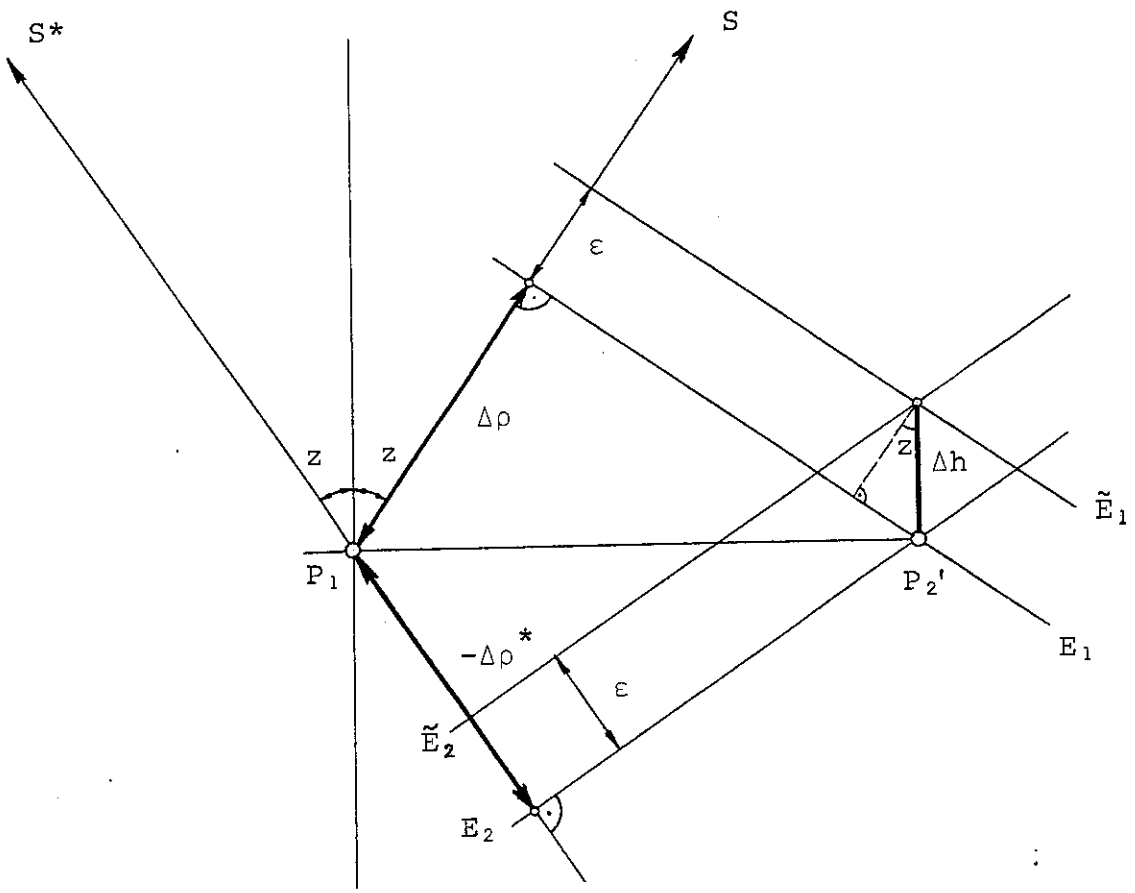

Figure 2: Influence of a class 1 bias ε on a baseline $\vec{b}$

Legend:

S: Satellite at zenith distance z, azimuth a
S^*: " " " " z, " a+180°
P_1: Location of receiver 1
P_2: Normal projection of receiver location P_2 on plane SP_1S^*

planes E_1, E_2: Locus 1, 2 of point P_2 (no biases)
planes $\tilde{E}_1, \tilde{E}_2$: " 1, 2 " " P_2 (bias ε of class 1)
z: Zenith distance of observations

$\Delta\rho, \Delta\rho^*$: Unbiased observables
Δh: Height errors induced by biased observations $\Delta\rho+\varepsilon$, $\Delta\rho^*+\varepsilon$

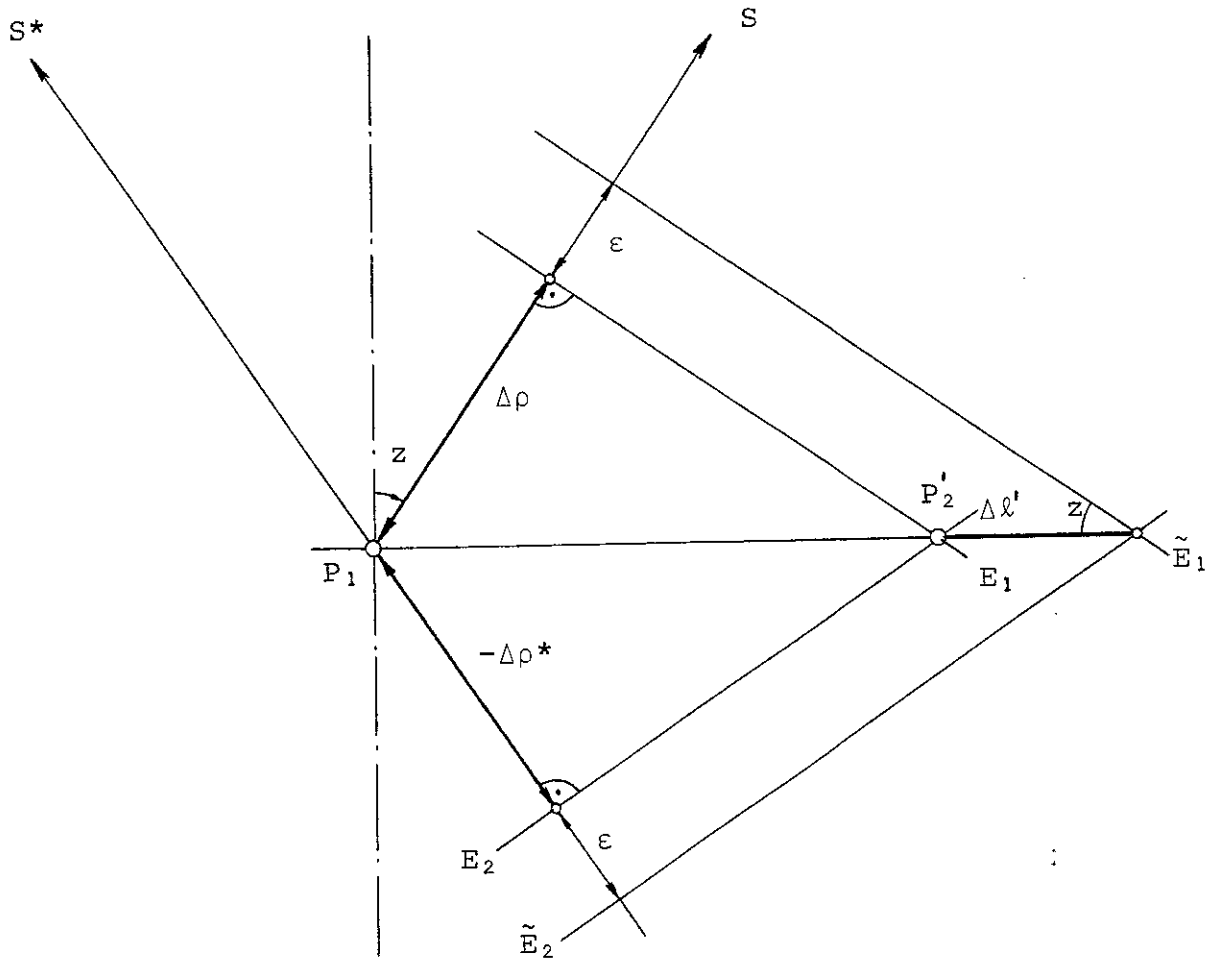

Figure 3: Influence of a class 2 bias on a baseline $\vec{b}$

Legend:

S: Satellite at zenith distance z, azimuth a
S^*: " " " " z, " a+180°
P_1: Location of receiver 1
P_2: Normal projection of receiver location P_2 on plane SP_1S^*
planes E_1, E_2: Locus 1,2 of point P_2 (no biases)
" $\tilde{E}_1, \tilde{E}_2$: " " " P_2 (bias ε of class 2)
z: Zenith distance of observations
$\Delta\rho, \Delta\rho^*$: Unbiased observables
$\Delta\ell'$: Projection of length error $\Delta\ell$ by bias ε on plane SP_1S^*

$$\Delta h\ (a,z) = \frac{\varepsilon(a,z)}{\cos z} \tag{5}$$

whereas the other baseline components remain unaffected. Of course eqn. (5) only characterizes the influence of the pair $\Delta\rho$, $\Delta\rho^*$ of observations. The influence of all observations is then computed as the mean value of all $\Delta h(a,z)$ as given by eqn. (5), where we assume a homogeneous distribution of satellites:

$$\Delta h = \frac{\int_0^{\pi}\int_0^{z_{max}} \Delta h(a',z')\cdot\sin z'\cdot dz'da'}{\pi\cdot(1-\cos z_{max})} \tag{6}$$

Figure 3 reveals that a bias ε of class 2 induces a length bias of

$$\Delta\ell(a,z) = \frac{\varepsilon(a,z)}{\sin z\cdot\cos\Delta a} \tag{7}$$

where $\Delta a = a - a_o$
a = azimuth of topocentric satellite (as seen from P_1)
a_o = azimuth of baseline b (as seen from P_1).
Again we may compute the influence of all observation pairs $\Delta\rho$, $\Delta\rho^*$ by taking the mean value of all $\Delta\ell$ in eqn. (7):

$$\Delta\ell = \frac{\int_0^{\pi}\int_0^{z_{max}} \Delta\ell(a',z')\cdot\sin z'\cdot dz'da'}{\pi\cdot(1-\cos z_{max})} \tag{8}$$

In the following sections we will discuss and classify the following important biases:

- Relative troposphere errors
- Neglected troposphere
- Neglected ionosphere
- "Wrong" GM-value (change of WGS-72 to WGS-84)
- Receiver location kept fixed at a wrong position
- Along track orbit errors

2. RELATIVE TROPOSPHERE ERRORS

Usually it is recommended by GPS instrument manufacturers to measure atmospheric pressure p, temperature T, and humidity H (or an equivalent set) at each receiver site e.g. all 15 minutes and then to account for the tropospheric refraction effect for each station separately using one of the well known refraction formulae (e.g. Hopfield, Saastamoinen). This certainly is an excellent advise for large scale analyses (baseline lengths 100 km or more). For small scale networks the advise may be not the best (see e.g. (Gurtner et al., 1987)) due to the inevitable instrument errors (calibration) of standard meteo equipment and due to local micro-climate effects (e.g. fog, inversion situations). In order to assess the order of magnitude for these relative troposphere errors we use (a simplified version of) the Saastamoinen formula (Bauersima, 1983):

$$\Delta r(z) = \Delta r(0)/\cos z \qquad (9)$$

where $\Delta r(z)$ is the refraction correction at a zenith distance z, $\Delta r(0)$ is the corresponding correction at $z=0$.

$$\Delta r(0) = 2.277 \cdot \left[p + \left(\frac{1255}{273+T} + .05 \right) \cdot e \right] \qquad (10)$$

where: $\Delta r(0)$ is the zenith correction in millimeters
p is the atmospheric pressure in mbar
T is the temperature in $^\circ$ Celsius
e, the water vapour pressure, is given by the formula

$$e = \frac{H}{100} \cdot \exp(-37.2465+0.213166 \cdot (T+273)-0.000256908 \cdot (T+273)^2) \qquad (11)$$

where H is the humidity in % .

In Table 1 we give the partial derivatives of $\Delta r(0)$ with respect to T, p, and H. They define (after division by cosz, see eqn. (9)) the bias introduced into the observable $\Delta\rho$ or $\Delta\rho^*$, if one of the stations shows a wrong temperature of 1°C resp. a wrong pressure of 1 mbar resp. a wrong humidity of 1 % .

Table 1
Meteo-Dependence of Tropospheric Refraction Correction $\Delta r(z=0)$

T °C	P mbar	H %	$\left\|\frac{\partial \Delta r}{\partial T}\right\|$ mm/°C	$\left\|\frac{\partial \Delta r}{\partial P}\right\|$ mm/mbar	$\left\|\frac{\partial \Delta r}{\partial H}\right\|$ mm/(1%)
0°	1000	100	5	2	0.6
30°	1000	100	27	2	4
0°	1000	50	3	2	0.6
30°	1000	50	14	2	4

First we see that these partial derivatives all are of the order of millimeters or more: A bad omen for small scale applications where usually we are hunting millimeters! Moreover it is obvious that high temperatures and high humidity will be very bad for GPS results. This underlines what we pointed out at the beginning of this section: Using erroneous meteo data in small scale networks may be quite destructive (remember that a bias of 1 cm is 10 ppm on a 1 km baseline, but only 0.01 ppm on a 1000 km baseline). Let us now assume that station 1 shows a troposphere bias of ε_o in the term $\Delta r(0)$ with respect to station 2. (If the thermometer at station 1 would have a calibration error of 1°C, and if no other error sources are present we would have ε_o=27mm for T=30°, p=1000mbar, H=100 % at P_1). If the meteorological conditions do not change between the observation epochs for observations $\Delta\rho$, $\Delta\rho^*$, both observations will be biased by exactly the same ε_o. Therefore we may conclude that relative troposphere errors cause class 1 biases in the observable.
Let us now study the influence of the bias ε_o in $\Delta r(0)$ on the estimated height of point P_2. First, due to eqn. (9), we have for the bias at zenith distance z:

$$\varepsilon(z) = \frac{\varepsilon_o}{\cos z} \tag{12}$$

According to eqn. (6) observations $\Delta\rho$, $\Delta\rho^*$ cause a height error of

$$\Delta h(z) = \frac{\varepsilon(z)}{\cos z} = \frac{\varepsilon_o}{\cos^2 z} \tag{13}$$

Since we have no azimuth dependence here we may write eqn. (6) as

$$\Delta h = \frac{1}{1-\cos z_{max}} \cdot \int_o^{z_{max}} \Delta h(z') \cdot \sin z' \cdot dz' \tag{14}$$

Introducing eqn. (13) into eqn. (14) gives the very simple formula

$$\Delta h = \frac{1}{\cos z_{max}} \cdot \varepsilon_o \qquad (15)$$

This means that relative troposphere errors cause height errors which are amplified by the factor $1/\cos z_{max}$ (2.9 for $z_{max}=70^\circ$) in the estimated receiver heights. We should mention that these height errors induce also scale errors depending on the inclination of the baseline b. This is only of importance if we leave assumption 2, of course.
Let us state at the end of this section that relative troposphere errors really introduce strong biases into GPS solutions.

3. ABSOLUTE TROPOSPHERE ERRORS

Let us assume in this section that we have identical meteorological conditions at both ends of our baseline. At first sight one might think that by completely neglecting tropospheric refraction no bias would be introduced in this case. That this is not the case follows from the fact that (in general) the two receivers at P_1 and P_2 do not see the satellite under the same zenith distance (see Figure 4).

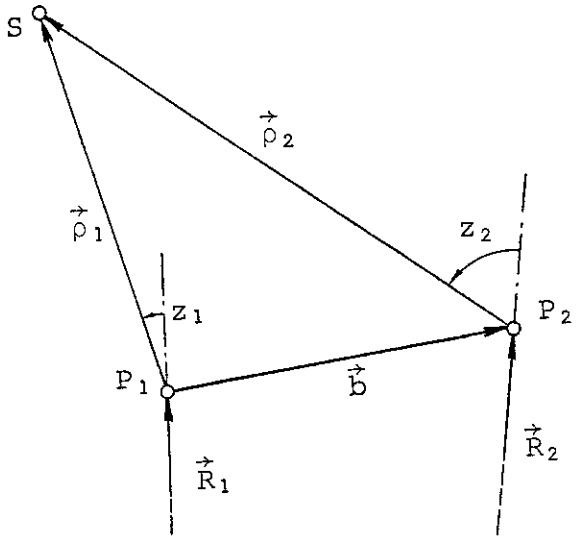

Figure 4: Geometry governing tropospheric refraction.

Legend:
S: Observed satellite
$\underline{P}_i$: Location of receiver i, i=1,2
$\underline{R}_i$: Geocentric positions of receivers
$\underline{\rho}_i$: Topocentric positions of satellite
b: Observed baseline
z_i: Zenith distances of satellite from P_i

Under the assumption mentioned (identical meteorological conditions at both ends of the baseline) the bias introduced into the observable by neglecting the troposphere may be written as

$$\varepsilon(a,z) = \Delta r(0) \left\{ \frac{1}{\cos z_1} - \frac{1}{\cos z_2} \right\} \tag{16}$$

where $\Delta r(0)$ is the troposphere zenith correction defined in eqn. (9).
From Figure 4 we see that we may put

$$\vec{\rho}_i \cdot \vec{R}_i = \rho_i R_i \cos z_i \quad , \quad i=1,2$$

Therefore we may write the bracket {...} in expression (16) as

$$\frac{1}{\cos z_1} - \frac{1}{\cos z_2} = \frac{\vec{\rho}_1 \cdot \vec{R}_1}{\vec{\rho}_1 \cdot \vec{R}_1} - \frac{\vec{\rho}_2 \cdot \vec{R}_2}{\vec{\rho}_2 \cdot \vec{R}_2} \tag{17}$$

Let us now eliminate $\vec{\rho}_2$, $\vec{R}_2$ in eqn. (17) by putting:

$$\rho_2^2 = (\vec{\rho}_1 - \vec{b})^2 \approx \rho_1^2 - 2\vec{\rho}_1 \cdot \vec{b}$$

or

$$\rho_2 = \rho_1 \cdot \left(1 - \frac{\vec{\rho}_1 \cdot \vec{b}}{\rho_1^2} \right) \tag{18}$$

and $$\vec{\rho}_2 \cdot \vec{R}_2 = (\vec{\rho}_1 - \vec{b})(\vec{R}_1 + \vec{b}) \approx \vec{\rho}_1 \cdot \vec{R}_1 + \vec{\rho}_1 \cdot \vec{b} \tag{19}$$

Putting $\vec{b}^2 \approx 0$, $R_2 \approx R_1$, and since $R_1 \cdot \vec{b} = 0$ due to assumption 2.

Using eqns. (18) and (19) in eqn. (17) gives

$$\frac{1}{\cos z_1} - \frac{1}{\cos z_2} = \frac{\rho_1 \cdot R_1}{\vec{\rho}_1 \cdot \vec{R}_1} \cdot \vec{\rho}_1 \cdot \vec{b} \cdot \left(\frac{1}{\rho_1^2} + \frac{1}{\vec{\rho}_1 \cdot \vec{R}_1} \right) \tag{20}$$

It is instructive to compute the scalar products in eqn. (20) in the azimuth elevation system of point P_1:

$$\begin{aligned} \vec{R}_1 &= (0, 0, R_1) \\ \underline{\rho}_1 &= \rho_1 \cdot (\cos a \sin z_1, \ \sin a \sin z_1, \ \cos z_1) \\ b &= \ell \cdot (\cos a_o \ , \ \sin a_o \ , \ 0 \ ) \end{aligned}$$

$$\vec{R}_1 \cdot \vec{\rho}_1 = R_1 \cdot \rho_1 \cdot \cos z_1$$

$$\vec{\rho}_1 \cdot \vec{b} = \rho_1 \cdot \ell \cdot \cos(a-a_0) \cdot \sin z_1$$

We may therefore rewrite eqn. (20) as

$$\frac{1}{\cos z_1} - \frac{1}{\cos z_2} = \frac{1}{\cos z_1} \cdot \rho_1 \cdot \ell \cdot \cos(a-a_0) \cdot \sin z_1 \cdot \left\{ \frac{1}{\rho_1^2} + \frac{1}{\rho_1 R_1 \cdot \cos z_1} \right\} \tag{21}$$

$$= \tan z_1 \cdot \cos(a-a_0) \cdot \ell \cdot \left\{ \frac{1}{\rho_1} + \frac{1}{R_1 \cos z_1} \right\}$$

The final result giving the bias in the observable $\Delta\rho$ follows by introducing eqn. (21) into eqn. (16):

$$\underline{\varepsilon(a,z) = \Delta r(0) \cdot \tan z_1 \cos(a-a_0) \cdot \ell \cdot \left\{ \frac{1}{\rho_1} + \frac{1}{R_1 \cdot \cos z_1} \right\}} \tag{22}$$

Next we have to compute the bias in the observable $\Delta\rho^*$. Since we observe at the same zenith distance z but at the azimuth a+180°, and since the topocentric satellite distance is the same for both observations we may conclude from eqn. (22)

$$\underline{\varepsilon(a+180^\circ, z) = -\varepsilon(a,z)} \tag{23}$$

Eqn. (23) tells us that <u>a neglected troposphere</u> (or a <u>common troposphere error</u> at both ends of the baseline) will cause a <u>class 2 bias in the observations</u>.
The length bias introduced by the observations $\Delta\rho$, $\Delta\rho^*$ is given by eqn. (7). If we introduce eqn. (22) into this equation we obtain

$$\Delta\ell(a,z) = \Delta\ell(z) = \Delta r(0) \cdot \frac{1}{\cos z_1} \cdot \ell \cdot \left\{ \frac{1}{\rho_1} + \frac{1}{R_1 \cdot \cos z_1} \right\} \tag{24}$$

and we see that this result is no longer azimuth dependent. Therefore we may simplify eqn. (8) as follows:

$$\Delta\ell = \frac{1}{1-\cos z_{max}} \cdot \int_0^{z_{max}} \Delta\ell(z') \cdot \sin z' \cdot dz' \tag{25}$$

Introducing eqn. (24) into this last equation and evaluating the integral gives the result

$$\frac{\Delta\ell}{\ell} = \frac{\Delta r(0)}{\rho} \cdot \frac{|\ell n \cos z_{max}|}{1-\cos z_{max}} + \frac{\Delta r(0)}{R_1} \cdot \frac{1}{\cos z_{max}} \tag{26}$$

If we retain only the more important term in eqn. (26) we may write approximately

$$\frac{\Delta\ell}{\ell} = \frac{\Delta r(0)}{R_1} \cdot \frac{1}{\cos z_{max}} \qquad (27)$$

Neglecting tropospheric refraction lengthens the GPS derived baselines. Since the entire troposphere effect is of the order of 2.25 meters and since for $z_{max}=70^\circ$ $1/\cos z_{max} \approx 2.9$, we may expect a scale error of the order of

$$\frac{\Delta\ell}{\ell} \approx 1 \cdot 10^{-6} \qquad (z_{max}=70^0) \qquad (28)$$

if we neglect tropospheric refraction completely. Of course the Saastamoinen and the Hopfield formulae account for the troposphere much better than that. In actual applications it may happen however, that there are serious errors in the wet component (at about 10 % of the entire effect). It is therefore possible, that troposphere induced scale errors of the order of 0.1 ppm may be in GPS results, if no reliable meteo data are available. It should be stated however, that relative troposphere errors are a much greater danger for GPS results.

4. IONOSPHERIC REFRACTION

The simplest model to account for ionospheric refraction is the single layer model. There it is assumed, that all free electrons in the atmosphere (which cause this effect) are concentrated in a spherical layer of infinitesimal thickness at height H above the earth's surface (see Figure 5). In this section we furthermore assume a uniform density of E electrons per m^2 in the layer.

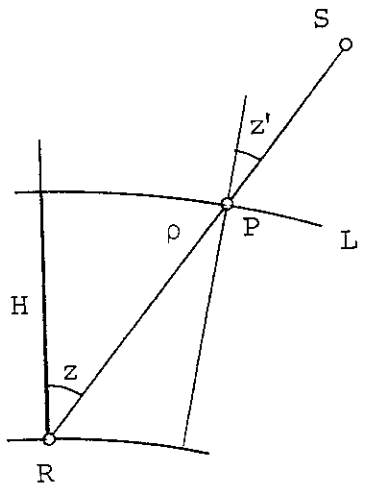

Figure 5: Single layer model for the ionosphere

Legend:

S: Satellite
R: Receiver
L: Ionosphere layer of infinitesimal thickness
H: Height of the ionosphere layer
z: Zenith distance of satellite as seen from receiver
z': Zenith distance of satellite as seen from intersection point P of signal path with ionosphere layer

The refraction effect seen from one receiver - to be added to the measurements in order to give the geometrical distance - is computed as

$$d\rho = \frac{41}{\nu^2} \cdot E \cdot \frac{1}{\cos z'} \tag{29}$$

in this model (see e.g. (Bauersima, 1983)). ν is the frequency of the observed carrier.

The bias introduced into the single difference observation by an unmodelled ionosphere then equals

$$\varepsilon(z,a) = - \frac{41}{\nu^2} \cdot E \cdot \left(\frac{1}{\cos z'_1} - \frac{1}{\cos z'_2} \right) \tag{30}$$

Obviously this bias is a close relative of the absolute troposphere bias (16). Apart from the proportionality factor the difference lies in the use of the zenith distances at the height H of the layer and not of the zenith distance at the receiver locations.
Let us now express the z'_i by the z_i:

We have: $$\sin z'_i = \frac{R}{R+H} \cdot \sin z_i \tag{31}$$

Where R is the earth radius,
H is the height of the layer.

We have $$\cos^2 z'_i = 1 - \sin^2 z'_i$$

$$= 1 - \frac{R^2}{(R+H)^2} \sin^2 z_i$$

Since H/R is a small quantity we may write

$$\cos^2 z'_i = 1 - \left(1 - 2 \cdot \frac{H}{R}\right) \sin^2 z_i$$

$$= \cos^2 z_i \cdot \left(1 + 2 \frac{H}{R} \tan^2 z_i\right)$$

$$\frac{1}{\cos z'_i} = \frac{1}{\cos z_i} \cdot \left(1 - \frac{H}{R} \tan^2 z_i\right) \tag{32}$$

Introducing this last result into eqn. (30) and approximating $\tan z_2$ by $\tan z_1$ we obtain

$$\varepsilon(z,a) = \frac{-41}{\nu^2} \cdot E \cdot \left(1 - \frac{H}{R}\tan^2 z_1\right) \cdot \left\{\frac{1}{\cos z_1} - \frac{1}{\cos z_2}\right\} \qquad (33)$$

Since we already developed the bracket {...} in expression (33) (see eqn. (21)) we may at once write the final result for the ionosphere bias as

$$\varepsilon(z,a) = -\frac{41}{\nu^2} \cdot E \cdot \left(\tan z_1 - \frac{H}{R}\tan^3 z_1\right) \cdot \cos(a-a_0) \cdot \ell \cdot \left\{\frac{1}{\rho_1} + \frac{1}{R_1 \cos z_1}\right\} \qquad (34)$$

Since we have for the layer height

$$250 \text{ km} \lesssim H \lesssim 400 \text{ km}$$

we have $$\frac{H}{R} \approx 0.05$$

and we may very well omit the term $H/R \cdot \tan^3 z_1$ in eqn. (34):

$$\varepsilon(z,a) = -\frac{41}{\nu^2} \cdot E \cdot \tan z_1 \cdot \cos(a-a_0) \cdot \ell \cdot \left\{\frac{1}{\rho_1} + \frac{1}{R_1 \cos z_1}\right\} \qquad (35)$$

Obviously the bias introduced into the observable by a neglected ionosphere is proportional to the bias introduced by a neglected troposphere (compare eqn. (22)). Therefore (if we observe only one frequency) it is not possible to separate the two effects by GPS measurements. Of course the ionosphere bias is a class 2 bias. In analogy to eqn. (27) we obtain the final result

$$\frac{\Delta\ell}{\ell} = -41 \cdot \frac{E}{\nu^2} \cdot \frac{1}{R_1} \cdot \frac{1}{\cos z_{max}} \qquad (36)$$

Using the L_1 carrier frequency $\nu_1 = 1.57542 \cdot 10^9$ Hz and expressing the scale factor in mm/km (ppm) we obtain the formula

$$\frac{\Delta\ell}{\ell} = -0.7 \cdot 10^{-17} \cdot E \qquad (37)$$

to compute the baseline shortening introduced into GPS results by a neglected ionosphere.
Because the ionosphere content E may vary from $E \approx 0.5 \cdot 10^{17}$ (night time observations) to $E \approx 5 \cdot 10^{17}$ (two hours after local noon in latitudes ± 20°), the ionosphere induced scale error may vary from $\Delta\ell/\ell \approx 0.35$ ppm to $\Delta\ell/\ell \approx 3.5$ ppm for L_1 observa-

tions. But day time changes are not the only variations: Although the 1984 and the 1986 Alaska GPS campaigns took place during the same time of the year and approximately at the same day time, we observed a scale bias of ~ 1.4 ppm in 1984 (Beutler et al., 1987_1) but only one of ~ 0.4 ppm in 1986. The problem of estimating model ionospheres from dual frequency GPS data has been considered by several authors. Y. Georgiadou and A. Kleusberg (1987) use the observations of one dual frequency receiver to estimate a local single layer model. They show, that the scale bias of single frequency instruments operating in the vicinity may be eliminated by using this model. We suggest to use all observations made in a regional permanent tracking network to give ionosphere model for the entire region. As opposed to Georgiadou et al. we use the double difference observable to estimate the model parameters (Beutler et al., 1987_2).

5. BIAS IN THE GM-VALUE

When we switched from the WGS-72 value for GM,

$$GM_{72} = 398.6008 \cdot 10^{12} , \tag{38}$$

to the WGS-84 value

$$GM_{84} = 398.60044 \cdot 10^{12} \tag{39}$$

in our GPS processing system, we asked ourselves whether this would change appreciable the geometry of our GPS results. We were especially afraid of a scale factor - remembering the days of optical satellite tracking, where indeed scale was uniquely determined by the adopted GM value. Indeed at first sight one might expect a scale error of the order of 10^{-6}, since the difference between the two GM values (38, 39) is 1 ppm. We will show in this section, that the change of GM-value indeed produces a scale factor, but one which is an order of magnitude smaller. We point out that the following deduction only holds for the single difference (or double difference) observable and not for the phase observable. It is easy to compute the influence on the semimajor axis of a GPS satellite using Kepler's third law.

$$n^2 \cdot a^3 = GM \tag{40}$$

where a is the semimajor axis (m)
n is the mean motion (radius/sec)

Variation of eqn. (40) gives

$$2na^3 \cdot \Delta n + 3n^2 \cdot a^2 \Delta a = \Delta GM. \tag{41}$$

If satellite orbits are estimated with the same set of observations but with two different GM-values, the mean motion

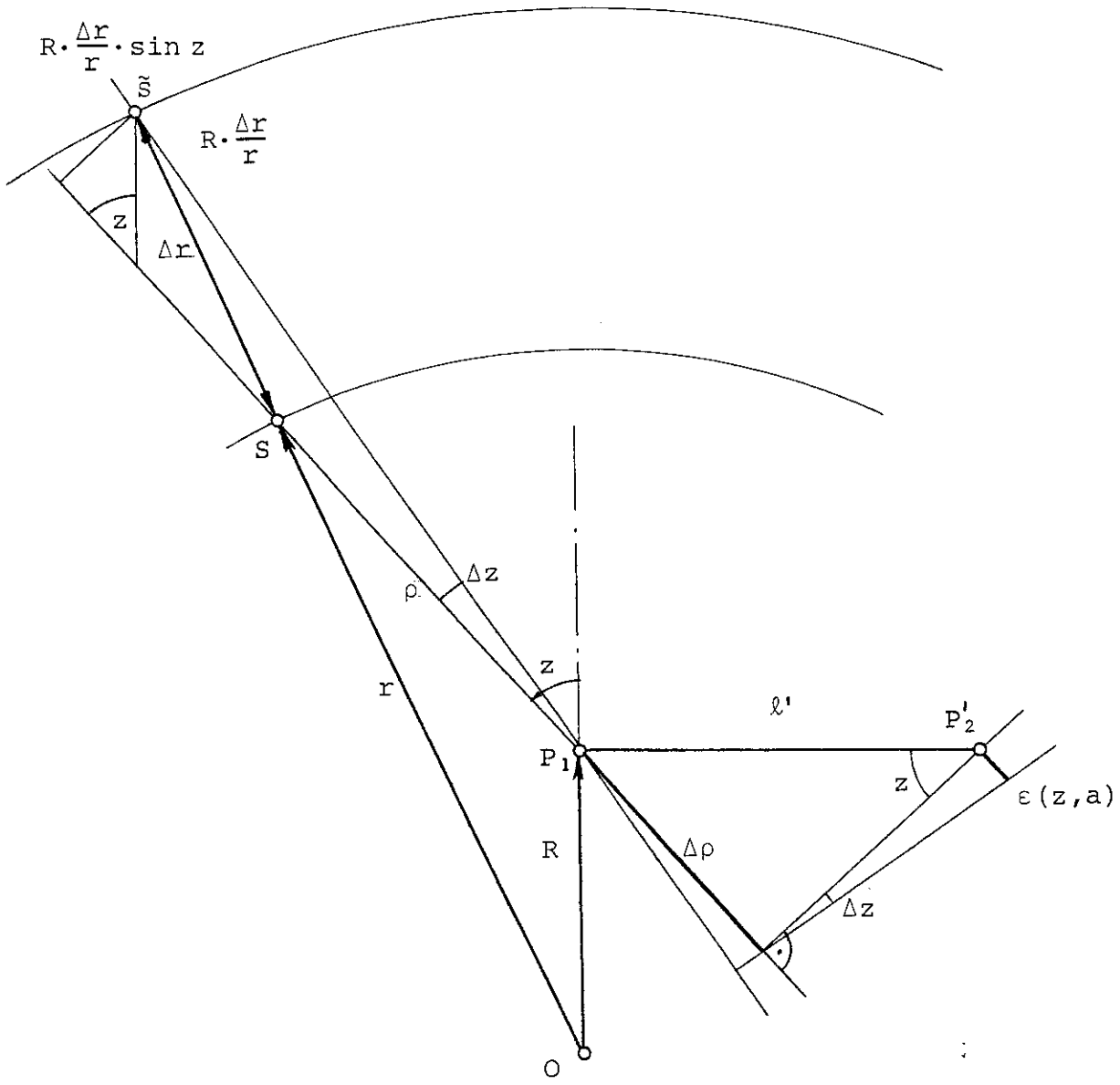

Figure 6: Bias in observable $\Delta\rho$ due to a radial bias Δr in all satellite orbits

Legend:

O: Center of earth
S, $\tilde{S}$: True resp. biased satellite positions
P_1: Location of receiver 1
r, R: Geocentric position vectors of S, P_1. $r=|\vec{r}|$, $R=|\vec{R}|$
ρ: Topocentric distance of S from P_1
z: Zenith distance of S
Δr: Bias in r
Δz: Bias in z due to Δr
$\Delta\rho$: Unbiased observable
ℓ': Length of projection of baseline $\vec{b}$ on plane OP_1S
$\varepsilon(z,a)$: Bias in the observable due to Δr

will be the same in both orbit determinations. Therefore we may put

$$\Delta n = 0 \tag{42}$$

for this special problem. Introducing eqn. (42) into eqn. (41) allows us to compute the bias introduced into the semimajor axis by a bias ΔGM in the gravity constant:

$$\Delta a = \frac{1}{3} \frac{\Delta GM}{n^2 a^2} = \frac{1}{3} \cdot \frac{\Delta GM}{GM} \cdot a$$

or

$$\frac{\Delta a}{a} = \frac{1}{3} \frac{\Delta GM}{GM}$$

Since GPS orbits are almost circular, a bias in a causes "only" a bias in the radius of the circle. We may therefore put:

$$\frac{\Delta r}{r} = \frac{1}{3} \cdot \frac{\Delta GM}{GM} \tag{43}$$

where r is the radius of the circular orbit.

We see that a change of 1 ppm in the GM value only introduces a change of 1/3 ppm, in the satellites' distances from the geocenter. Does this now mean that the scale of GPS derivered networks changes by 1/3 ppm if the new GM_{84} value is used instead of the old GM_{72} value? The answer is given in Figure 6. There we see that the bias $\varepsilon(z,a)$ introduced by a bias Δr equals

$$\begin{aligned} \varepsilon(z,a) &= \ell' \cdot \cos z \, \Delta z \\ &= \ell \cdot \cos(a-a_o) \cdot \cos z \cdot \Delta z \end{aligned}$$

where $$\Delta z = \sin z \cdot \left(R \cdot \frac{\Delta r}{r} \right) / \rho$$

Thus

$$\varepsilon(z,a) = \ell \cdot \cos(a-a_0) \cdot \cos z \cdot \frac{R}{\rho} \cdot \frac{\Delta r}{r} \sin z \quad . \tag{44}$$

The error in the baseline length introduced by the pair of observations made at (z,a) and at $(z,180^\circ+a)$ follows by introducing eqn. (44) into eqn. (7):

$$\Delta \ell(z) = \ell \cdot \frac{R}{\rho} \cdot \frac{\Delta r}{r} \cos z \tag{45}$$

Again we see that the length bias is proportional to the baseline length ℓ (indicating a net scale effect), and that $\Delta \ell(z)$ is not azimuth dependent. Therefore the scale effect introduced by all observation pairs may be written as

$$\frac{\Delta\ell}{\ell} = \frac{R}{\rho} \cdot \frac{\Delta r}{r} \quad \frac{1}{1-\cos z_{max}} \int_0^{z_{max}} \cos z' \cdot \sin z' \cdot dz'$$

$$\underline{\frac{\Delta\ell}{\ell} = \frac{R}{\rho} \cdot \frac{1}{2} \cdot \frac{\sin^2 z_{max}}{1-\cos z_{max}} \cdot \frac{\Delta r}{r}} \qquad (46)$$

where we use a mean value for the topocentric distance ρ. Therefore formula (46) holds only approximately.

Using $\rho \approx 22'000$ km
$R = 6'378$ km
$z_{max} = 70^\circ$

We obtain

$$\frac{\Delta\ell}{\ell} = 0.20 \cdot \frac{\Delta r}{r} \qquad (47)$$

To answer our original question in this section, we have to substitute eqn. (43) into eqns. (46) and (47):

$$\frac{\Delta\ell}{\ell} = \frac{1}{6} \frac{R}{\rho} \cdot \frac{\sin^2 z_{max}}{1-\cos z_{max}} \cdot \frac{\Delta GM}{GM} \qquad (48)$$

$$\underline{\frac{\Delta\ell}{\ell} = 0.07 \cdot \frac{\Delta GM}{GM}} \quad , \quad \underline{\text{for} \quad z_{max} := 70^\circ} \qquad (49)$$

This proves what we stated at the beginning of this section: An erroneous GM value indeed causes a scale error in relative GPS network results. But this scale error is less than a tenth of the relative error in the GM value. Certainly formulae (48) and (49) allow the conclusion, that biases introduced by a still erroneous WGS-84 value for GM are smaller than 0.01 ppm and therefore unimportant.

6. BIAS INTRODUCED BY AN ERRONEOUS STATION HEIGHT

Usually the position of one receiver is kept fixed when processing GPS data in the relative mode. Here we investigate the bias introduced by an error in the height of the fixed station. This error source is not important, if there is a reliable geocentric position available for one of the receiver locations (e.g. from a laser observatory). It has to be considered however, if the fixed position is derived from a single point positioning using GPS code measurements.

Figure 7 reveals the geometry of this bias type:

$$\varepsilon(z,a) = \ell' \cdot \cos z \cdot \Delta z$$
$$\Delta z = \Delta h \cdot \sin z / \rho$$

Thus:

$$\varepsilon(z,a) = \ell \cdot \cos(a-a_0) \cdot \frac{\Delta h}{\rho} \sin z \cdot \cos z \qquad (50)$$

Clearly this last expression is closely related to the GM bias discussed in the previous section. Again we have a class 2 bias. The length error introduced by the two observations made at (z,a) and $(z,a+180^\circ)$ respectively follows by introducing eqn. (50) into eqn. (7):

$$\Delta\ell(z) = \ell \cdot \cos z \cdot \frac{\Delta h}{\rho} \qquad (51)$$

and the effect by all observations is computed as usual by introducing eqn. (51) into eqn. (8):

$$\frac{\Delta\ell}{\ell} = \frac{1}{1-\cos z_{max}} \cdot \frac{\Delta h}{\rho} \int_0^{z_{max}} \cos z' \cdot \sin z' \cdot dz'$$

$$\frac{\Delta\ell}{\ell} = \frac{\Delta h}{\rho} \cdot \frac{1}{2} \cdot \frac{\sin^2 z_{max}}{1-\cos z_{max}} = \frac{\Delta h}{R} \cdot \frac{R}{\rho} \cdot \frac{1}{2} \cdot \frac{\sin^2 z_{max}}{1-\cos z_{max}} \qquad (52)$$

where R is the radius of the earth.
Using again

$$\rho = 22'000 \text{ km}$$
$$z_{max} = 70^\circ$$

gives the following formula for the scale error introduced due to an error of Δh in the height of the station kept fixed:

$$\frac{\Delta\ell}{\ell} = 0.20 \cdot \frac{\Delta h}{R} \qquad (53)$$

This means that an error of 6 m in the station height will cause a scale error of 0.20 ppm in the GPS network.
If $\Delta h/R$ is caused by a wrong GM value used in the single point positioning, it is easy to show that

$$\frac{\Delta h}{R} = \frac{1}{6} \cdot \frac{\Delta GM}{GM} \frac{\sin^2 z_{max}}{1-\cos z_{max}}$$

and by substitution in eqn. (53):

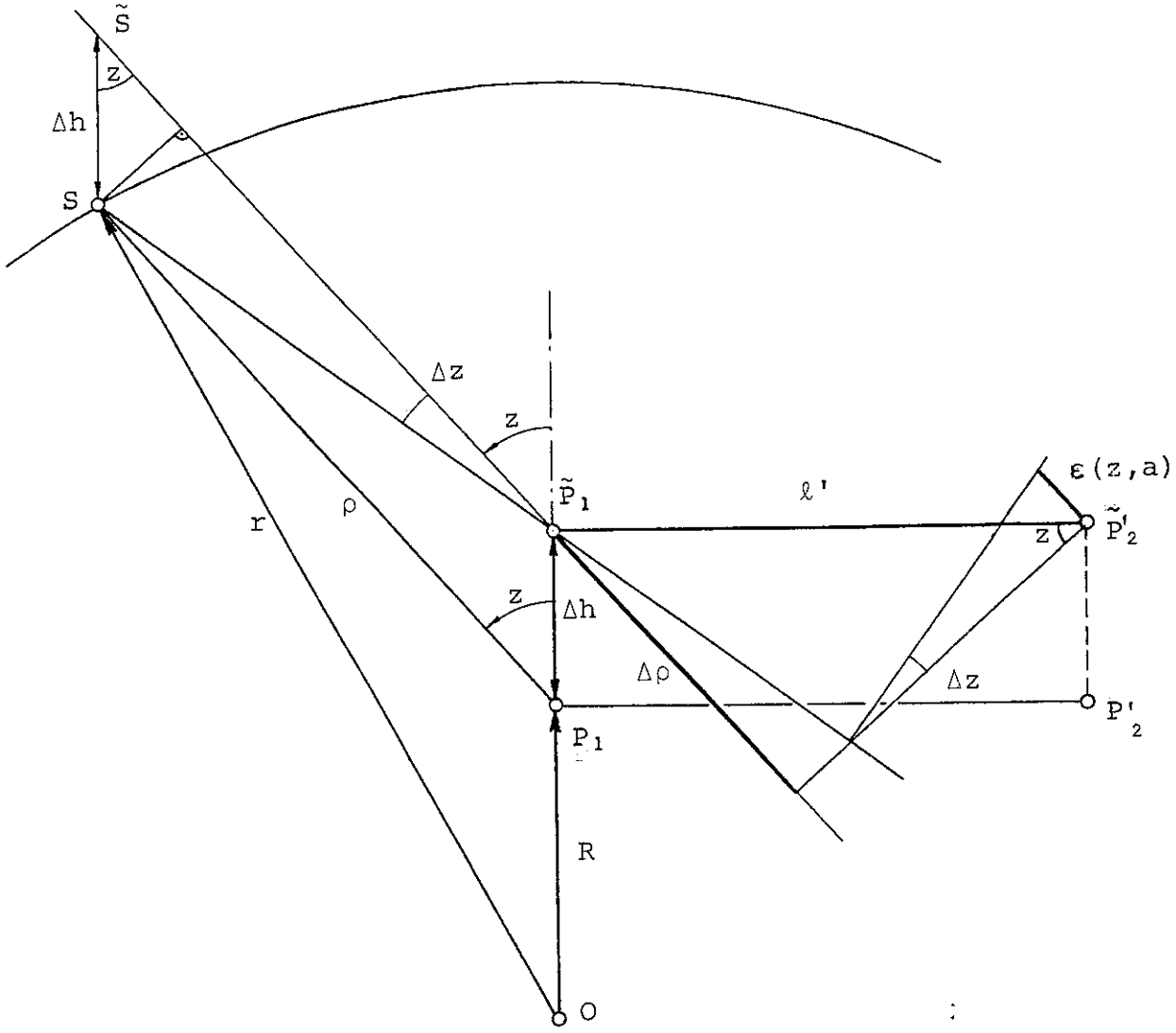

Figure 7: Bias in observable $\Delta\rho$ due to a bias Δh in height of station P_1

Legend:

O:	Center of earth
S, $\tilde{S}$:	Satellite position, Satellite position shifted by Δh
P_1, $\tilde{P}_1$:	True position, biased position of receiver 1
r, R:	Geocentric position vectors of S_1 and P_1; $R=\lvert \vec{R} \rvert$, $r=\lvert \vec{r} \rvert$
ρ:	Topocentric distance of S from P_1
z:	Zenith distance of S
$\Delta\rho$:	Unbiased observable
Δh:	Height bias of station P_1
ℓ':	Length of projected baseline $\vec{b}$ on plane OP_1S
P_2', $\tilde{P}_2'$:	Projections of P_2, P_2 parallelly shifted by Δh along OP_1 on plane OR_1S

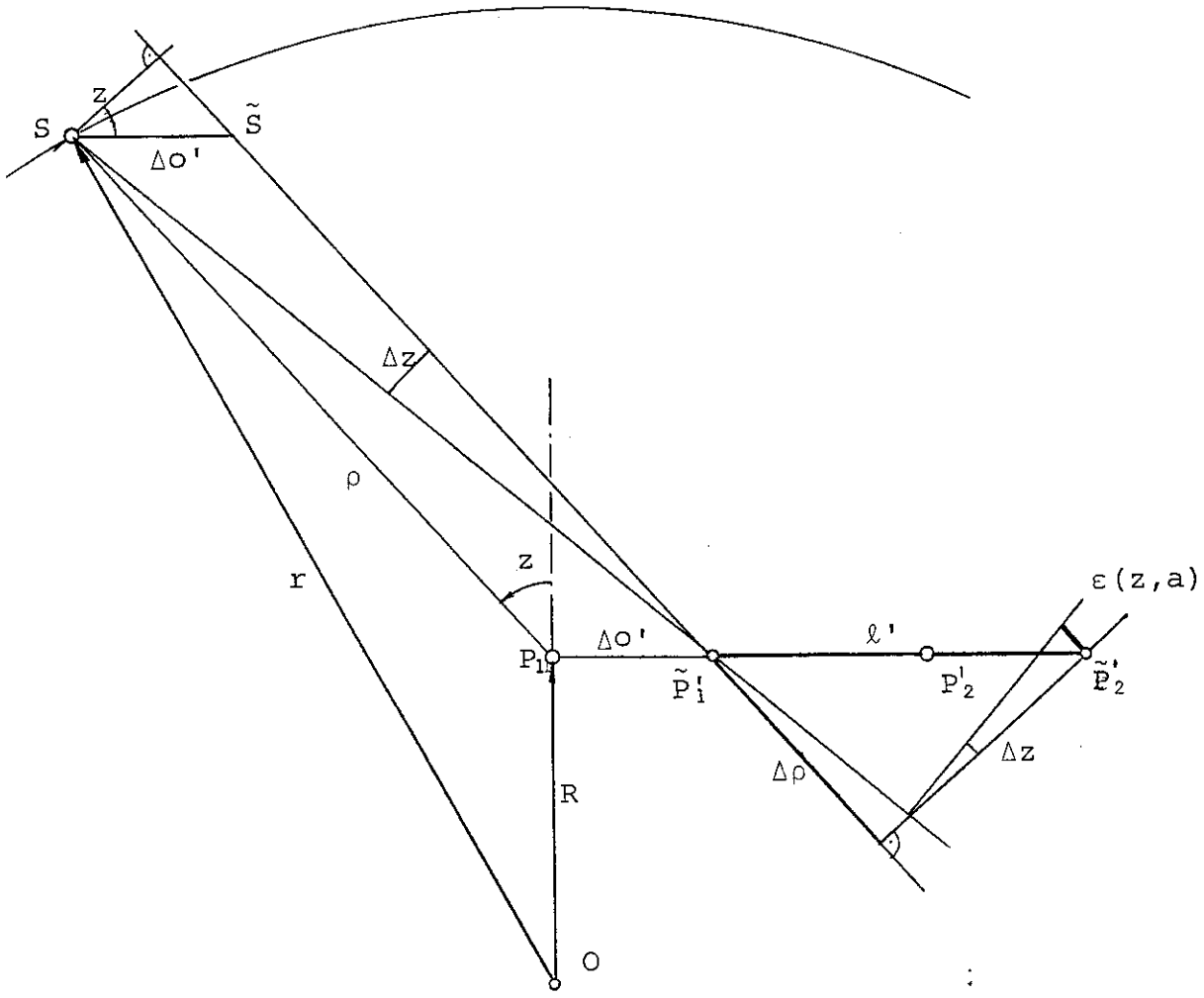

Figure 8: Bias in observable $\Delta\rho$ due to a bias $\Delta 0$ in horizontal coordinates of fixed station P_1

Legend:

0: Center of earth
S, $\tilde{S}$: Satellite position, Satellite position shifted by $\Delta 0'$
P, $\tilde{P}'$: True position, projection of biased position of fixed receiver
$\vec{r}$, $\vec{R}$: Geocentric position vectors of S, P_1, $R=|\vec{R}|$, $r=|\vec{r}|$
ρ: Topocentric distance of S from P_1
z: Zenith distance of S from P_1
$\Delta\rho$: Unbiased observable
$\Delta 0'$: Projection of horizontal position bias on plane SOP_1
ℓ': Length of projected baseline b on plane SOP_1
$\varepsilon(a,z)$: bias in $\Delta\rho$ due to $\Delta 0$

$$\frac{\Delta \ell}{\ell} = 0.05 \cdot \frac{\Delta GM}{GM} \quad , \text{(indirect } \Delta GM\text{-effect)} \qquad (54)$$

Therefore, if the coordinates of the station(s) kept fixed in the single (or double) difference analysis have been determined previously using the code observations of the same satellite passes and a biased GM value, the total scale error will be the difference of the scale errors in eqns. (49) and (54). The resulting effect will therefore almost vanish. If the coordinates of the fixed station are known from a different source (e.g. Laser ranging), the GM induced scale error is given by eqn. (49) uniquely.

7. BIASES IN HORIZONTAL COORDINATES OF FIXED STATION

Let us assume in this section that the station P_1 is kept fixed at a wrong horizontal position

$$\vec{R} = \vec{R} + \Delta\vec{0} \qquad (55)$$

where $$\vec{R} \cdot \Delta\vec{0} = 0 \qquad (56)$$

Figure 8 shows the bias $\varepsilon(a,z)$ caused by the horizontal bias vector $\Delta 0$:

$$\varepsilon(a,z) = \ell' \cdot \cos z \cdot \Delta z = \ell' \cdot \cos z \cdot \Delta 0' \cdot \cos z/\rho \qquad (57)$$

where ℓ', $\Delta 0'$ are the projections of vectors $\vec{b}$, $\Delta\vec{0}$ on the plane $0\ P_1\ S$:

$$\begin{aligned} \ell' &= \ell \cdot \cos(a-a_0) \\ \Delta 0' &= \Delta 0 \cdot \cos(a-a_1) \end{aligned} \qquad (58)$$

where a, a_0, a_1 are the azimuths of the satellite position, the baseline and the bias vector $\Delta 0$. Due to the change of sign of Δz and of $\cos(a-a_0)$, if a is replaced by $a+180°$, the bias discussed in this section is a class 1 bias influencing heights. According to eqn. (5) the influence of the observations made at (z,a) and $(z,a+180°)$ is (eqns. (57), (58)):

$$\Delta h(a,z) = \ell \cdot \cos(a-a_0) \cdot \cos(a-a_1) \cdot \cos z \cdot \frac{\Delta 0}{\rho} \qquad (59)$$

Writing $$\begin{aligned} \cos(a-a_1) &= \cos(a-a_0-(a_1-a_0)) \\ &= \cos(a-a_0)\cdot\cos(a_1-a_0)-\sin(a-a_0)\cdot\sin(a_1-a_0) \end{aligned}$$

it is easy to show that by introducing eqn. (59) into eqn. (6) one obtains for the integral height effect

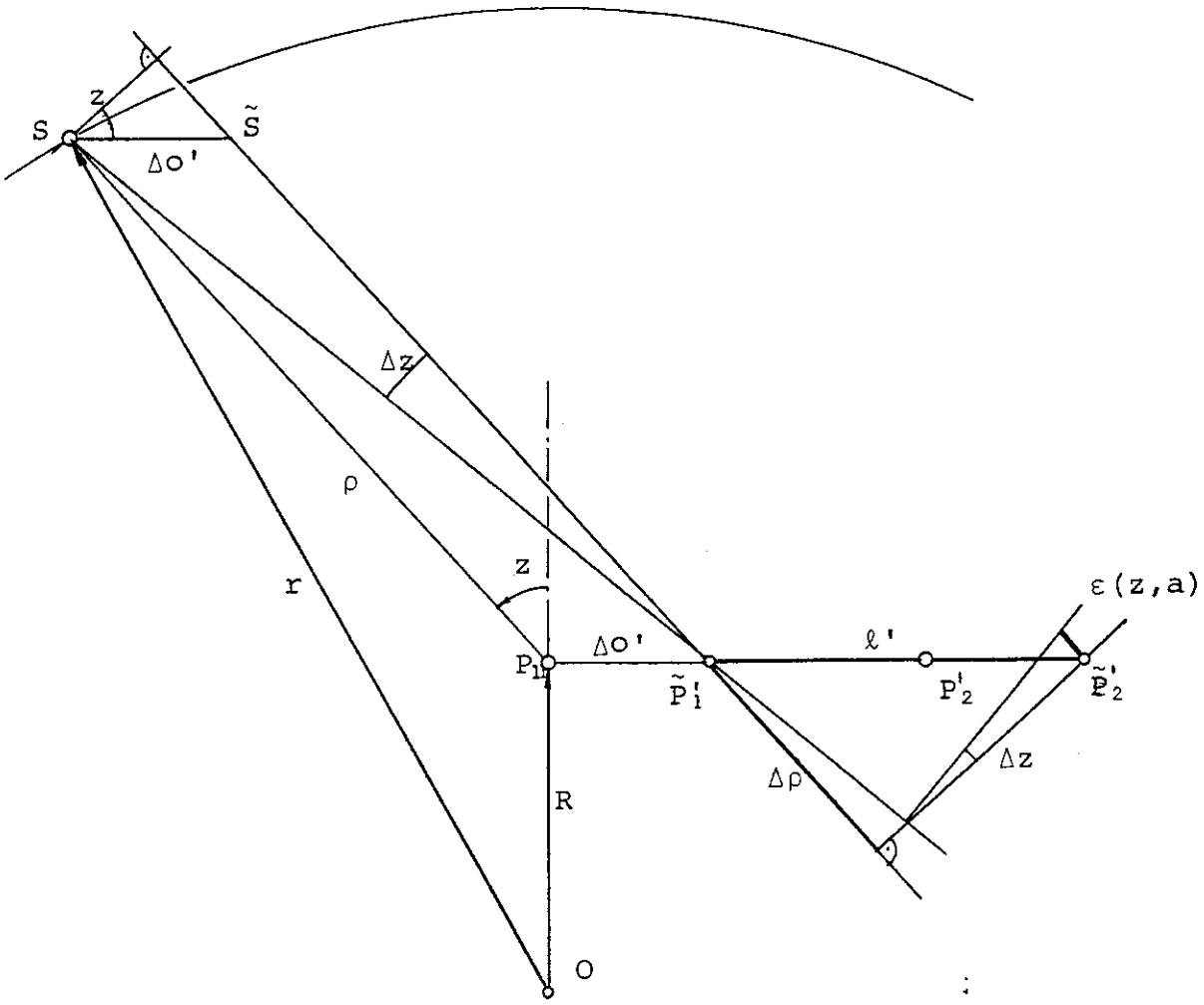

Figure 8: Bias in observable $\Delta\rho$ due to a bias $\Delta 0$ in horizontal coordinates of fixed station P_1

Legend:

0: Center of earth
S, $\tilde{S}$: Satellite position, Satellite position shifted by $\Delta 0'$
P, $\tilde{P}'$: True position, projection of biased position of fixed receiver
$\vec{r}, \vec{R}$: Geocentric position vectors of S, P_1, $R=|\vec{R}|$, $r=|\vec{r}|$
ρ: Topocentric distance of S from P_1
z: Zenith distance of S from P_1
$\Delta\rho$: Unbiased observable
$\Delta 0'$: Projection of horizontal position bias on plane SOP_1
ℓ': Length of projected baseline b on plane SOP_1
$\varepsilon(a,z)$: bias in $\Delta\rho$ due to $\Delta 0$

$$\frac{\Delta h}{\ell} = \frac{1}{4} \cdot \frac{\sin^2 z_{max}}{1-\cos z_{max}} \cdot \frac{\Delta 0}{\rho} \cos (a_1 - a_0) \qquad (60)$$

Indeed quite a special effect in height!: If we consider an entire network (baselines at azimuths a_{0i}, i=1,2,...) eqn. (60) tells us that the entire network will be rotated about an axis in the horizontal plane perpendicular to the bias vector $\Delta 0$. The rotation angle ω (expressed in radians) follows from eqn. (60) as

$$\omega = \frac{1}{4} \cdot \frac{\sin^2 z_{max}}{1-\cos z_{max}} \cdot \frac{\Delta 0}{\rho} \qquad (61)$$

In order to assess the order of magnitude, let us use

$$z_{max} = 70^\circ$$
$$\Delta 0 = 10 \text{ m}$$
$$\rho \approx 22'000 \text{ km}$$

We obtain

$$\omega = 0''.03 \qquad (62)$$

It is instructive also to rewrite eqn. (61) as

$$\omega = \frac{1}{4} \frac{\sin^2 z_{max}}{1-\cos z_{max}} \cdot \frac{R}{\rho} \cdot \frac{\Delta 0}{R} \qquad (63)$$

Now, $\Delta 0/R$ may be interpreted as the angular bias measured at the surface of the earth. We may therefore conclude that, if we keep a station fixed at 1" from the true position, the GPS network will be rotated by an angle 0".1.

Apart from the rotation discussed above there is a side effect due to the circumstance that in general point $\tilde{P}_1$ in Figure 8 does not lie in the plane OP_1S. It is interesting to note that this side effect is of bias class 2. We do not consider it further here.

8. ALONG TRACK ORBIT ERRORS

In section 5 we considered radial orbit biases common to all satellites. We showed that the consequence is a scale factor in GPS results which may be written as (compare eqn. (47))

$$\frac{\Delta\ell}{\ell} = 0.2 \cdot \frac{\Delta r}{r} \qquad (64)$$

Comparing that to the formula given by (Bauersima, 1983)

$$\frac{\Delta b}{b} = \frac{\Delta r}{\rho} \qquad (65)$$

where Δb stands for the length of the induced baseline error, we conclude that radial orbit errors show a much more favourable propagation into GPS results. Does this statement also hold for other than radial orbit errors? In order to answer that question we discuss a very simple special case of an along track error in this section, namely a constant along track error $\Delta 0$ of an orbit going through the zenith of station P_1. Approximating the topocentric orbit (as seen from station P_1) by a vertical plane with azimuth a, we see the geometry involved for this bias type in Figure 9. We have

$$\begin{aligned} \varepsilon(z,a) &= \ell' \cos z \cdot \Delta z \\ &= \ell' \cos z \cdot \Delta 0 \cdot \cos\zeta/\rho \end{aligned} \qquad (66)$$

Since $\zeta \leq 14^\circ$ for $z \geq 20^\circ$ and
$\ell' = \ell \cdot \cos(a-a_0)$

we may approximate eqn. (66) as

$$\varepsilon(z,a) = \ell \cdot \cos(a-a_0) \cdot \cos z \cdot \frac{\Delta 0}{\rho} \qquad (67)$$

Since the angle Δz and the term $\cos(a-a_0)$ will change sign if a is replaced by $a+180^\circ$, the bias $\Delta 0$ causes a class 1 bias in the observable. The height error associated with the two observations at (z,a) and at $(z,a+180^\circ)$ (see eqn. (5)) is

$$\Delta h(a,z) = \ell \cdot \cos(a-a_0) \cdot \frac{\Delta 0}{\rho} \qquad (68)$$

Because the assumption that other satellites show the same along track error $\Delta 0$ does not make sense, an integration over the azimuth a does not make sense either. Introducing therefore eqn. (68) into eqn. (6) (without integrating over a) gives

$$\frac{\Delta h}{\ell} = \cos(a-a_0) \cdot \frac{\Delta 0}{\rho} \qquad (69)$$

Two comments concerning the final result (69) seem appropriate:

(1): Along track errors may propagate into GPS results in a much less favourable way than radial errors. As a matter of fact, if the baseline lies in the orbit plane, the height component is influenced exactly in the way predicted by the rule (65) (Bauersima, 1983).

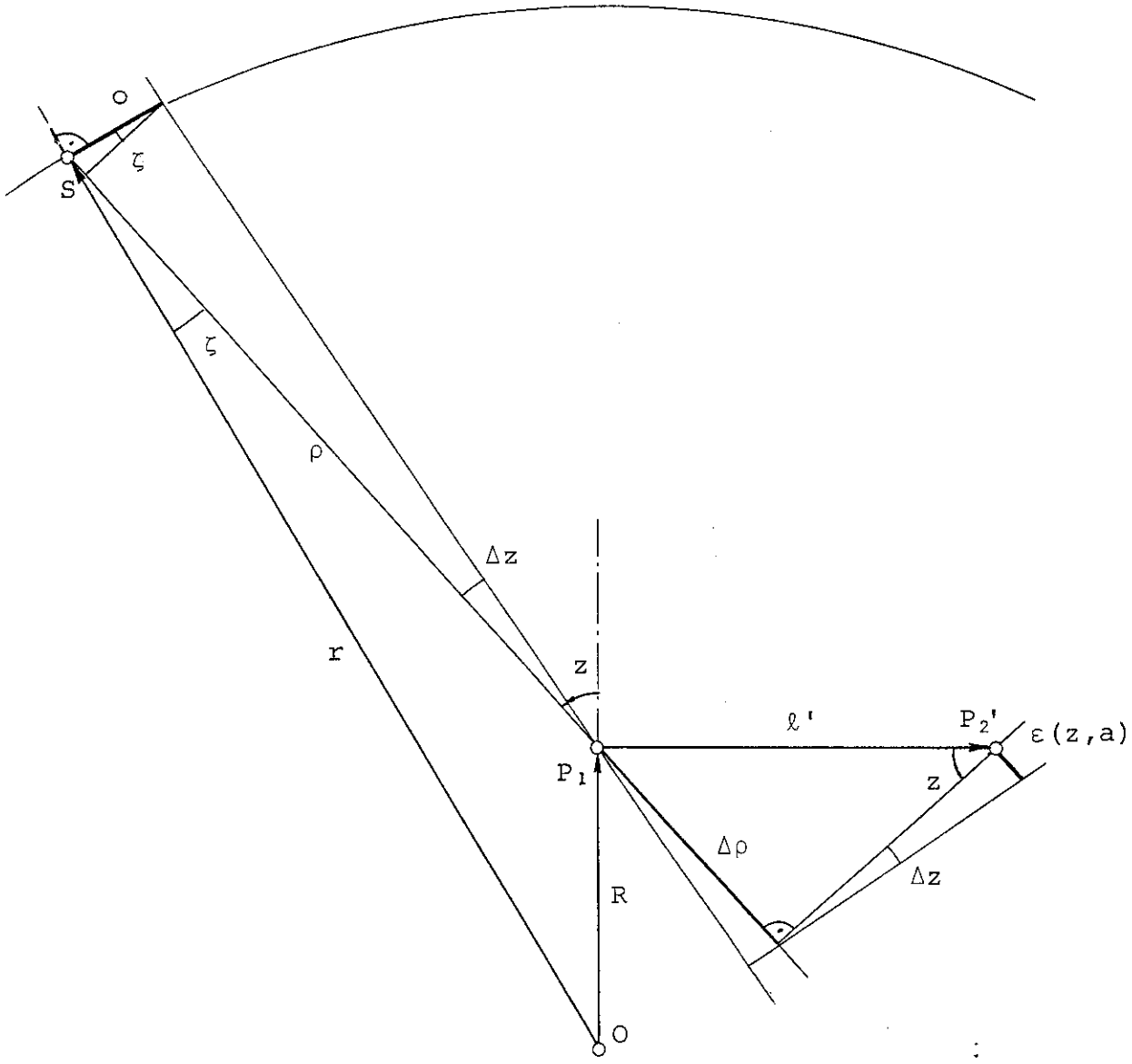

Figure 9: Bias in observable $\Delta\rho$ due to an along track orbit error $\Delta 0$ (satellite pass through zenith of P_1 assumed)

Legend:

0:	Center of earth
Π_1:	Location of receiver 1
P_2':	Projection of second receiver location on plane $0P_1S$
$\underline{S}, \tilde{\underline{S}}$:	True position, biased position of satellite
r, R:	Geocentric position vectors of S_1 and P_1. $r=\lvert \vec{r} \rvert$, $R=\lvert \vec{R} \rvert$
ρ:	Topocentric distance of S from P_1
z:	Zenith distance of S
$\Delta\rho$:	Unbiased observable
$\Delta 0$:	Along track error
ζ =	$(S0, SP_1)$
$\varepsilon(z,a)$:	bias in $\Delta\rho$ due to $\Delta 0$

(2): From eqn. (69) we conclude that an along track error $\Delta 0$ in one satellite would cause a GPS network to rotate about an axis perpendicular to the orbit plane by an angle of $\Delta 0/\rho$. This is of the same order of magnitude as the rotation we would expect, if working with ranges instead of range differences (the rotation angle would be $\Delta 0/r$ in the latter case).

Reality will be somewhat different from our simple special case. We think that at this point simulation techniques should replace the geometrical method developed in this paper. In this context we think that the approach chosen by A. Geiger (1987) is most promising.

9. NON SYMMETRICAL SATELLITE DISTRIBUTIONS

Assumption 1 (uniform satellite distribution in a cone around the vertical axis of the station kept fixed, see section 1) was vital for the deduction of the simple formulae given in the preceeding sections. Certainly, in real applications, this assumption will never be perfectly satisfied. In future, when the final configuration will become available (1991(?)), it will be one important aspect for campaign designers to schedule sessions in order to have a uniform satellite distribution. Certainly under these circumstances the rules given here will be good approximations of the real situation. We had some question marks however concerning the applicability to the test configuration of GPS. We used the method of simulation to find an answer to this question. For the satellite distribution presently available we simulated observations (four sessions) for a network (50 × 50 × 1 km) in Switzerland to test our theory. We found the results most encouraging. In all cases the predicted main effect was actually "observed", its size always was within 50 % of the theoretically predicted effect. We therefore conclude that the predictions given here are most useful even if the satellite distribution is not symmetrical. We have to mention however that our test sample was limited.

10. DOUBLE DIFFERENCE VERSUS SINGLE DIFFERENCE PROCESSING

The theory presented in the preceeding chapters was developed for the single difference observable (see Figure 1). In GPS processing however usually the "double difference observation"(the difference of two single differences of two satellites observed at the same time by the same receiver pair) is analyzed. The reason for this differencing technique is the cancellation (actually only a strong reduction) of receiver clock errors. In principle it is possible to develop a

pure geometrical bias theory for the double difference observable, but this approach proves to be rather complicated. Moreover in our opinion it is not necessary to do so because in all cases considered here the absolute values of biases obtained using double differences were of the order of magnitude predicted by our single difference theory. It is interesting to note that the signs of height biases (class 1 biases) may change if single difference is replaced by the double difference processing.

11. SUMMARY

In this paper we showed that many important biases occuring in GPS are members of two classes. Class 1 biases are identical for observations at (z,a) and at (z+180°,a), class 2 biases are identical in absolute value but of opposite sign. We showed that class 1 biases produce height effects, which in some cases could be interpreted as rotations, whereas class 2 biases give rise to scale errors. Table 1 summarizes the essential results:

Table 2
Influence of biases on GPS results

Bias	Class	Influence	
		Type	Order of magnitude
Troposphere (relative)	1	Height	A bias of 1mm in zenith direction of tropospheric correction causes a height bias of ~2.9mm
Troposphere (absolute)	2	Scale	A bias of 1m in zenith direction of tropospheric correction causes a scale effect of 0.4ppm (If troposphere is neglected, baselines are longer.)
Ionosphere	2	Scale	Network contracts by 0.7ppm if an electron content of 10^{17} electrons/m^2 in zenith direction is neglected.
GM-value	2	Scale	If GM is increased by 1ppm, the scale of the GPS net is increased by 0.05ppm.
Fixed station height	2	Scale	A height bias of 10m introduces a scale effect of 0.4ppm (If station height is too big, scale is too small.)

Fixed station horizontal coordinates	1	Rotation	An error of 1" in horizontal position causes the network to rotate 0".1 about a horizontal axis perpendicular to the station bias vector.
Along track orbit error	1	Rotation	An along track orbit error of 1" rotates the GPS network 1" about an axis perpendicular to the orbit plane.

REFERENCES

Bauersima, I. (1983). "NAVSTAR/Global Positioning System (GPS), (II)." Mitteilungen der Satellitenbeobachtungsstation Zimmerwald, Nr. 10, Astronomical Institute, University of Berne, Switzerland.

Beutler, G., I. Bauersima, W. Gurtner, M. Rothacher, T. Schildknecht (1987_1). "Evaluation of the Alaska Global Positioning System Campaign with the Bernese Software." Journal of Geophysical Research, Vol. 92, No. B2, pp. 1295-1303, 1987.

Beutler, G., I. Bauersima, S. Botton, W. Gurtner, M. Rothacher, T. Schildknecht (1987_2). "Accuracy and biases in the goedetic application of the Global Positioning System." Paper presented at the XIX General Assembly of the International Union of Geodesy and Geophysics (IUGG), Vancouver, Canada, 1987.

Bock, Y., R.I. Abbot, C.C. Counselman, S.A. Gourevitch, R.W. King, A.R. Paradis (1984). "Geodetic accuracy of the Macrometer Model V-1000." Bulletin Géodésique, Vol. 58, No. 2, pp. 211-221, 1984.

Geiger, A. (1987). "Simplified error estimation of satellite positioning." Paper presented at the GPS Technology Workshop, Jet Propulsion Laboratory, Pasadena, March 23, 1987.

Georgiadou, Y., A. Kleusberg (1987). "On the effect of ionospheric delay on geodetic relative positioning." Manuscripta geodaetica 1987, in press.

ATMOSPHERIC REFRACTION ON THE RESULTS OF GPS PHASE DIFFERENTIAL MEASUREMENTS

P. Shi

Abstract

This paper deals with the effects of atmospheric refraction on the results of NAVSTAR GPS phase differential measurements. A simplified model has been proposed to remove the normal parts with a great saving of the computer time. From this investigation, we realize that it is not necessary to observe the weather conditions very frequently for a baseline shorter than 10 km. Only about 1 cm random error will be left in the solution vector, if we just use approximate mean values in a preprocessing program to calculate differential observations. For long distance baseline measurements and for more accurate results, we should generate a more complicated mathematical and physical model to estimate the corrections for the phase differential observations. In addition careful measurements of weather parameters are necessary in order to estimate the meteorological data along the wave paths. If all other error sources, such as ephemeris, ionospheric delay, clock error, etc., are reduced below the 0.01 ppm level, we can excpect that baseline results from GPS phase differential measurements, in the near future, will be better than 0.01 to 0.02 ppm if their lengths are longer than 1000 km. Such a high relative accuracy will be comparable to the results of VLBI and SLR measurements -- the most precise methods known to the geodetic community.

In Brunner, F.K. (Ed.), 1988, "Atmospheric Effects on Geodetic Space Measurements", *Monograph 12, School of Surveying, University of New South Wales, pp. 45-62.*

1. INTRODUCTION

As a well-known fact, atmospheric refraction is one of the most important biases in the results of GPS observations. Previous investigations put their view point onto the range corrections and derived a series of experimental model to estimate them. When a baseline measurement with GPS is performed in a relative positioning mode, experience told us that there was no serious effect caused by atmospheric refration. An explanation for the cancellation of refraction effects on relative positioning is that they are correlated each other reaching a very high level, when the observations of two stations are acquired simutaneously from the same space vehicle.

There are some questions: (1) Are all of these models for range corrections equivalent in their effectiveness and shall we choose which one for data processing? (2) Under what conditions, we can ignore real time observation of meteorological data or do a relative positioning without atmospheric correction? (3) How accuracy and what kind of requirements shall be specified for the acquisition of weather parameters to ensure 0.01 to 0.02 ppm relative precission for a long baseline? In this paper, author will discuss these problems and give some his suggestion.

2. ATMOSPHERIC EFFECT ON GPS CARRIER PHASE MEASUREMENTS

Electro-magnetic waves transmitted by GPS satellite are refracted when they pass through the medium of atmosphere surrounding the earth. For the convenience of study and discussion, refraction effects are almost always divided into two components, "dry" and "wet". As a well-known fact, about 80 - 90% of effects on L band signal will come from the dry part and remains are caused by wet component which is variable due to the quantity and to the distribution of aqueus vapour in atmosphere. Range error will also be related to the elevation angle of satellite above horizon inversely (Wells 1986). In other words, the higher the elevation of the satellite, the lower the effect of refraction. At the zenith, the refractional correction to a path length of microwaves is bit more than 2 metres which is about 12 times of wave-length of L1 carrier; closing to the horizon, refraction errors will be getting higher and higher, almost reach 100 metres (see fig. 1).

In fact, when the elevation angle is lower than 10 degrees, not only increase the effects rapidly, but also get higher and higher the rates of effects, so we are hardly to determine the correction in a reasonable precision which will cause the reduce of the accuracy in the results of positioning.

Table 1a:

Range and Phase Corrections vs the Elevation

(h=0m, t=20°c, P=1014.0mb, e=0.0mb)

Ele.	dr/dL	Bo	B	H	S
5	dr(m)	23.447	23.620	23.757	23.412
(deg)	dL1(C)	123.13	124.04	124.76	122.95
	dL2(C)	95.95	96.65	97.21	95.80
6	dr	20.189	20.310	20.443	20.320
	dL1	106.02	106.66	107 35	106.71
	dL2	82.61	83.11	83.65	83.15
8	dr	15.719	15.788	15.877	15.859
	dL1	82.55	82.91	83.38	83.28
	dL2	64.32	64.60	64.97	64.90
10	dr	12.834	12.879	12.933	12.932
	dL1	67.40	67.63	67.92	67.91
	dL2	52.52	52.70	52.92	52.92
15	dr	8.785	8.805	8.823	8.823
	dL1	46.13	46.24	46.33	46.33
	dL2	35.95	36.03	36.10	36.10
20	dr	6.698	6.710	6.716	6.716
	dL1	35.17	35.24	35.27	35.27
	dL2	27.41	27.46	27.48	27.48
30	dr	4.608	4.613	4.614	4.613
	dL1	24.20	24.22	24.23	24.22
	dL2	18.86	18.88	18.88	18.88
40	dr	3.592	3.595	3.594	3.593
	dL1	18.86	18.88	18.87	18.87
	dL2	14.70	14.71	14.71	14.70
50	dr	3.017	3.019	3.018	3.017
	dL1	15.84	15.85	15.85	15.84
	dL2	12.35	12.35	12.35	12.35
70	dr	2.461	2.462	2.462	2.461
	dL1	12.92	12.93	12.93	12.92
	dL2	10.07	10.07	10.07	10.07
90	dr	2.314	2.314	2.314	2.313
	dL1	12.15	12.15	12.15	12.15
	dL2	9.47	9.47	9.47	9.46

* Values in column B and Bo are taken from simplified Black model and those with bending corrections, H for Hopfield and S for eq. (1).

Table 1b:

Range and Phase Corrections vs the Elevation

(h=0m, t=20°c, P=1014.0mb, e=25.0mb)

Ele.	dr/dL	Bo	B	H	S
5	dr(m)	26.082	26.273	26.382	26.034
(deg)	dL1(C)	136.97	137.97	138.54	136.72
	dL2(C)	106.73	107.51	107.96	106.53
6	dr	22.409	22.542	22.660	22.537
	dL1	117.68	118.38	119.00	118.35
	dL2	91.70	92.24	92.72	92.22
8	dr	17.405	17.461	17.564	17.546
	dL1	91.40	91.69	92.24	92.14
	dL2	71.22	71.45	71.87	71.80
10	dr	14.193	14.242	14.294	14.293
	dL1	74.53	74.79	75.06	75.06
	dL2	58.08	58.28	58.49	58.49
15	dr	9.702	9.724	9.741	9.742
	dL1	50.95	51.06	51.15	51.16
	dL2	39.70	39.79	39.86	39.86
20	dr	7.394	7.407	7.413	7.412
	dL1	38.83	38.90	38.93	38.92
	dL2	30.26	30.31	30.33	30.33
30	dr	5.085	5.090	5.090	5.090
	dL1	26.70	26.73	26.73	26.73
	dL2	20.81	20.83	20.83	20.83
40	dr	3.963	3.966	3.965	3.965
	dL1	20.81	20.83	20.82	20.82
	dL2	16.22	16.23	16.22	16.22
50	dr	3.329	3.331	3.330	3.329
	dL1	17.48	17.49	17.49	17.48
	dL2	13.62	13.63	13.63	13.62
70	dr	2.715	2.716	2.716	2.715
	dL1	14.26	14.26	14.26	14.26
	dL2	11.11	11.11	11.11	11.11
90	dr	2.553	2.553	2.553	2.552
	dL1	13.41	13.41	13.41	13.40
	dL2	10.45	10.45	10.45	10.44

* Values in column B and Bo are taken from simplified Black model and those with bending corrections, H for Hopfield and S for eq. (1).

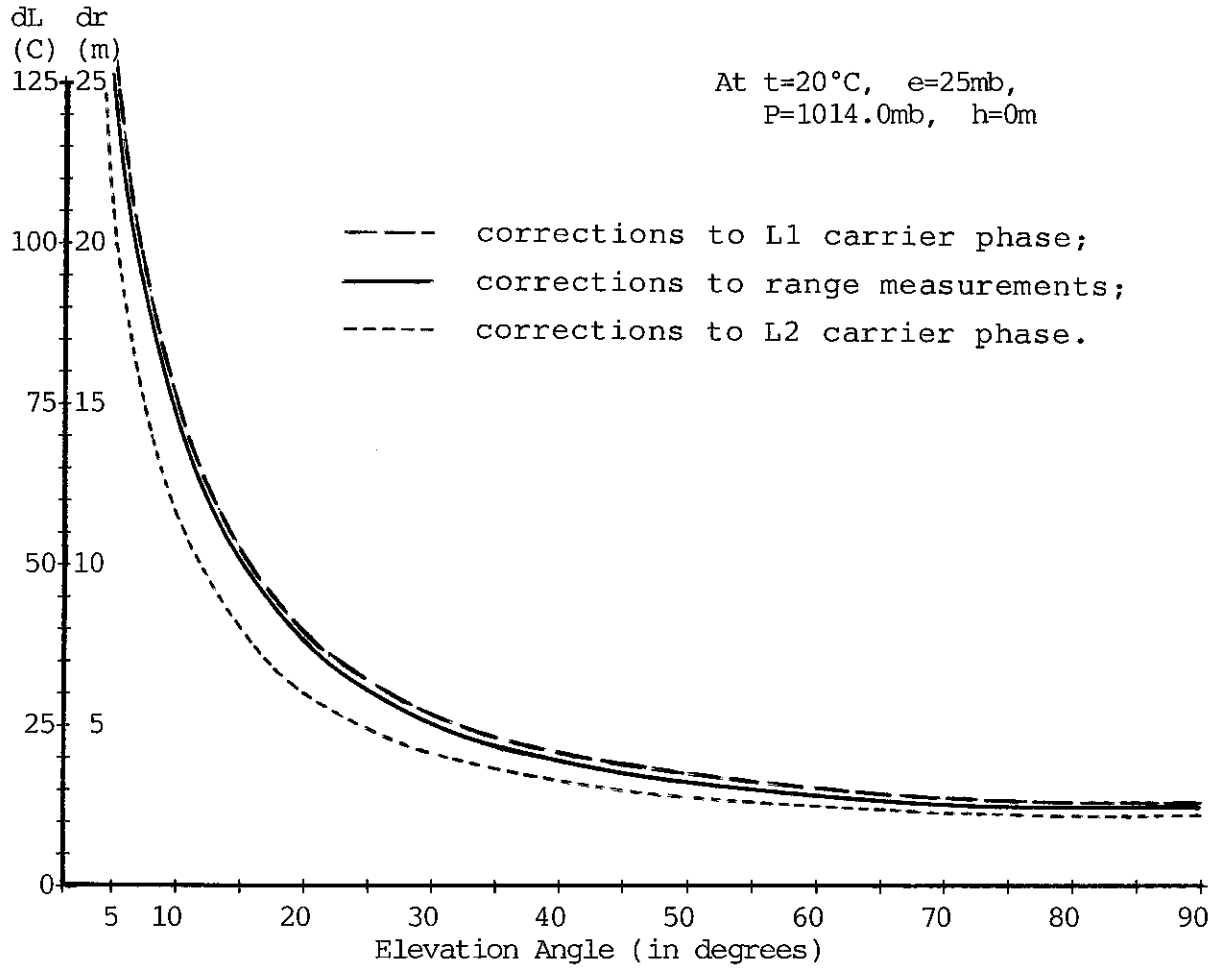

Fig 1 Range & Phase Corrections with Respect to Elevation Angle

To guarantee the quality of results against atmospheric uncertainty, the observation schedule usually choose the elevation of 10 or even 15 degrees as cut off angle.

In practice, various models may be employed in estimating the corrections to the GPS range measurements. The most famous formulae mentioned by other literature frequently and written into computer programs are those followed by names of Black (1978), Hopfield (1969) and Saastamoinen. Although they are not the same in their appearance and in computational efficiency, they almost provide the same corrections to the range measurements when the elevation of satellite is high above 15 degrees.

In table 1a and 1b, you can find the corrections from different models under the same weather conditions: t=20°C, P=1014.0mb, h=0metre, e_w=0 and e_w=25mb respectively. Last column labled with S gives the values from an experimental function derived by author.

$$\Delta 1 = (D - C / E^2) / \text{Sin } E \qquad (1)$$

where E is the elevation angle of satellite; D indicates the correction for the path from zenith including dry component A and wet component B as usual; And C is a linear combination of A and B which just makes a small modification to the main term D.

The geometrical and physical explanation of eq. (1) is so clear that you can find your answer from fig. 2.

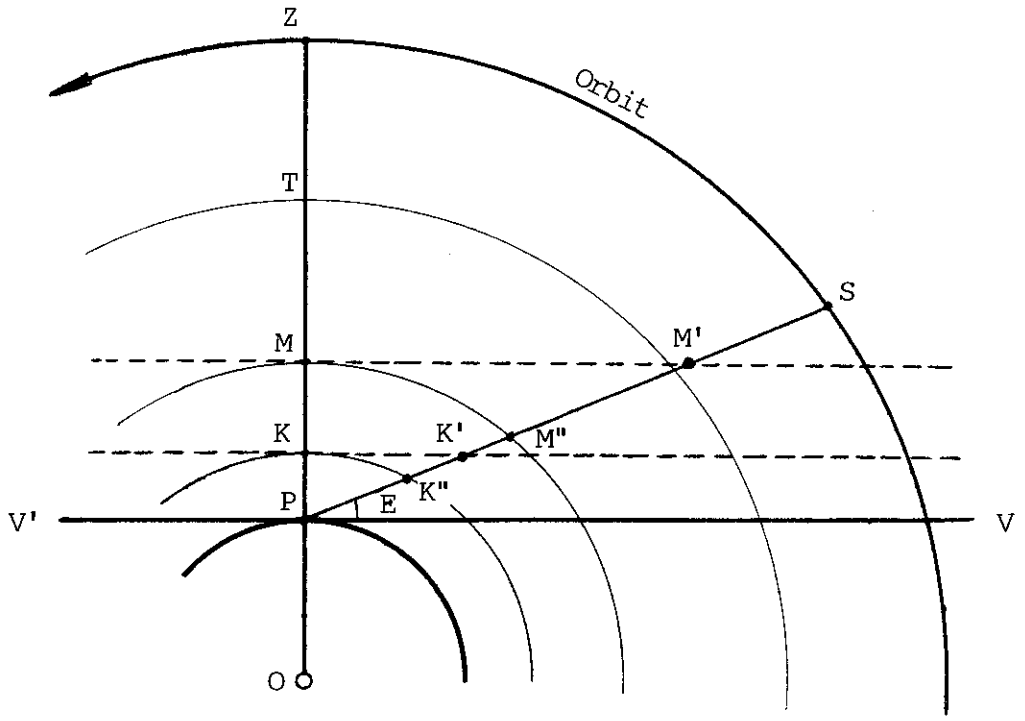

Fig 2 Explanation for Modifying the Atmospheric Effect with Elevation E vs that to the Direction of Zenith.

If the isodensity surfaces of air are parallel to the horizontal plane of the station, refractional correction for path with elevation, E, which will equal D / Sin E. Actually, the isodensity surfaces are curved and parallel to the earth surface; Furthermore, the height of top atmosphere is far less than the radius of the earth and the height of the satellite being observed. The correction for the interval M'M" is a small term and inversely proportional to the value of E^2. Thus, the full set of expressions for calculating range/phase corrections are as following:

$$D = A + B$$
$$C = c_1 A + c_2 B$$
$$= 9.0 \times 10^{-4} A + 3.3 \times 10^{-4} B$$
$$A = (0.00228 - 1.552 \times 10^{-7} h / T_k) P$$
$$B = (821.2 - 0.0746h) e / T_k^2 \qquad (2)$$

$$T_k = 273.16 + t_d$$

$$e = e_w - 4.5\times10^{-4}[1+1.68\times10^{-3}(t_w+273.16)](t_d-t_w)P$$

$$e_w = 6.126+(0.4503+(0.001389+(2.35\times10^{-4}+ +4.847\times10^{-6}t_w)t_w)t_w)t_w$$

$$(-15°C \leq t_w \leq 45°C)$$

here, h is height of station above mean sea level (in metres); t_d, t_w and P are temperature of air, wet bulb, and air pressure (in °C and mb) respectively; e is the pressure component of water vapour in the air, and e_w is saturated vapour pressure of water at t_w calculated from a numerical formula (Shi 1981). Their units are in mb., and it is valid for t_w between -15 and 45°C.

For obtaining the corrections to L1 and L2 carrier phase measurements in GPS positioning, range corrections should be divided by the wavelengths of carriers, L1 and L2 respectively.

From the computational point of view, above formulae are about 5-10 times faster than other models and need less memories to set them.

3. ATMOSPHERIC EFFECT ON PHASE DIFFERENTIAL OBSERVATIONS

3.1 Outline

The effect of atmosphere on a single phase differential observation between stations is far less than those on the range/phase measurements of GPS. There is a very high relativity for a pair of observations to the same satellite simutanueously observed by two stations at the ends of a baseline if it is short enough. The most of main term for range corrections will be cancelled out, so that a great deal of software packages for GPS data processing of short distances simply ignore their existance.

As we have mentioned before, we should make sure that if the real time meteorological data records are ignored, what about the influence on the results compared with other error sources? Also, we would like to know if we want to get the most precise results, what efforts shall we do to keep the refraction effects as low as posible? In following three sub-sessions, three aspects will be discussed:

(1) Refraction effects yield from the difference of elevation angles at two ends of the baseline;

(2) Refraction effects caused by the error from the

meteorological data records and data interpolation;

(3) Effects come from the difference of the weather conditions between stations.

3.2 Effects from the Difference of Elevation Angles

Table 1a and 1b have shown that the corrections for range and phase are mainly dependent on the elevation of the satellite above the horizon of the tracking station. At this stage we may ignore the influence introduced by other omitted parameters, and assume the tropospheric correction as a function of E.

$$\Delta l = f (E) \qquad (3)$$

from fig. 3, we have the equation (4):

$$E_i = \arcsin \frac{\bar{l}_i \cdot \bar{R}_i}{|\bar{l}_i| \, |\bar{R}_i|} , \quad (i=1,2) \qquad (4)$$

where $\bar{l}_1, \bar{l}_2$ are values from station 1 and 2 to the same

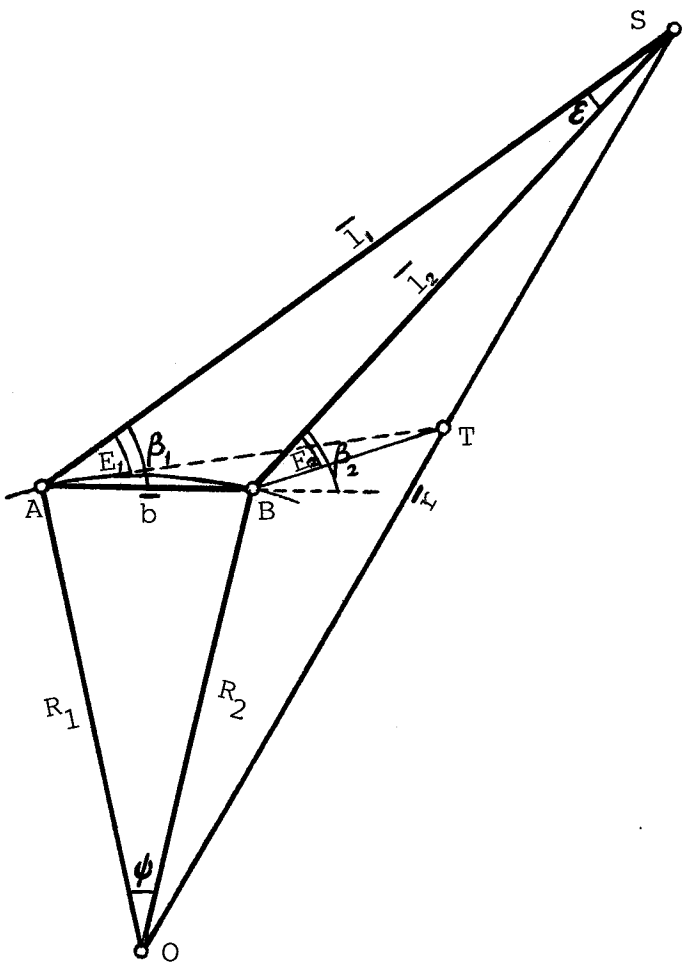

Fig 3 Delta Elevation and Delta Angle Beta.

satellite; $\overline{R}_1$, $\overline{R}_2$ are the radius - vectors of the earth centre to the stations. Because $|\overline{l}_i|$ and $|\overline{R}_i|$ (i=1,2) far larger than the vactor of the baseline, $\overline{b}$. For analysing the error source only, we further assume $R_1 = R_2 = R$, then we can prove

$$\Delta E = E_2 - E_1 \leqslant \psi + \varepsilon \qquad (5)$$

In eq. (5) ψ is the geocentric angle of baseline,

$$\psi \doteq b / R, \quad \text{(in radians)} \qquad (6)$$

and ε is the angle of parallax at the satellite S.

$$\varepsilon \doteq b \sin \beta / l \leqslant b / l \qquad (7)$$

If and only if S is falling onto the plane of $\overline{R}_1 \times \overline{R}_2$, the equality will be true. At that time, the intersection angles β_i for $\overline{AB}$ and $\overline{l}_i$ are equal to $E_i \pm \psi / 2$.

$$\begin{aligned} \Delta E = E_2 - E_1 &= (\beta_2 + \psi / 2) - (\beta_1 - \psi / 2) \\ &= (\beta_2 - \beta_1) + \psi \\ &= \varepsilon + \psi \leqslant b (1 / R + 1 / l) \end{aligned} \qquad (8)$$

We take the maximum value for estimating the error rising from ignoring the difference of elevation angles between stations. Table 2 shows the maximum errors for phase differential observations.

$$\begin{aligned} \Delta\Phi_{12} &= f' (E) \cdot dE / \lambda_{L1} \\ &= dl \cdot \cot E \cdot dE / \lambda_{L1} \end{aligned} \qquad (9)$$

Table 2:

Max. Errors(in circles) with Respect to dE for a Baseline

E°	b=1km	2km	5km	10km	20km	50km	100km
10	0.06	0.12	0.30	0.64	1.21	3.03	6.07
15	0.03	0.07	0.17	0.37	0.70	1.74	3.48
20	0.02	0.04	0.10	0.26	0.39	0.98	1.95
30	0.01	0.02	0.04	0.08	0.17	0.42	0.84
50	0.00	0.01	0.01	0.03	0.05	0.13	0.27
90	0.00	0.00	0.00	0.00	0.00	0.00	0.00

Taking 0.4 circles as upper limit, if the campaign area is with its diameter less than 20 kms, we can ignore the difference of elevation angles from station to station, so that we may use the central point and calculate its correction, then evaluate the modifications (ref. to next sub-session) to all other stations from the differences of weather parameters compared with the central station.

If we calculate the standard divation of $\Delta\Phi$ throughout the srea τ (E from 15° to 90° and b from 0 to 10 kms), we have:

$$\sigma_{\Delta\phi} = \sqrt{\frac{\int_\tau (\Delta\Phi)^2 d\tau}{\int_\tau d\tau}} \approx 0.06 \text{ (circles)} \qquad (10)$$

Obviously that for general purpose, ignoring the effect of elevation difference between two stations is accepted.

3.3 Effects from the Accuracy of the Weather Parameters

We take partial derivatives of eq. (1) with respect to the weather parameters x, (x=t,P,e) at t_o= 0°C, P_o= 1014mb, h_o= 0m, e_o= 25mb, and ignore the small term of C / E^2. Thus

$$\frac{\partial \Delta l}{\partial x} = \frac{\partial \Delta l}{\partial D}\frac{\partial D}{\partial x} = \left(\frac{\partial A}{\partial x} + \frac{\partial B}{\partial x}\right) / \sin E, \quad (x = t, P, e) \qquad (11)$$

From eq. (2), we have

$$\frac{\partial \Delta l}{\partial t} = \left(\frac{a_2 P}{T_k} - 2B\right) / (T_k \sin E)$$

$$\frac{\partial \Delta l}{\partial P} = A / (P \sin E) \qquad (12)$$

$$\frac{\partial \Delta l}{\partial e} = B / (e \sin E)$$

where $a_2 = 1.552 \times 10^{-5} h$.

Set unit increment of dt = 1°C, dP = 1mb, and de = 1mb too, we can evaluate the changes in range corrections (see table3). It seems not too difficult to make an acceptable record of temperature or pressure. If dt and dP are not greater than 1°C and 1mb respectively with elevatoin angle higher than 15 degrees, then, the range difference will be within 1 to 2 cm. Also we should note that it is very sensitive about the change of water vapour pressure in the air. 1mb change in vapour pressure may cause 5 times of change in range correction from temperature and air pressure with unit changes. So that we should pay more attention to the acquisition of the temperature difference $t_d - t_w$ and temperature of wet bulb.

Because an increment of e may be represented as (not rigorously):

Table 3:

Changes in Correction vs Unit Weather Parameters

(h=0m, eo=25.0mb, Po=1014.0mb, to=0°C)

Ele.	dr/dL	Values	dt=1°C	dP=1mb	de=1mb
5	dr (m)	26.411*	-0.0231	0.0262	0.1263
(deg)	dL1(C)	138.70	-0.121	0.137	0.663
	dL2(C)	108.08	-0.095	0.107	0.517
10	dr	14.488	-0.0116	0.0131	0.0634
	dL1	76.08	-0.061	0.069	0.333
	dL2	59.28	-0.047	0.054	0.259
15	dr	9.873	-0.0078	0.0088	0.0425
	dL1	51.85	-0.041	0.046	0.223
	dL2	40.40	-0.032	0.036	0.174
20	dr	7.512	-0.0059	0.0067	0.0322
	dL1	39.45	-0.031	0.035	0.169
	dL2	30.74	-0.024	0.027	0.132
30	dr	5.158	-0.0040	0.0046	0.0220
	dL1	27.09	-0.021	0.024	0.116
	dL2	21.11	-0.016	0.019	0.090
40	dr	4.018	-0.0031	0.0035	0.0171
	dL1	21.10	-0.016	0.019	0.090
	dL2	16.44	-0.013	0.015	0.070
50	dr	3.373	-0.0026	0.0030	0.0144
	dL1	17.72	-0.014	0.016	0.075
	dL2	13.80	-0.011	0.012	0.059
70	dr	2.752	-0.0021	0.0024	0.0117
	dL1	14.45	-0.011	0.013	0.062
	dL2	11.26	-0.009	0.010	0.048
90	dr	2.586	-0.0020	0.0023	0.0110
	dL1	12.14	-0.011	0.012	0.058
	dL2	10.58	-0.008	0.009	0.045

* The normal values are taken from Hopfield model.

Table 4:

Changes of Vapour Pressure (in mb) for dtw=1°C at P=1014mb

tw(°C)	-15	- 5	5	15	25	35	45
de(mb)	1.19	1.14	1.17	1.40	1.95	2.93	4.45
σe(mb)	1.37	1.33	1.35	1.56	2.06	3.01	4.51
σe(mb)	2.47	2.37	2.44	2.88	3.96	5.89	8.93

$$de = \frac{\partial e_w}{\partial t_w} dt_w - 6.75\times10^{-4}\,[\,P\,(dt_d - dt_w) - \Delta t \cdot dP\,]$$

$$=(.4503+(.002778+(7.05\times10^{-4}+1.939\times10^{-5}t_w)t_w)t_w)dt_w$$

$$-6.75\times10^{-4}P\cdot(dt_d - dt_w) \qquad (13)$$

Last term related to dP is small term and omitted. We find that the partial de from t_d is close to 0.68 mb (at P=1014mb, dt_d=1°C). The most important part comes from dt_w. Results from eq.(13) are listed in table 4, where values, de, are the increments of e from dt_w only, the standard deviations of σ'_e are those for dt_w= 2°C and dt_d=1°C.

Now we can understand why we are not effectively making the correction for wet component. One of the reasons is that we have a very poor method to get the information of vapour pressure in the air. It asks to record t_w and t_d in an accuracy of 0.01 to 0.1°C to match the same accuracy for dry component with 1mb for P and 1°C for the air temperature.

In fact it is imposible to acquisite temperature of wet bulb with precission higher than dry bulb in the field at present unless and until we have another method to determine the water vapour pressure directly with the accuracy one order higher than P and t_d determined.

3.4 Effects on the Phase Differential Observations

Single phase differential observations are taken from the differences of observed phase between two stations at the same epochs. Fig.4 shows the range difference with the relationship:

$$dl = l_2 - l_1 = (\phi_2 - \phi_1)\cdot\lambda = d\phi\cdot\lambda \qquad (14)$$

We can image that the true range is composed of an ideal observation l_{io} perfectly corrected for all other error sources except the atmospheric refraction, and a absolutely correct troposheric delay Δl_i.

$$l_i = l_{io} + \Delta l_i \qquad (15)$$

Assuming tropospheric refractional effect may be further dissociated into four parts: the model correction Δl_{io}, systematic bias from the model, Δl_{is}, the representation error of the model, Δl_{ri}, and the observational errors of weather parameters, Δl_{ie}. So

$$l_i = \Delta l_{io} + \Delta l_{is} + \Delta l_{ir} + \Delta l_{ie} \qquad (16)$$

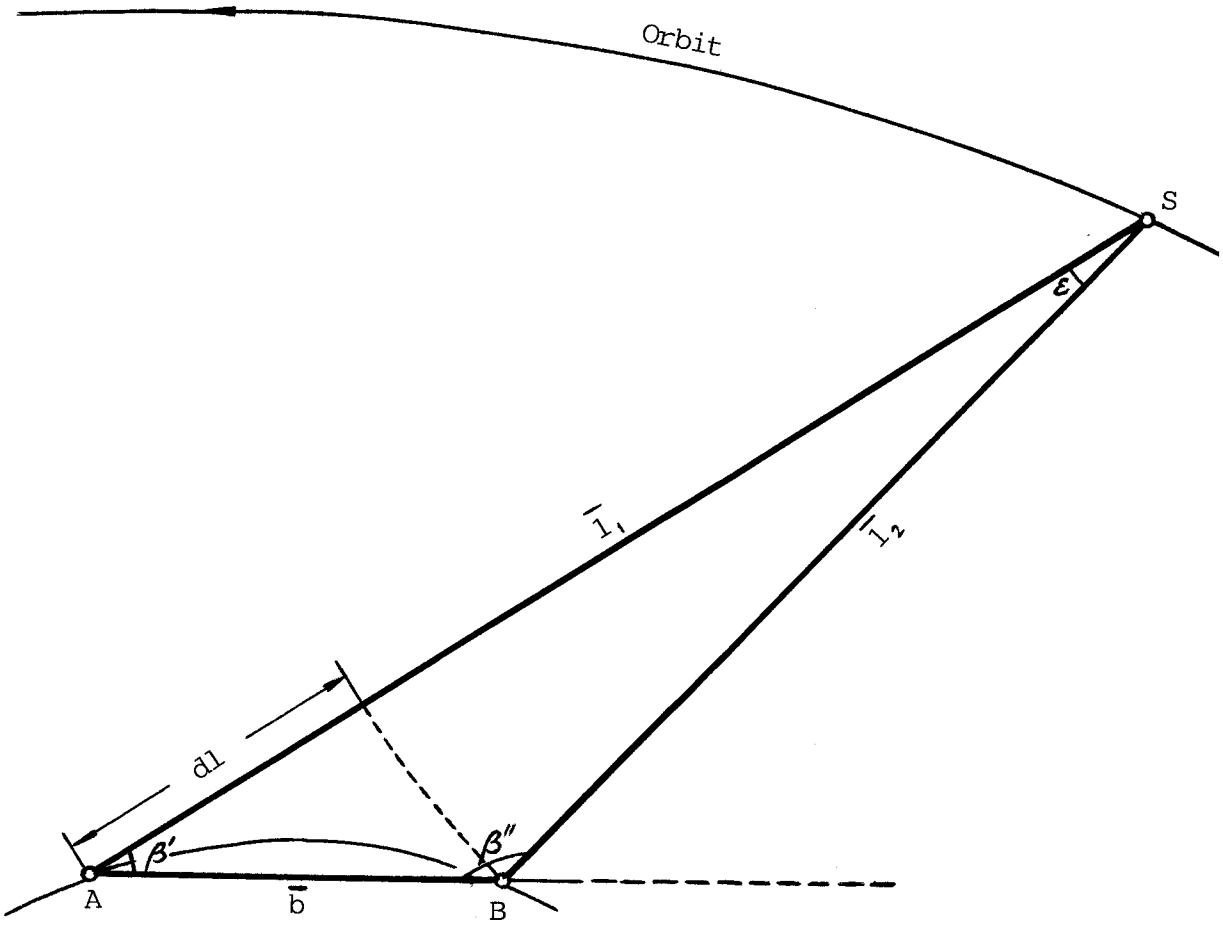

Fig 4 Phase Differential Observations as a Function of Delta Beta.

From precise GPS data processing point of view, we have to distinguish their contributions to the relative positioning results:

(1) Model correction may be calculated as precise as required mathematically speaking. It is not necessary to account its influence to the total error except which will be considered by items (2) and (3).

(2) Model error yielded from the unperfectness of the model being used. Its quantity is the function of input parameters (t_d, t_w, and P) and some unestimated parameters (e.g. windage, cloudage etc). Within an adjacent area and small enough with a specific set of parameters, it would be a constant or appears to be linear variated gently. The main part of this variation may be evaluated with the increments of dry and wet temperature, and air pressure with respect to the given parameters. Thus, the remainder unevaluable parts would be very small and may put them into the representation error together.

When a pair of stations is satisfied with above conditions, these errors for the two stations are related at a high level, and may be cancelled out during taking the phase

difference between stations. It is irrelative to the length of the baseline! Whether it is in an alluvial plain or in a plateau area, if they are with similar weather conditions for the pair of stations, and without significant variations along the baseline and its adjacency, the cancellation will still be very strongly effective even for a quite long distance; Inversely, model error can not cancel out althrough the baseline may be only few kilometres long in horizontal projection, especially in the mountain area like Tibet, Qinghai, Yunnan, Guizhou and some other places in China. If we want to determine the relative position for two separated stations situated on the top of a mountain and the bottom of the valley respectively, the local climate differences may reach 5-15°C in temperature, 200-500 mb in air pressure, and significant changes in water vapour pressure content, because there is a large difference in heights (1500-3000 metres). From table 1 and 3, this error will be 2-30 cm. and depend upon the elavation angle to the SV. Sometime it causes bad results.

(3) Representation error is a kind of model error too. It is assumed that two stations have the same weather records without any errors, therefore the model corrections to the pair of observations must be the same. If they are not close to each other, the actual path delays will not be the same.

It is dependent on the differences of some unevaluated parameters at the observation time and the non-homogeneous gradient variations of tempressure, air pressure and water vapour pressure.

When the length of a baseline is far less than 10 km and no significant microclimate over the the surveying area, the representation error should be largely related; For a long baseline determination, the representation error will be independent from station to station. According to some invesitigations using local weather records, this error is about 1 - 2 cm in the direction of azimuth (Kaniuth, 1986).

(4) The last term of error is a random noise, and dependent on the accuracy of weather records, this error is not related from station to station. Testing shows that the standard deviations are 0.3°C for temperature, 0.5°C for wet bulb and 0.2 mb for air pressure under careful performance of a calibrated weather station. The total values of this random noise for phase differencial observations (at p_o=1014mb, e_o=25mb)

$$\sigma_{\Delta l_E} = \sqrt{2\left[\sigma^2_{\Delta l_{td}} + \sigma^2_{\Delta l_p} + \sigma^2_{\Delta l_s}(P, t_d, t_w)\right]} \qquad (17)$$

are listed in table 5. As it has been mentioned that the main effects come from t_w.

Table 5:

Random Noise from Weather Records (in metres)

(P_o=1014mb, e_o=25mb)

tw(°C)	-15	- 5	5	15	25	35	45
E=10°	0.072	0.070	0.071	0.081	0.106	0.150	0.218
15	0.048	0.047	0.048	0.055	0.071	0.100	0.146
20	0.036	0.035	0.036	0.041	0.054	0.076	0.111
30	0.030	0.029	0.029	0.033	0.044	0.062	0.090
40	0.025	0.024	0.025	0.028	0.037	0.052	0.076
50	0.022	0.021	0.022	0.025	0.032	0.045	0.066
70	0.019	0.019	0.019	0.022	0.029	0.040	0.059
90	0.018	0.017	0.017	0.020	0.026	0.037	0.054

3.5 Relative Errors

From last section we have an idea about the quantity of atmospheric refraction errors introduced into the phase differential observations, but we are much more interested to know the relative error, R, for a baseline, i.e., we have to estimate the value of Δl / dl. Refer to fig. 3 and 4, we get

$$\begin{aligned} R &= \Delta b / b = \Delta l / dl \\ &= \Delta l / b \cos\beta \\ &= \Delta l_{90} / b \sin E \cos\beta \leqslant 2\Delta l_{90} / b \sin(2\beta) \end{aligned} \qquad (18)$$

where the differences of β_1, E_1 and β_2, E_2 are ignored.

Eq.(18) tells us that the relative error is not only dependent upon the atmospheric refraction error itself, but also on the value of angle β. It means that the observations to an SV will contribute nothing to the results if the SV moves towards or backwards the baseline perpendicularly and the angle β is close to 90° during the observation time.

(1) For a baseline, b=100km, in a hilly territory with 250 metres height difference (cause about 29.7mb change in P), assume dt=2°C, de=5mb at t_o=0°C, e_o=25mb, p_o=1014mb, and h_o=0m, if we process data without any meteorological corrections, the omitted effects in phase differential observations will cause about 4ppm in relative error (see Table 6 and Fig. 5).

(2) If we introduce some correction under normal weather conditions (say t_d=20°C, t_w=15°C, P_o=1014mb at h_o=0m, and modified by station heights). The error may reduce down by 80-90% in each nondifferental phase observation. The improvement to the single phase differential observations between stations will be only 20-50% compared with that without correction.

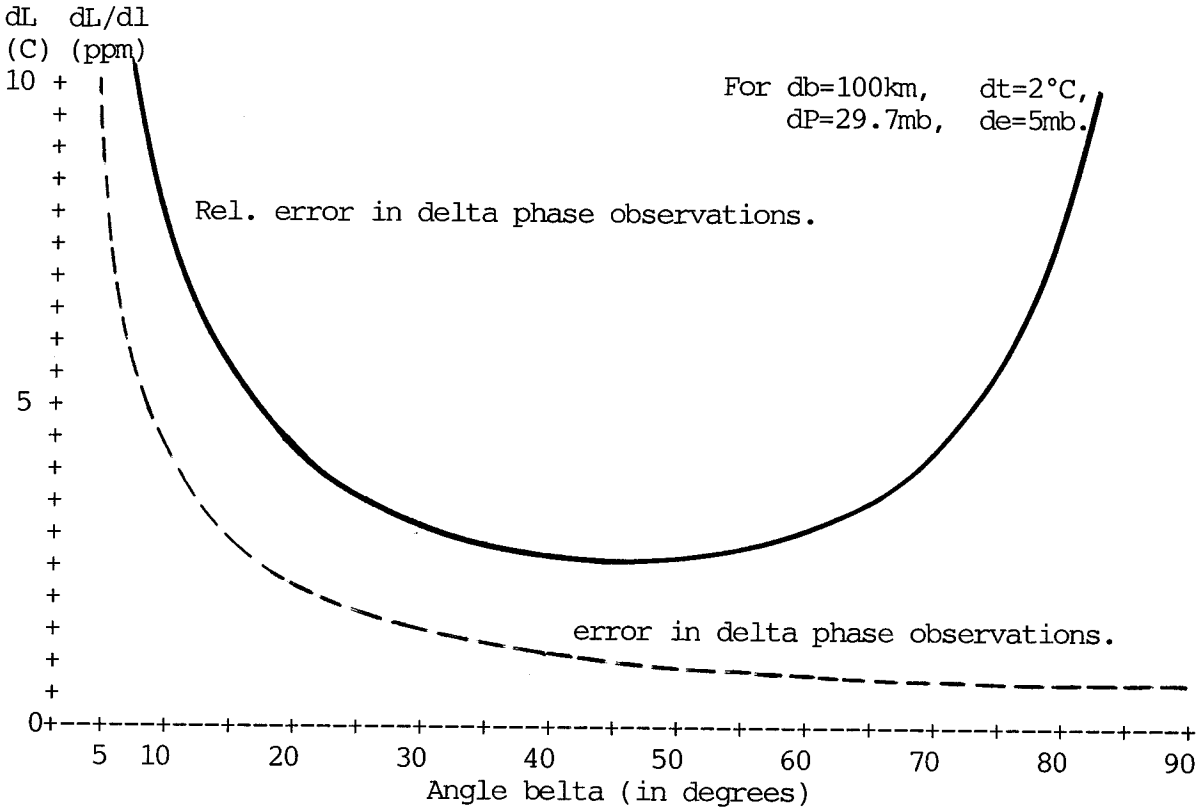

Fig 5 Typical Effects on Phase Differences between a Pair of Stations (without Atmospheric Corrections)

Table 6:

Effect on a Set of Differential Obs. w/o Atmospheric Correction

(b=100km, dt=2°C, de=5mb, dP=29.7mb)

Delta Beta(deg)	5	10	15	20	30	40	50	60	70	80	90
Delta Phase (C)	7.8	4.1	2.8	2.1	1.5	1.1	0.96	0.86	0.78	0.75	0.73
Rel. Error(ppm)	14.9	7.9	5.5	4.3	3.3	2.7	2.8	3.3	4.3	8.2	----

(3) When some real weather records are employed to the data processing, 90-95% effects from refraction can be cancelled out due to the distribution characteristics of atmosphere refractivity being modelled and the relativity between stations, the remainder Δl will be of 2-5cm at the direction of the zenith for above typical baseline. In this situation, the average relative accuracy will be around 0.5 ppm. The longer the baseline, the smaller the relative error from refraction in results.

(4) At present, the total expectable model error will not be better than 1-2 cm. It leads to about 0.2 ppm relative accuracy for a baseline normally.

(5) If all other errors (ephemerides, clock, multipath, circle slips, ambiguity and so forth) are removed perfectly and their residuals are limited within 0.01ppm. We can expect a baseline with its final accuracy higher than 0.02 ppm, if it is satisfied with:

* The baseline should be longer than 1000km, repeat measurements not less than 4 sessions and each session at least has 7 different SVs to be observed normally.

* meteorological data are carefully and automatically recorded regularly in every few minutes. The instrument of the weather station should be calibrated to ensure its accuracy not worse than 0.2°C for temperature, 0.2mb for air pressure and 0.05-0.1mb for water vapour pressure in the air.

* Best observation time interval is at night, which would not only reduce the ionospheric error, but also decrease the tropospheric effect from the uncertainty of the humidity determination. Anyway, it should be avoided to carry a high precision GPS surveying campaign in summer at tropics or the places with a tropical climate.

* It should be noted that the best geometry for point positioning may not be that for relative positioning from the view point of main error sources.

4. DISCUSSION AND RECOMMENDSATION

Some discussion and commendation have been already made in previous sections. What should be further mentioned is that if we want to get high precision results from GPS which will be comparable with VLBI and SLR in the near future, we have to improve the mathematical model first in order to reduce the model error and representation error. It should be helpful to evaluate the differential refraction effects between two stations. And we should develop some compact instrument to be able to measure the gradient of temprature, and vapour pressure in the air precisely and directly.

Inversely, if relative observations free of other error sources and the weather records are precise enough, we can make closely investigation in the local model for the correction of tropospheric delay with the help of GPS measurements. Up to now, all models for the purpose are derived from some specific area using limited data available, unfortunately, no models for mountain area and for tropics.

On the other hand, for a short baseline ($b < 10$km) under normal condition, it is posible to carry GPS relative positioning without real meteorological records and obtain a final results in few centimetres. But the author still recommend to estimate the correctons before data editing.

5. REFERENCES

Black, H. D. (1978) An Easily Implimented Algorithm for the Tropospheric Range Correction, J.G.R., V83 No.84 pp1825-1828.

Brown, A. K., Sturza, M. A. (1985) Static Point Positioning with an L1, C/A Code GPS Receiver, Proceedings of the 1st int. symps. on precise positioning with GPS, Rockville, Maryland, US, pp161-175.

Hopfield, H. S. (1969) Two Quartic Tropospheric Refractivity Profiles for Correcting Satellite Data, J.G.R., V74 No.1 pp4487-4499.

Kaniuth, K. (1986) A Local Model for Estimating the Tropospheric Path Delay at Microwave Frequencies, Proceedings of the 4th int. geodetic symps. on sat. positioning, Austin, Texas, US, pp589-601.

Kroger, P. M. et al (1985) Sensitivity of GPS Caribbean Baseline Performance to the Location of a Southerly Fiducial Station, Proceedings of the 1st int. symps. on precise positioning with GPS, Rockwille, Maryland, US, pp447-456.

Shi, P. (1981) A Practical Formula for Calculating Saturated Vapour Pressure of Water, presented at UNSW, Australia.

Wells, D. E., Vaníček, P. and et al (1986) Guide to GPS Positioning, printed in Fredericton, UNB, Canada.

MICROWAVE RADIOMETRY IN MEASUREMENT OF RADIO PATHLENGTH THROUGH THE TROPOSPHERE

D.C. Hogg and J.B. Snider

Abstract

The design of millimeter-wave radiometers for accurate measurement of integrated water vapor on earth-space paths to provide radiowave excess pathlength for satellite based surveying systems is given. Effects of fluctuations in the integrated vapor and comparison of excess delay computed from radiosonde measurements of vapor are discussed. The utility of radiometric measurements in improving attainable accuracy of baseline estimation using the GPS system is illustrated by an example.

In Brunner, F.K. (Ed.), 1988, "Atmospheric Effects on Geodetic Space Measurements", *Monograph 12, School of Surveying, University of New South Wales, pp. 63-70.*

1. INTRODUCTION

Fluctuations in satellite-earth pathlength and therefore in the phase of radio waves limit significantly the accuracy obtainable by coherent surveying systems such as the Global Positioning System (GPS) (see for example, Bossler et al., 1980). In the troposphere, the most serious spatial and temporal variations in radio refractive index are caused by water vapor. The excess pathlengths (ℓ_V) experienced by the radiowave are related to the integrated water vapor (V) on the path (expressed as an equivalent layer thickness of liquid water) by Hogg et al., 1981a)

$$\ell_V = 6.5V \ , \qquad (1)$$

both being in centimeters.

Most continuous measurements of V are made by dual-channel microwave radiometers. These passive instruments are sensitive to emission from the water (both vapor and liquid) in the troposphere. The operating wavelengths for the channels are typically about 1 and 1.4 cm. This choice is made because the latter is near a maximum in sensitivity to vapor emission whereas the former is sensitive primarily to liquid. In this way, the radiometric instrument can, through appropriate processing of the radiometric emissions, measure the amounts of vapor and liuqid during both clear and cloudy conditions on the earth-space paths. Vapor is also measured accurately in the presence of clouds formed of ice particles since ice produces negligible emission at these wavelengths. These instruments are used extensively, and typical descriptions are given by Guiraud et al. (1979), Zhao et al. (1985) and Resch (1982).

2. ZENITH PATHS

2.1 Calibration

The only routine method of measuring integrated water vapor that can be used for independent comparison with the product of the radiometric instruments is the balloon-borne radiosonde. This device provides, point-by-point, vertical profiles of temperature and relative humidity. The profile of vapor computed from those data is then integrated, resulting in a radiosonde vertical-path vapor, V_r, that can in turn be used in Eq. (1) to compute excess path length.

A 2-week comparison from a 6 month sample of such data is shown in Fig. 1 (Guiraud et al. 1979). The triangular dots plotted every 12 hours are ℓ computed from the radiosonde V_r whereas the quasi-continuous plot is ℓ computed from data measured by a dual-channel radiometer. Rapid changes in ℓ such as the one between August 14 and 15 clearly mandate almost continuous observations. Statistical treatment of all data of the 6-month sample results in a root-mean-square instrumental error of

about 5 mm in ℓ. More modern radiometers have resulted in a slightly improved value. The short-term (hours) performance of these instruments has been observed to be a factor of 10 better than the long-term behavior, i.e., instrumental precision of about 0.5 mm.

2.2 Effect of Liquid

As mentioned above, dual-channel instruments measure simultaneously and separately both integrated vapor and liquid. Figure 2 shows an example of the variations in ℓ prior to and during a heavy rain event (day 140). During the week in Oklahoma beginning day 133, dry and stable conditions prevailed until liquid-bearing clouds appeared on day 138. The excess zenith pathlength built up to more than 25 cm on day 140 where a gap appears in the record; this is caused by (electronic) saturation of the radiometers, which results in unreliable values of vapor. The general result of experience with such situations is that the instruments measure vapor and therefore ℓ to good accuracy during cloudy conditions, provided the clouds are non-rain-producing, although reasonable data are also obtained during some light rains. Note that the excess radio pathlength (phase shift) produced by the liquid per se under these limited rain conditions is negligible.

When pathlengths are to be meaured in the presence of liquid-bearing clouds, it is important that the antenna beams of the two radiometric channels be of equal width and coaxial (Guiraud et al., 1979). If they are not, the cloud will affect one channel differently from the other, and correct values of integrated vapor will not be obtained.

2.3 Short-Term Fluctuations in ℓ

The spatial distribution of vapor in the troposphere is often governed by turbulence that produces a spectrum of scale sizes. Although the spatial distribution of these variaions in water vapor is not necessarily isotropic, the scale sizes cover about three orders of magnitude (see, for example, Gossard et al., 1984). As these inhomogeneities are moved through the earth-space path by the wind, temporal fluctuations in emission are observed by the radiometer.

An example of a spectrum of the resultant short-term temporal variations in excess zenith pathlength is given in Fig. 3 (Hogg et al., 1981b). For the 1-day cycle, the variation in pathlength is about 0.5 cm. The slope of the spectrum approximates the law $S(F) = KF^{-5/3}$ indicated by the dashed line; this is the classical one-dimensional behavior calculated for isotropic turbulence.

3. STEERABLE WATER-VAPOR RADIOMETERS

3.1 Instrumentation

In applications such as GPS, the antenna beams of the radiometric instruments must be pointable at satellites over most of a hemisphere. Various designs have been implemented, one of the major considerations being portability.

A trailer-mounted NOAA design in which the dual-channel electronics and antenna per se remain stationary is discussed by Hogg et al., 1983; pointing of the equal and coaxial antenna beams (2.5 degrees in width) is accomplished by flat reflectors. Access by road to the measuring site is necessary with this type of instrument. Models have been implemented by the Jet Propulsion Laboratory, and a prototype designed specificaly for GPS pathlength measurements has been built by Janssen (1985). In this case, the electronics package and antenna all rotate in azimuth and the antenna beams are directed in elevation angle by a rotating reflector; the beamwidths are about 9 and 6 degrees. Elgered et al. (1982) from Chalmers University discussed a fairly portable implementation that incorporates two antennas, resulting in 6-degree-wide beams at both frequencies. This design uses an elevation over azimuth mount for beam pointing.

3.2 Test Measurements

One way of checking the relative accuracy of such radiometers is to scan a sector of the sky with two colocated instruments and compare the measured excess pathlengths. A measurement of that type, taken during cloudy conditions but with negligible liquid present, is given by Heggli et al., 1987. Figure 4 shows these data, taken as an azimuth scan with a fixed elevation angle of 15 degrees. The solid line is measured by a NOAA instrument and the dots by an essentially identical instrument of the U.S. Bureau of Reclamation. Analysis of this sample shows that the root-mean-square difference between the two sets of pathlength measurements is 0.45 cm, which is about 2.5 percent of the mean of 17.55 cm.

3.3 Some Measured GPS Data

The two instruments just discussed were used by Ware et al. (1985) near Boulder, Colorado, to evaluate the improvement obtainable in a GPS-measured baseline of about 22 km by incorporating the radiometrically determined pathlength corrections (due to water vapor). Weather conditions were disturbed during the measurement. Using optimum processing, it was found that the corrected values improved the baseline repeatability by a factor of 5 (±45 mm to ±9 mm) and that a 10-cm foreshortening of the baseline existed. In this case, the achievable accuracy after including pathlength corrections was better than one part per million.

4. REFERENCES

Bossler, J.D., C.C. Goad and P.L. Bender, 1980, Using the global positioning system (GPS) for geodetic surveying, Bull. Geod., 54, 553-563.

Elgered, G., B.O. Rönnäng and J.I.H. Askne, 1982, Measurements of atmospehric water vapor with microwave radiometry, Radio Science, 17, 1258-1264.

Gossard, E.E., R.B. Chadwick, T.R. Detman and J. Gaynor, 1984, Capability of surface-based clear-air Doppler radar for monitoring meteorological structure of elevated layers, J. Climate Appl. Meteorol., 23, 474-485.

Guiraud, F.O., J. Howard and D.C. Hogg, 1979, A dual-channel microwave radiometer for measurement of precipitable water vapor and liuqid, IEEE Trans. Geosci. Electron., Ge 17, 129-136.

Heggli, M., R.M. Rauber and J.B. Snider, 1987, Field evaluation of a dual-channel microwave radiometer designed for measurement of integrated water vapor and cloud liquid in the atmosphere, J. Atmos. Ocean Tech., 4, 204-213.

Hogg, D.C., F.O. Guiraud and W.B. Sweezy, 1981a, Measurement of excess radio transmission length on earth-space paths, Astron. Astrophys., 95, 304-307.

Hogg, D.C., F.O. Guiraud and W.B. Sweezy, 1981b, The short-term temporal spectrum of precipitable water vapor, Science, 213, 1112-1113.

Hogg, D.C., F.O. Guiraud, J.B. Snider, M.T. Decker and E.R. Westwater, 1983, A steerable dual-channel microwave radiometer for measurement of water vapor in the troposphere, J. Appl. Meteorol., 22, 789-806.

Janssen, M.A., 1985, A new instrument for the determination of radio path delay due to atmospheric water vapor, IEEE Trans. Geosci. Remote Sensing, GE-23, 485-490.

Resch, G.M., 1982, Description and overview of an instrument designed to measure line-of-sight delay due to water vapor, Jet Propulsion Laboratory TDA Report, 42-72.

Ware, R.H., C. Rocken and J.B. Snider, 1985, Experimental verification of improved GPS-measured baseline repeatability using water-vapor radiometer corrections, IEEE Trans. Geosci. and Remote Sensing, 23, 467-473.

Zhao, B., H. Li and Q. Han, 1985, Atmospheric microwave radiation and remote sensing of atmospheric water vapor content, Kexue Tongbao, 30, 85-89.

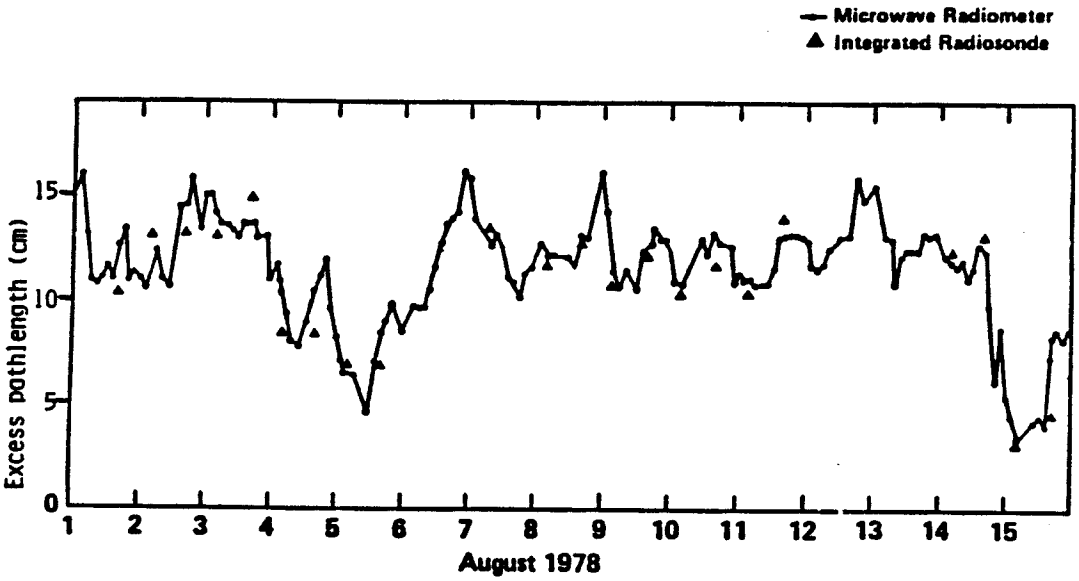

Fig. 1 Original measurements of excess zenith pathlength due to water vapor using dual-channel radiometry at Denver, CO

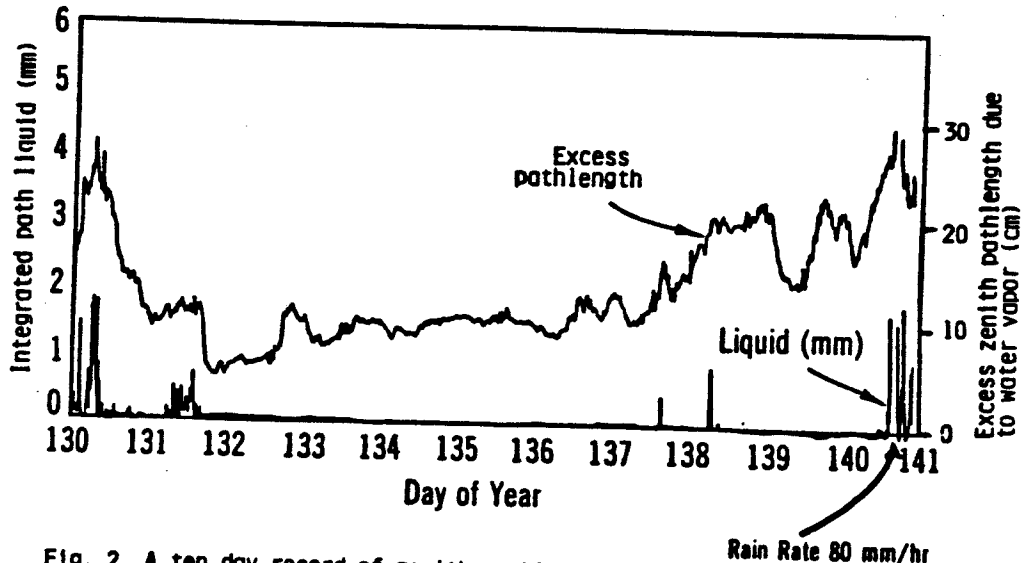

Fig. 2 A ten day record of zenith pathlength fluctuations taken during clear and cloudy conditions using dual-channel radiometry at Fort Sill, OK

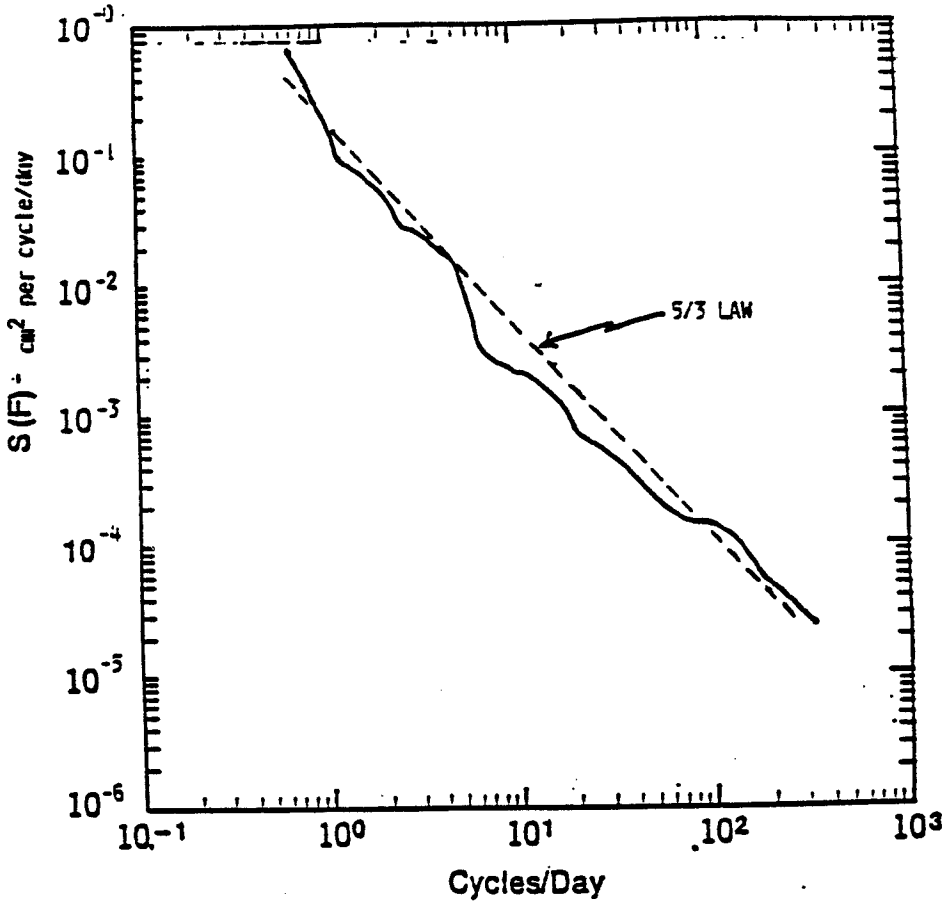

Fig. 3 Spectrum of excess zenith radio pathlength due to water vapor (Denver, CO)

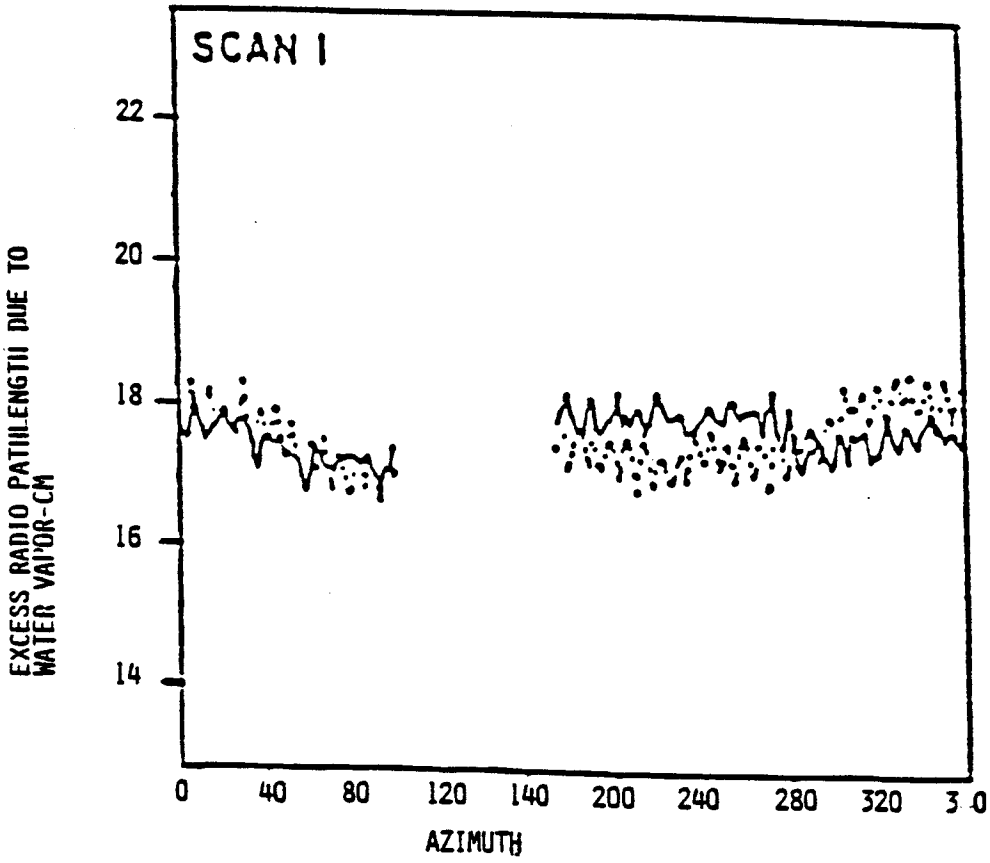

FIG. 4 DATA FROM TWO COLOCATED DUAL-CHANNEL RADIOMETERS SCANNING IN AZIMUTH AT AN ELEVATION ANGLE OF 15°; STEAMBOAT SPRINGS, CO

LOCAL MODELING OF THE TROPOSPHERIC WET PATH DELAY

K. Kaniuth

Abstract

This paper is a continuation of a study recently performed by the author. It aims at contributing to an improvement of the predictability of the tropospheric wet path delay by local modeling. The analysis is based on a total of 270 radiosonde launches acquired over a five year period. The results indicate that the height of the troposphere effective for the wet path delay may be described by a simple periodic function. The rms agreement between the derived local model, predicting the zenith wet path delay from surface meteorological data only, and the radiosonde data set is 1.66 cm.

In Brunner, F.K. (Ed.), 1988, "Atmospheric Effects on Geodetic Space Measurements", *Monograph 12, School of Surveying, University of New South Wales, pp. 71-79.*

1. INTRODUCTION

Range and range rate measurements at microwave frequencies will in the near future be the dominant technique for precise trakking of satellites as well as geodetic positioning applying satellite orbits. However, one of the errors considerably affecting microwave ranging is the path delay due to the refractivity of the propagation medium. This delay consists of an ionospheric part caused by the free electron content and a neutral part. Since the refraction in the ionosphere is frequency dependent this effect can to a large extent be removed by tracking at two preferably high and sufficiently different frequencies.

This is not true for the un-ionized air in stratosphere and troposphere being dispersive in the optical but not in the radio wavelength range up to frequencies of about 30 GHz. The path delay arising in this lower part of the atmosphere is commonly termed tropospheric refraction because most of the effect is caused in the troposphere, below the tropopause.

The tropospheric path delay is usually split into a "dry" term caused by the dry air and a "wet" term caused by the water vapor content. The dry component amounts to a zenith path delay of 2.3 m and can be estimated from surface meteorological data with 1 cm accuracy or even better. On the other hand, the wet component varies between very few and more than 30 cm in zenith direction and is much more difficult to predict because the water vapor is often not well mixed with the dry air. The wet path delay can be derived from water vapor radiometer measurements simultaneously performed with the microwave ranging; but due to several reasons the application of this technique will remain restricted to permanent tracking stations and particular research projects, and therefore modeling the wet component is equally important.

Since models derived for global application may regionally or locally yield systematic errors the author has recently tried to derive a local model for both the dry and wet path delay for a particular site from radiosonde data acquired at an adjacent meteorological observatory (Kaniuth 1986). The zenith path delay predicted by the model agreed with that derived from the radiosonde data with 1.62 cm rms for the wet term and 0.21 cm rms in case of the dry term indicating again the good predictability of the dry component.

Therefore this paper is restricted to the modeling of the wet path delay and is based on an extended data set of 270 radiosonde launches acquired during the period 1982 - 1986 (Deutscher Wetterdienst 1982 - 1986). The basic idea and the estimation procedure applied in this analysis can be summarized as follows:

- Estimation of the actual troposphere height effective for the wet path delay for each radiosonde data set and subsequently derivation of a model enabling to predict the effective troposphere height;

- Integration of the refractivity profiles up to the troposphere height predicted by the model and then adjustment of a local model for estimating the wet path delay as function of surface meteorological data only.

2. EFFECTIVE HEIGHT OF THE TROPOSPHERE

The radiosonde launches provide profiles of temperature, pressure, dew point temperature and relative humidity up to heights approaching the tropopause. These data allow to derive profiles of the "wet" refractivity N_W according to Smith and Weintraub (1953)

$$N_W = 3{,}73 \cdot 10^5 \cdot \frac{e}{T^2} \qquad (1)$$

and integration of the N_W-profile yields the zenith wet path delay

$$dL_W\ [cm] = \int_{H_S}^{H_W} N_W\, dH = 3.73 \int_{H_S}^{H_W} \frac{e}{T^2}\, dH \qquad (2)$$

where T = absolute temperature [°C]
e = partial pressure of water vapor [hPa]
H_S = station height [km] } above the geoid
H_W = effective troposphere height [km] } above the geoid

The integration requires an estimate of the actual height of the troposphere effective for the wet path delay being defined by $N_W = 0$. By the way, the knowledge of H_W is also a prerequisite for applying any of the established general models (Goad and Goodman 1974, Hopfield 1969). For deriving the actual H_W the refractivity profile of each of the 270 radiosonde launches has been smoothed by applying the following procedures:

- Fitting a polynomial subject to the constraint of negative slope at all data points,

- fitting a cubic spline in the least squares sense providing the possibility of individual fixing of interior knots.

The actual troposphere heights resulting from both algorithms did not differ significantly; those of the cubic splines fitting have been applied to the adjustment of a local model for predicting H_W. The reason for this is indicated in figure 1 presenting two examples of N_W-profiles which can be considered representative for all 270 data sets: there is a remarkable change of the refractivity gradient appearing in winter typically already in 2 - 3 km height and then being much more striking than in summer time when this discontinuity occurs in roughly 5 km height. This feature could best be met by placing interior knots in this area.

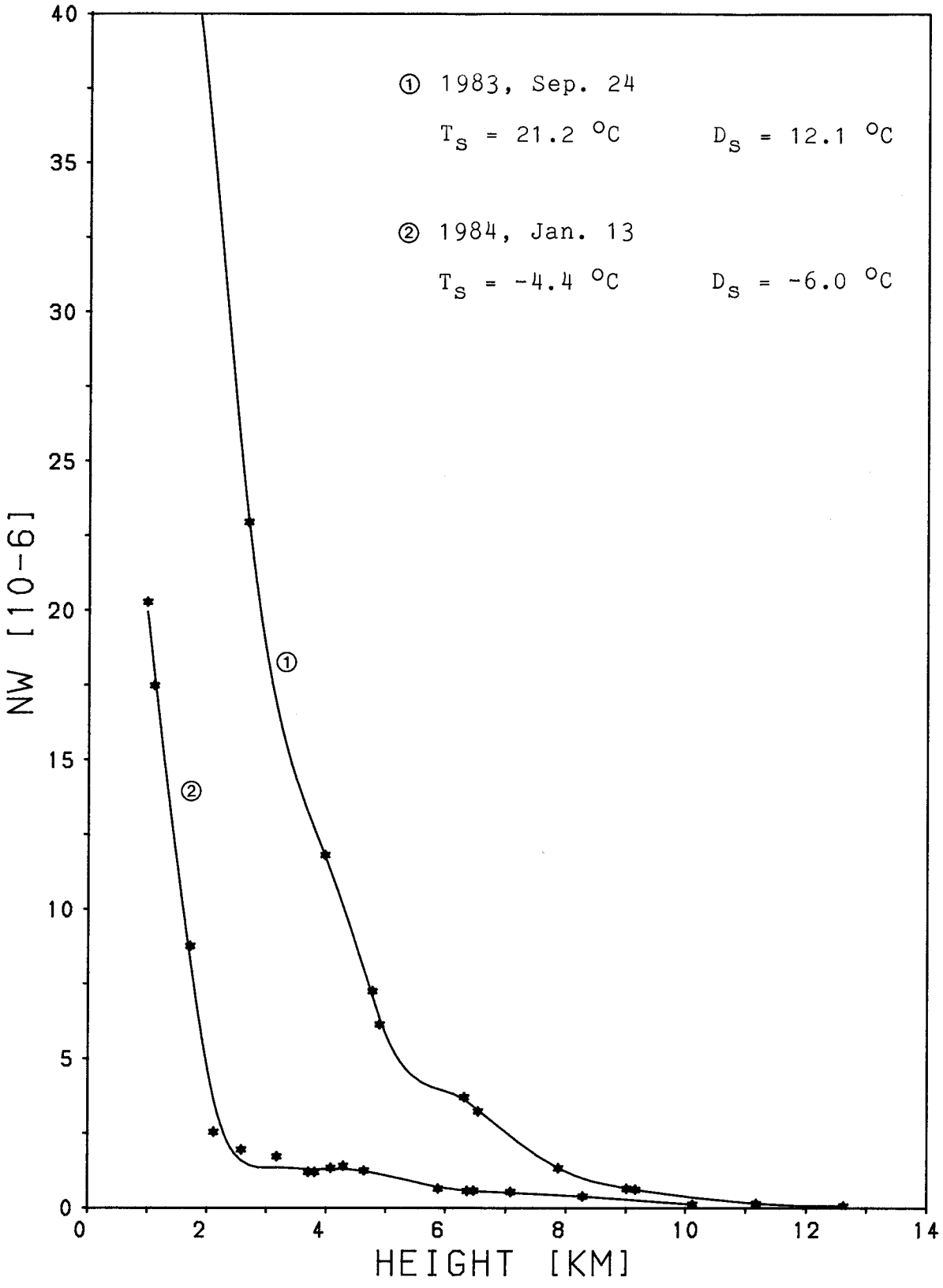

Figure 1 N_W-profiles derived from radiosonde data
T_S = surface temperature
D_S = surface dew point temperature

The former analysis (Kaniuth 1986) yielded a simple linear relation between the effective height of the troposphere H_W and the surface temperature. Also in this paper a model has been set up describing H_W as a function of surface meteorological data only, and the parameters following from the least squares adjustment agreed quite well with the previous result. In addition, H_W was modeled by a periodic function

$$H_W = C_0 + C_1 \sin 2\pi\Theta + C_2 \cos 2\pi\Theta + C_3 \sin 4\pi\Theta + C_4 \cos 4\pi\Theta \qquad (3)$$

allowing a one-year and a half-year period, Θ being measured in fraction of year. The adjustment yielded the following significant result

$$\begin{aligned} H_W\ [km] = \ & 12.151 \pm 0.042 \\ & -(0.585 \pm 0.061) \sin 2\pi\Theta \\ & -(0.593 \pm 0.058) \cos 2\pi\Theta \end{aligned} \qquad (4)$$

and indicated that

- there is no half-year but only a one-year periodic variation amounting to about 1.7 km, and that
- the extended set of radiosonde data acquired over a 5-year period can be fitted better by a model of type (3) than by a function of surface meteorological data.

A graphical representation of the model (4) enabling to predict the local height of the troposhere as function of epoch only is given in figure 2.

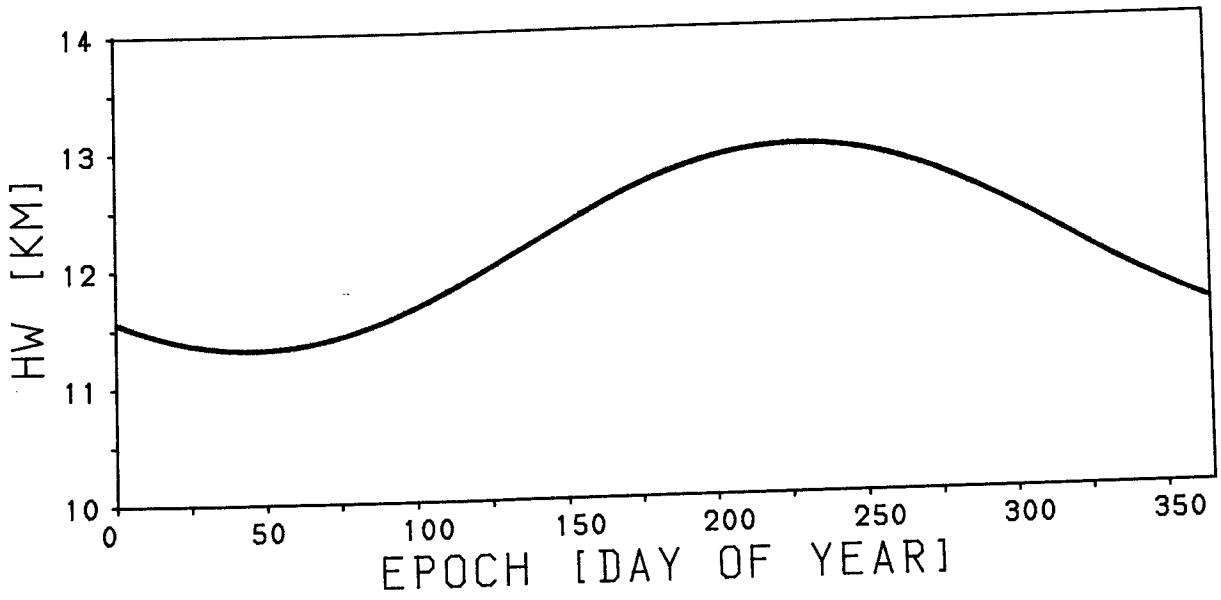

Figure 2 Local troposphere height H_W effective for the wet path delay

3. WET PATH DELAY MODEL

The estimation of the wet path delay according to (2) requires the integration of the N_W-profile up to the height predicted by the model (4). Instead of integrating the piecewise given profile the integral of the fitted cubic spline was computed from its B-spline representation (de Boor 1978). Then the model for predicting the wet path delay dL_W was derived by a least squares adjustment from the 270 individual path delay values resulting from the integration.

Fitting, corresponding to (3), a simple periodic function requiring no estimates of the actual meteorological parameters yielded the following result:

$$\begin{aligned} dL_W\ [cm] = \; & 8.20 + 0.15 \\ & -(1.87 \pm 0.22) \sin 2\Pi\Theta \\ & -(4.00 \pm 0.20) \cos 2\Pi\Theta \\ & +(0.65 \pm 0.21) \sin 4\Pi\Theta \\ & +(0.30 \pm 0.21) \cos 4\Pi\Theta \end{aligned} \qquad (5)$$

Figure 3 presents a graphical representation of equation (5). However, the rms agreement between the adjusted model and the radiosonde results was not better than 2.41 cm, indicating that this model obviously does not well match the input data.

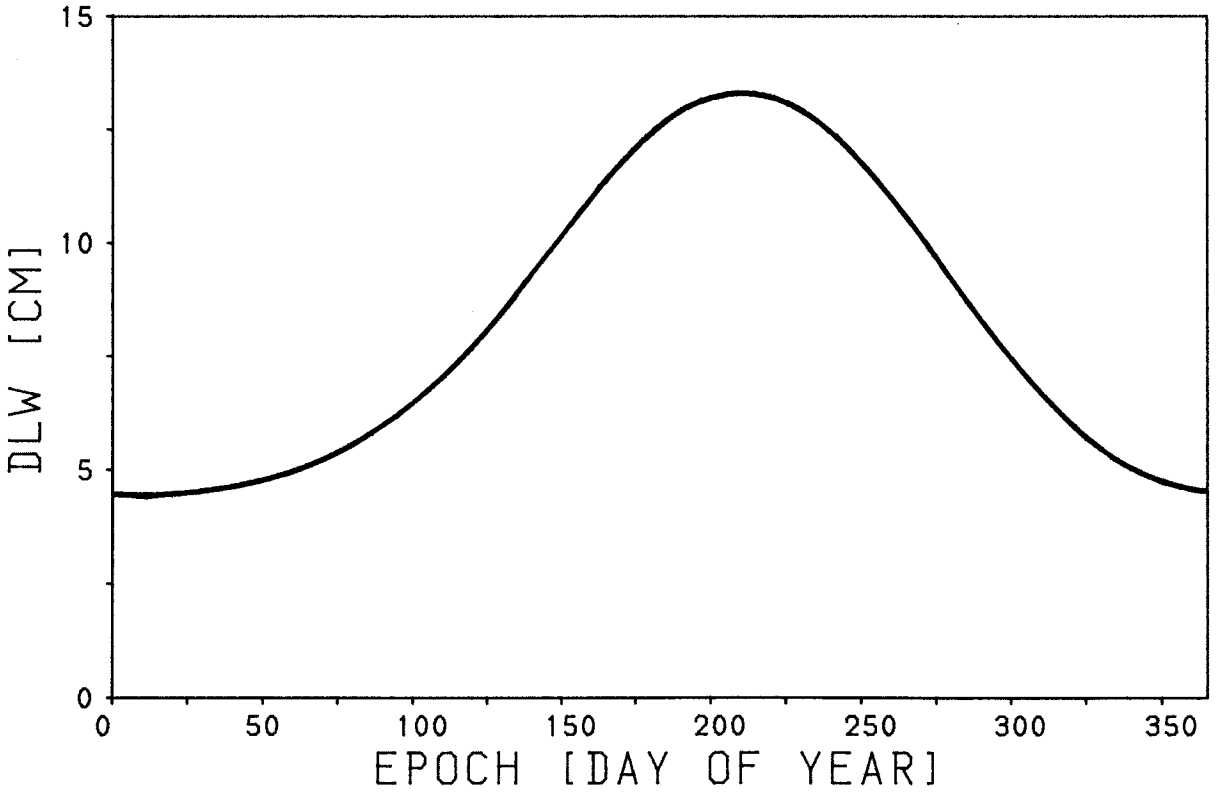

Figure 3 Wet path delay dL_W modeled by a periodic function

Therefore, as in (Kaniuth 1986) a model expressing dL_W as a function of surface meteorological data has also been derived.

The adjustment model set up was

$$dL_W = p_W\ (T_S,\ D_S) \tag{6}$$

where p_W stands for low order polynomials of temperature T_S and dew point temperature D_S respectively. Because of the physical correlation between T_S and D_S the nonlinear dependence of dL_W on temperature can to a certain extent be described either by T_S or D_S. The model yielding the best rms fit to the data of 1.66 cm and a minimum number of significant parameters was found to be

$$\begin{aligned} dL_W\ [cm] \;=\; & 6.452 \pm 0.143 \\ & -(0.008 \pm 0.003)\ D_S\ (T_S - D_S) \\ & +(0.485 \pm 0.019)\ D_S \\ & +(0.014 \pm 0.002)\ D_S^2 \end{aligned} \tag{7}$$

with T_S and D_S measured in ^{o}C.

A comparison of this local wet path delay model with two general models is given in the following paragraph.

4. COMPARISON WITH GENERAL MODELS

Due to the adjustment procedure the derived local model (7) is a bias free solution with respect to the radiosonde data set and is based on the relation (4) for predicting the effective height of the troposphere. The following two general models for estimating the wet path delay from surface meteorological data were compared with the path delay resulting from the radiosonde launches, and in this way indirectly also with the local model:

- The well known original Hopfield model (Hopfield 1969, 1977) being based on the relation

$$N_W = \frac{N_{W,S}}{(H_W - H_S)^4}\ (H_W - H)^4 \tag{8}$$

  for predicting the wet refractivity N_W of height H as a function of station height H_S, troposphere height H_W and surface wet refractivity $N_{W,S}$;

- A modified Hopfield model proposed by Goad and Goodman (1974) as outlined in (Remondi 1984) which in case of estimating only the zenith path delay reduces to a simple linear function of H_W and the surface partial pressure of water vapor.

The results of this comparison are summarized in table 1 and imply that

- the bias found for the original Hopfield model agrees within 0.1 cm with the result obtained in (Kaniuth 1986),

- there is a systematic difference of 0.7 cm in zenith direction between the original and the modified Hopfield model,
- each of the models could be applied provided the height of the troposphere is properly , but not necessarily realistically, chosen.

Table 1 Bias in zenith wet path delay [cm] between the local model (7) and general models for various troposphere heights H_W

H_W	Hopfield	mod. Hopfield
Model (4)	-0.34 ± 0.11	-1.05 ± 0.13
11 km constant	+0.73 ± 0.11	+0.04 ± 0.10
12 km constant	-0.02 ± 0.10	-0.73 ± 0.11

5. CONCLUSIONS

The results obtained from the analysis of the meteorological data of the total of 270 radiosonde launches allows the following conclusions to be drawn:

- Provided a sufficiently large radiosonde data set is available, local or regional modeling of the wet path delay will certainly match the particular meteorological conditions better than general models. This is indicated by the rms agreement of 1.66 cm between the derived local model and the radiosonde data compared to results of 3-4 cm at best achieved elsewhere (Askne et al. 1986, Coco and Clynch 1982). Moreover general models may yield a bias of up to a few cm.

- The definition of a model for estimating the local effective height H_W of the troposphere seems to be essential for improving the predictability of the wet path delay. The result that the variations of H_W were found to be better described by a periodic function of epoch than by a function of meteorological parameters indicates that the surface defined by the effective troposphere height is rather stable and is not directly reflecting short-term variations of temperature and humidity on the earth's surface.

REFERENCES

Askne J, Elgered G, Nordius H (1986) Atmospheric Water Vapour Corrections for Altimetry Measurements. In: Proceedings of IGARRS 86 Symposium, Zürich, Switzerland, ESA SP-254, pp 1543-1548

Coco DS, Clynch JR (1982) The Variability of the Tropospheric Range Correction due to Water Vapour Fluctuations. In: Proceedings of the Third International Geodetic Symposium on Satellite Doppler Positioning, Las Cruces, N.M., USA, Vol. 1, pp 475-495

de Boor C (1978) A Practical Guide to Splines. Springer, New York, 1978

Deutscher Wetterdienst (1982-1986) Sonderbeobachtungen des Meteorologischen Observatoriums Hohenpeißenberg, No. 46-56

Goad CC, Goodman L (1974) A Modified Hopfield Tropospheric Refraction Correction Model. Paper presented at the Fall Annual Meeting of the AGU, San Francisco, Cal., Dec. 1974

Hopfield HS (1969) Two-quartic Tropospheric Refractivity Profile for Correcting Satellite Data. JGR 74: pp 4487-4499

Hopfield HS (1977) Tropospheric Correction of Electro-Magnetic Ranging Signals to a Satellite: Study of Parameters. In: Proceedings of the International Symposium on Electromagnetic Distance Measurement and the Influence of Atmospheric Refraction, Wageningen, The Netherlands, May 1977, pp 205-213

Kaniuth K (1986) A Local Model for Estimating the Tropospheric Path Delay at Microwave Frequencies. In: Proceedings of the Fourth International Geodetic Symposium on Satellite Positioning, Austin, Tx., USA, pp 589-601

Remondi BW (1984) Using the Global Positioning System (GPS) Phase Observable for Relative Geodesy: Modeling, Processing and Results. Ph.D. Dissertation, The University of Texas at Austin, Tx., USA

Smith EK, Weintraub S (1953) The Constants in the Equation for Atmospheric Refraction Index at Radio Frequencies. In: Proceedings of the I.R.E., 41, pp 1035-1057

IONOSPHERIC REFRACTION ERRORS AND OBSERVABLES

R. Leitinger and E. Putz

Abstract

Increasing accuracy requirements for the geodetic application of trans-ionospheric propagation of radio waves necessitates refined error assessment. To achieve this goal one has first to improve the formulae which relate propagation errors to parameters of the electron distribution in the ionosphere. The second step is to assess which quantities are measured or likely to be measured in the future and which data are available both for error assessment and error correction.

In the first part of this paper we give precise formulae for the higher order refraction errors for spherical electron density distributions. Second order errors depend on the square of (vertical) electron content, $(N_\perp)^2$, on equivalent slab thickness of the ionosphere, τ, on the height of the layer, and on a "shape factor", η.

In the second part of this paper we estimate the observability of these ionospheric parameters and we discuss the data base, observation methods, temporal and spatial resolution. Two of the more readily available empirical models for the F region of the ionosphere are discussed briefly, namely the so-called Bent model and the International Reference Ionosphere (IRI - 79).

In Brunner, F.K. (Ed.), 1988, "Atmospheric Effects on Geodetic Space Measurements", *Monograph 12, School of Surveying, University of New South Wales, pp. 81-102.*

1. Introduction

This paper makes use of the series expansion method for the ionospheric refractive index (Leitinger, 1974, Leitinger and Hartmann, 1977). It makes also use of the separation of the propagation errors in terms of increasing power of $(1/f^2)$, f being the frequency of the transmitted signal. We give rigorously derived formulae for second order refraction errors both for a planar and for a spherically layered ionosphere. The other errors of second order stem from the expansion of the refractive index and are explicitly given elsewhere (Leitinger, 1974, compare Hartmann and Leitinger, 1984). In previous papers we had used results of model calculations for the refraction errors of second order (e.g., Hartmann and Leitinger, 1984).

The following scenario is assumed: radiowaves emitted from a satellite, S, are received at an observing station, B, and signal phase is used for range measurement. The carrier phase is proportional to the length of the phase path (optical path), S_n. (In practice one is restricted to measure phase differences and therefore phase path differences can be considered to be the primary measured quantity. Our considerations can easily be transferred from range errors into range difference or range rate errors.) Propagation "error" means length of the optical path, S_n, minus true (geometrical) range, S_o. If we subdivide the error into two partial errors s_1 and s_2 we have $S_n = S_o+s_1+s_2$. Using the phase path element ds and the line element ds_o (straight line BS from the receiving station to the satellite) then $S_n = {}_B\int^S n\, ds$ and $S_o = {}_B\int^S ds_o$. Error distribution is done in such a way that $s_1 = {}_B\int^S n\, ds_o - {}_B\int^S ds_o$ and $s_2 = {}_B\int^S n\, ds - {}_B\int^S n\, ds_o$. s_1 comprises the first order error and those errors which stem from the series expansion of the refractive index. s_2 is the refraction error. Numerical model calculations and derivations for a homogeneous ionosphere (planar as well as spherical layering) have shown that s_2 contains no terms of order zero or one (Leitinger, 1974). Model calculations demonstrate that the birefringence (anisotropy) influence produces no errors of orders zero, one, two. Therefore restriction to error terms up to order two allows to use the "quasi-isotropic" approximation for the ray path, i.e., assuming the ray path to be identical with the wave normal. In the following chapter we give the highlights of the derivation only. For a more complete description see Leitinger, 1987 (English translation available).

2. The refraction error of order two

Figure 1 shows the geometry for planar layering (left hand part) and

for spherical layering (right hand part). We use the following conventions: the index "o" designates the location of the receiver, B, the index "s" designates the location of the satellite transmitter, S (Figure 1). ds be the ray path element, ds_o the straight line element along BS. Be α the zenith angle along the ray path, ζ the zenith angle along BS. The path elements are $ds = dh/\cos\alpha$, $ds_o = dh/\cos\zeta$ (h: height above B; for spherical layering $h = r - r_o$, $dh = dr$, when r is the distance from the centre, O, of the concentric spheres marking the layering).

For planar layers we use Cartesian coordinates (x, h), x being the horizontal coordinate. For spherical layers we use polar coordinates (r, θ), θ being the angular coordinate, measured from the line BS, i.e., $\theta_o = 0$ (Figure 1).

The height dependence of the square of the refractive index, n, be $n^2 = 1 - C(h)$. For the signal frequencies of practical value $C<<1$ and one can use an expansion in a power series of C when n is needed.

Refraction laws for

planar layers	spherical layers
$n \sin\alpha = n_o \sin\alpha_o = \text{const.};$	$n\, r \sin\alpha = n_o\, r_o \sin\alpha_o = \text{const.}$

For simplicity we assume in the following $n_o = 1$. This is no serious restriction: The refractive index can always be considered a relative number.

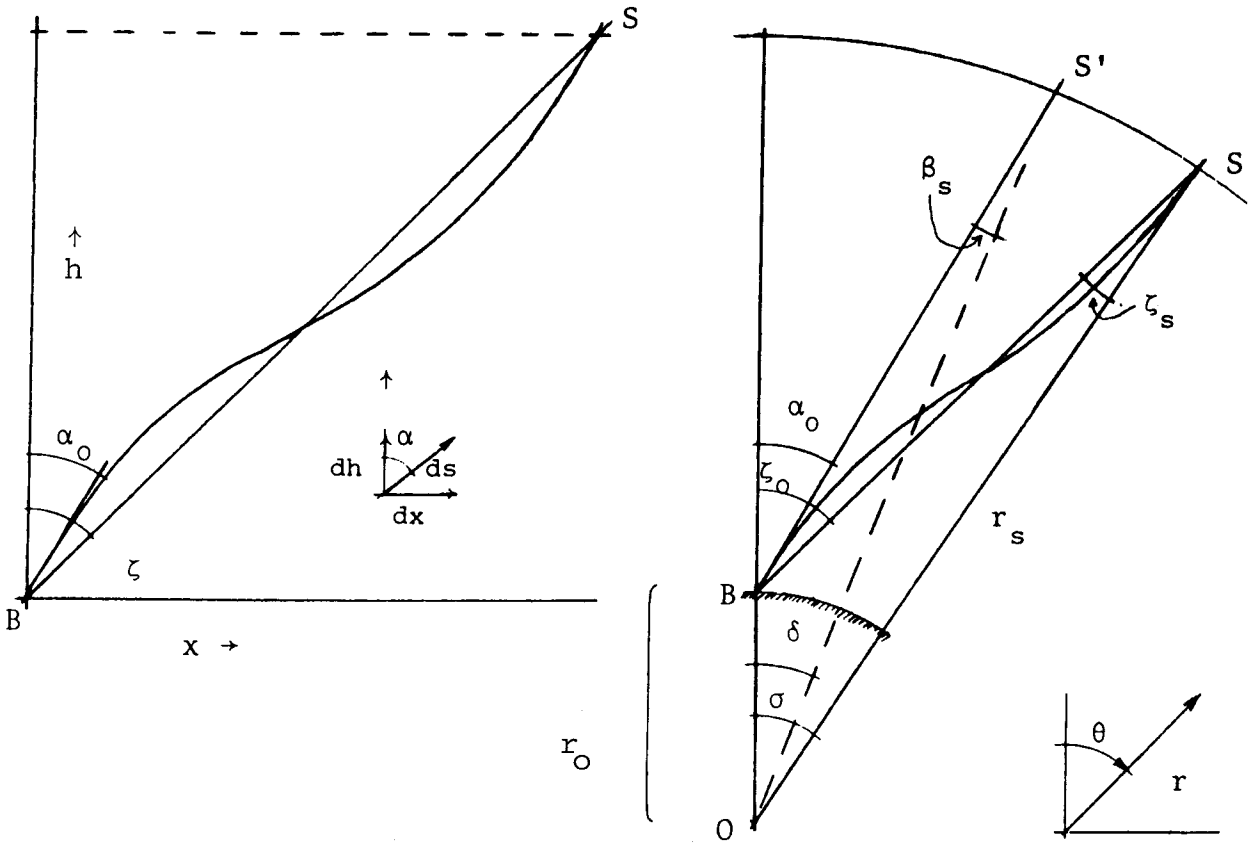

Figure 1: Geometry for planar layering (left) and spherical layering (right).

Planar layering:

Differential equation of the ray

$$dx = tg\alpha\ dh = \frac{\sin\alpha_o\ dh}{(n^2 - \sin^2\alpha_o)^{1/2}} = \frac{tg\alpha_o\ dh}{(1 - C(h)/\cos^2\alpha_o)^{1/2}}$$

Ray path element

$$ds = dh/\cos\alpha = \frac{n\ dh}{(n^2 - \sin^2\alpha_o)^{1/2}} = \frac{(1 - C(h))^{1/2}\ dh}{\cos\alpha_o\ (1-C(h)/\cos^2\alpha_o)^{1/2}}$$

Element of the optical path length

$$n\ ds = \frac{(1 - C(h))\ dh}{\cos\alpha_o\ (1-C(h)/\cos^2\alpha_o)^{1/2}}$$

Power of C series expansions:

$$dx = tg\alpha_o\ dh\ [1 + \frac{1}{2}\frac{C}{\cos^2\alpha_o} + \frac{3}{8}\frac{C^2}{\cos^4\alpha_o} + \cdots]$$

$$n\ ds = \frac{dh}{\cos\alpha_o}[1 - (1 - \frac{1}{2\cos^2\alpha_o})\ C + (\frac{3}{8\cos^4\alpha_o} - \frac{1}{2\cos^2\alpha_o})\ C^2 \pm \cdots]$$

Now the difference between α_o and ζ_o has to be taken into account. We define $tg\zeta_o = tg\alpha_o\ (1 + \varepsilon)$. Using the coordinates of the satellite (x_s, h_s) and the zenith angle of the straight line BS at B, $\zeta_o = \zeta$ (it is constant along BS) we obtain $tg\zeta = x_s/h_s$ and by means of integration follows

$$\varepsilon = \frac{1}{2}\frac{(I_1/h_s)}{\cos^2\alpha_o} + \frac{3}{8}\frac{(I_2/h_s)}{\cos^4\alpha_o} + \cdots, \quad \text{with} \quad I_n = {}_0\int^{} C^n\ dh\ .$$

One obtains for the refractive index integrated over the straight line BS

$${}_0\int^{h_s} n\ ds_o = \frac{1}{\cos\zeta}\ {}_0\int^{h_s} n\ dh = \frac{1}{\cos\zeta}\ (h_s - \frac{1}{2}\ I_1 - \frac{1}{8}\ I_2 - \cdots)$$

and with the series expansion for $1/\cos\zeta$

$${}_0\int^{h_s} n\ ds_o = \frac{h_s}{\cos\alpha_o} + \frac{I_1\ tg^2\alpha_o}{2\cos\alpha_o} + \frac{3}{8}\frac{I_2\ tg^2\alpha_o}{\cos^3\alpha_o} + \frac{I_1^2\ tg^2\alpha_o}{8\ h_s\cos\alpha_o} - \frac{I_1}{2\cos\alpha_o} - \frac{I_2}{8\cos\alpha_o} - \frac{I_1^2\ tg^2\alpha_o}{4\ h_s\cos\alpha_o} \pm \cdots$$

In a similar way integration of the element of the optical path length gives the first term of the refraction error s_2.

The difference gives $(s_2)_2$. Up to second order it is

$$(s_2)_2 = ({}_B\int^S n\ ds - {}_B\int^S n\ ds_o)_{o..2} = -\frac{tg^2\alpha_o}{8\cos\alpha_o}\ (I_2 - \frac{I_1^2}{h_s})$$

The outer index indicates that all expressions are to be developed up to order 2 in C. Therefore we had to keep I_1^2 and I_2 but not I_2^2, I_m with $m>2$, etc. The terms of order 0 and 1 in C (order 0 through 3 in 1/f) compensate. The refractive error s_2 is a quantity of order 2 in C, and order 4 in 1/f, respectively. The expression given above is complete, i.e., it comprises all terms of order 2 in C.

With sufficient accuracy we set for the ionosphere

$C = X = f_p^2/f^2 = A\,N/f^2$ (f_p: plasma frequency, f: transmitted frequency, N: electron density. With SI units the constant A = 80,6). It follows

$$I_1 = \frac{A}{f^2}\,{}_B\!\int^S N\,dh = \frac{A}{f^2}\,N_1 = \frac{A}{f^2}\,N_m\,\tau\;; \qquad I_2 = \frac{A^2}{f^4}\,{}_B\!\int^S N^2\,dh = \frac{A^2}{f^4}\,(N_1)^2\,\frac{\eta}{\tau}\;;$$

N_1: vertical electron content,

τ: "equivalent slab thickness",

N_m: maximal electron density ($\tau = N_1/N_m$),

η: shape factor, $\eta = (\tau\,{}_B\!\int^S N^2\,dh)\;/\;({}_B\!\int^S N\,dh)^2$.

Finally the second order refraction error for planar layering becomes

$$(s_2)_2 = \frac{A^2}{f^4}\,\frac{tg^2\alpha_o}{8\cos\alpha_o}\,(N_1)^2\,\left(\frac{\eta}{\tau} - \frac{1}{h_s}\right)$$

Spherical layering

We start with the expansion of the path elements. The outer index is used to indicate the order in C (the power of C to which the expression is proportional). We expand

$$ds = (ds)_0 + (ds)_1 + (ds)_2 + \cdots$$
$$ds_o = (ds_o)_0 + (ds_o)_1 + (ds_o)_2 + \cdots$$

With the expansion for the refractive index,

$$n = 1 - \frac{1}{2}\,C - \frac{1}{8}\,C^2 - \cdots, \qquad \text{we get}$$

$$n\,ds = (ds)_0 - \frac{1}{2}\,C\,(ds)_0 + (ds)_1 - \frac{1}{8}\,C^2\,(ds)_0 - \frac{1}{2}\,C\,(ds)_1 + (ds)_2 \pm \cdots$$
$$n\,ds_o = \underbrace{(ds_o)_0}_{o.\,0} - \underbrace{\frac{1}{2}\,C\,(ds_o)_0 + (ds_o)_1}_{\text{order 1}} - \underbrace{\frac{1}{8}\,C^2\,(ds_o)_0 - \frac{1}{2}\,C\,(ds_o)_1 + (ds_o)_2}_{\text{order 2}} \pm \cdots$$

Now we need the relation between the zenith angle of the satellite in B, ζ_o, the angle of arrival of the ray, α_o, and C. We define $\zeta_o = \alpha_o + \varepsilon$. We follow the tangent to the ray at B up to the height of the satellite (point S', see Figure 1) and gain the triangle OBS'. Let the angle at O and at S' be δ and β_s, respectively, then $\alpha_o = \beta_s + \delta$. Be ζ_s the zenith angle of the straight line BS at S, be $\sigma = \delta + \gamma$ the angle BOS and it follows $\zeta_o = \alpha_o + \varepsilon = \zeta_s + \delta + \gamma$.

The triangle BOS gives the relation $tg\,\zeta_o = \dfrac{\sin\sigma}{\cos\sigma - r_o/r_s}$

(r_o: distance OB; r_s: distance OS, $r_s = r_o + h_s$; h_s: height of S above B). Use of the triangle BOS gives after rearrangement and series expansion

$$tg\,\varepsilon = \frac{\cos\beta_s\,\sin\alpha_o}{\sin(\alpha_o - \beta_s)}\,\gamma + \left[\frac{1}{2}\,\frac{\sin\beta_s\,\sin\alpha_o}{\sin(\alpha_o - \beta_s)} - \frac{\cos\beta_s\,\sin\beta_s\,\sin\alpha_o}{\sin(\alpha_o - \beta_s)}\right]\gamma^2 \pm \cdots$$

From the Differential Equation of the ray, $d\theta = (1/r)\ \mathrm{tg}\ \alpha\ dr$, it follows

$$\sigma = \int_{r_o}^{r_s} \frac{n_o\, r_o \sin\alpha_o}{r\,(n^2 r^2 - n_o^2\, r_o^2 \sin^2\alpha_o)^{1/2}}\, dr. \qquad \text{Defining } \sin\beta = \frac{r_o}{r}\sin\alpha_o$$

one gets

$$\gamma = \sigma - (\alpha_o - \beta_s) = \int_{r_o}^{r_s} \frac{\sin\alpha_o\, dr}{r^2\,(1 - C - \sin^2\beta)^{1/2}} - \int_{r_o}^{r_s} \frac{r_o \sin\alpha_o\, dr}{r^2\,(1 - \sin^2\beta)^{1/2}} .$$

($n_o \equiv 1$, $n^2 = 1 - C$ were used and for $(\alpha_o - \beta_s)$ the integral from the Differential Equation of the tangent of the ray was used.). We combine the integrals, use series expansion and gain

$$\gamma = \int_{r_o}^{r_s} \frac{r_o \sin\alpha_o}{r^2 \cos\beta}\left[\frac{1}{2}\frac{C}{\cos^2\beta} + \frac{3}{8}\frac{C^2}{\cos^4\beta} + \frac{5}{16}\frac{C^3}{\cos^6\beta} + \cdots\right] dr = \gamma_1 + \gamma_2 + \gamma_3 + \cdots$$

With $-(r_o/r)\sin\alpha_o\, dr = \cos\beta\, d\beta$ we get

$$\gamma_1 = \frac{1}{2}\int_{r_o}^{r_s} \frac{C}{\cos^2\beta}\, d\beta, \quad \gamma_2 = \frac{3}{8}\int_{r_o}^{r_s} \frac{C^2}{\cos^4\beta}\, d\beta, \quad \gamma_3 = \frac{5}{16}\int_{r_o}^{r_s} \frac{C^3}{\cos^6\beta}\, d\beta, \text{ etc.}$$

With the zenith angle of the ray, α, we gain the ray path element

$$ds = \frac{dr}{\cos\alpha} = \frac{n\, dr}{[n^2 - (r_o/r)^2 \sin^2\alpha_o]^{1/2}} = \frac{(1 - C)^{1/2}\ dr}{\cos\beta\ (1 - C/\cos^2\beta)^{1/2}} .$$

Expanded: $ds = \frac{dr}{\cos\beta}\left(1 - \frac{1}{2}C - \frac{1}{8}C^2 - \cdots\right)\left(1 + \frac{C}{2\cos^2\beta} + \frac{3\,C^2}{8\cos^4\beta} + \cdots\right).$

With the conventions used above we get

$$(ds)_0 = \frac{dr}{\cos\beta},$$

$$(ds)_1 = \frac{1}{2}\,C\,\mathrm{tg}^2\beta\,\frac{dr}{\cos\beta} = -\frac{1}{2}\,r_o \sin\alpha_o\, C\,\frac{d\beta}{\cos^2\beta},$$

$$(ds)_2 = \frac{1}{8}\,C^2(3\,\mathrm{tg}^4\beta + 4\,\mathrm{tg}^2\beta)\,\frac{dr}{\cos\beta} = -\frac{1}{8}\,r_o \sin\alpha_o\, C^2\left(\frac{3\sin^2\beta}{\cos^4\beta} + \frac{4}{\cos^2\beta}\right) d\beta.$$

For the corresponding expansion of the path element along BS we use the zenith angle of this straight line, ζ:

$\sin\zeta = (r_o/r)\sin\zeta_o = (r_o/r)\sin(\alpha_o + \varepsilon)$

and it follows $ds_o = \frac{dr}{\cos\zeta} = \frac{dr}{[1 - (r_o/r)^2 \sin^2(\alpha_o + \varepsilon)]^{1/2}}$.

Insertion for $\sin^2(\alpha_o+\varepsilon)$ and expansion of the square root give

$$(ds_o)_0 = \frac{dr}{\cos\beta},$$

$$(ds_o)_1 = -\frac{1}{2}\left[\int_{\beta_s}^{\alpha_o} C\,\frac{d\beta}{\cos^2\beta}\right] r_o \sin\alpha_o\,\frac{\cos\alpha_o \cos\beta_s}{\sin(\alpha_o - \beta_s)}\,\frac{d\beta}{\cos^2\beta} .$$

We see that $(ds)_0 \equiv (ds_o)_0$.

Since $\int_{\beta_s}^{\alpha_o} \frac{d\beta}{\cos^2\beta} = \mathrm{tg}\,\alpha_o - \mathrm{tg}\,\beta_s = \frac{\sin(\alpha_o - \beta_s)}{\cos\alpha_o \cos\beta_s}$,

it follows $\int_{r_o}^{r_s} (ds_o)_1 = \frac{1}{2} r_o \sin\alpha_o \int_{\beta_s}^{\alpha_o} \frac{C}{\cos^2\beta}\, d\beta \equiv \int_{r_o}^{r_s} (ds)_1$.

Now we have demonstrated that $\int n\, ds$ and $\int n\, ds_o$ are identical in first and second order of C. Furthermore all expressions in higher order of C which are constructed either by means of $(ds)_o$ or by means of $(ds_o)_o$ are identical. We use an other approach to gain a suitable expression for comparison of $(ds_o)_2$ with $(ds)_2$. We need the integrals of $(ds)_o$ from B to S. Those can be found with the distance BS, s_o: $s_o = r_s \cos\zeta_s - r_o \cos\zeta_o$ (triangle BOS). With $\zeta_o = \alpha_o + \varepsilon$ and with $\zeta_s = \zeta_o - (\delta+\gamma) = \alpha_o+\varepsilon-\delta-\gamma = \beta_s+\varepsilon-\gamma$ we expand $\cos\zeta_o$ and $\cos\zeta_s$ and gain

$$s_o = \underbrace{(r_s\cos\beta_s - r_o\cos\alpha_o)}_{\text{order 0}} + \underbrace{(r_o\sin\alpha_o)\gamma_1}_{\text{order 1}} + \underbrace{\tfrac{1}{2}[(r_o\cos\alpha_o - r_s\cos\beta_s)\mathrm{tg}^2\varepsilon + (2r_s\cos\beta_s)\cdot\gamma_1\mathrm{tg}\varepsilon - (r_s\cos\beta_s)\gamma_1^2] + (r_o\sin\alpha_o)\gamma_2}_{\text{order 2}}$$

It is easily shown that the members of order 0 and 1 are identical with the integrals of the differentials $(ds_o)_o$ and $(ds_o)_1$, respectively. Using $(r_o/r_s) = \sin\beta_s/\sin\alpha_o$ we get

$$({}_B\int^S ds_o)_2 = \frac{1}{2}\frac{r_o}{\sin\beta_s}[(\cos\alpha_o\sin\beta_s)\mathrm{tg}^2\varepsilon - \sin\alpha_o\cos\beta_s(\mathrm{tg}\varepsilon-\gamma_1)^2] + (r_o\sin\alpha_o)\gamma_2$$

The first order term $(\mathrm{tg}\varepsilon-\gamma_1)_1 = [\frac{\cos\alpha_o\cos\beta_s}{\sin(\alpha_o-\beta_s)} - 1]\,\gamma_1 = \frac{\cos\alpha_o\sin\beta_s}{\sin(\alpha_o-\beta_s)}\,\gamma_1$ leads to

$$({}_B\int^S ds_o)_2 = -\frac{1}{2} r_o\sin\alpha_o \frac{\cos\alpha_o\cos\beta_s}{\sin(\alpha_o-\beta_s)}\gamma_1^2 + (r_o\sin\alpha_o)\gamma_2 =$$

$$= -\frac{1}{8} r_o\sin\alpha_o \frac{\cos\alpha_o\cos\beta_s}{\sin(\alpha_o-\beta_s)}\left[\int_{\beta_s}^{\alpha_o}\frac{C\,d\beta}{\cos^2\beta}\right]^2 + \frac{3}{8} r_o\sin\alpha_o \left[\int_{\beta_s}^{\alpha_o}\frac{C^2\,d\beta}{\cos^4\beta}\right]$$

Since

$$({}_B\int^S ds)_2 = -\frac{1}{8} r_o\sin\alpha_o\left[\int_{\beta_s}^{\alpha_o}\frac{C^2\,d\beta}{\cos^2\beta}\right] + \frac{3}{8} r_o\sin\alpha_o\left[\int_{\beta_s}^{\alpha_o}\frac{C^2\,d\beta}{\cos^4\beta}\right]$$

we get

$$({}_B\int^S ds)_2 - ({}_B\int^S ds_o)_2 = \frac{1}{8} r_o\sin\alpha_o\left\{\left[\int_{\beta_s}^{\alpha_o}\frac{C^2\,d\beta}{\cos^2\beta}\right] - \frac{\cos\alpha_o\cos\beta_s}{\sin(\alpha_o-\beta_s)}\cdot\left[\int_{\beta_s}^{\alpha_o}\frac{C\,d\beta}{\cos^2\beta}\right]^2\right\}.$$

With

$$({}_B\int^S C\,ds)_1 - ({}_B\int^S C\,ds_o)_1 = \frac{1}{2} r_o\sin\alpha_o\left\{\left[\int_{\beta_s}^{\alpha_o}\frac{C^2\,d\beta}{\cos^2\beta}\right] - \frac{\cos\alpha_o\cos\beta_s}{\sin(\alpha_o-\beta_s)}\cdot\left[\int_{\beta_s}^{\alpha_o}\frac{C\,d\beta}{\cos^2\beta}\right]^2\right\}$$ we get finally

$$(s_2)_2 = ({}_B\int^S n\,ds - {}_B\int^S n\,ds_o)_{o..2} = -\frac{1}{8} r_o\sin\alpha_o\left[\int_{\beta_s}^{\alpha_o}\frac{C^2\,d\beta}{\cos^2\beta} - \frac{1}{\mathrm{tg}\,\alpha_o-\mathrm{tg}\,\beta_s}\cdot\left(\int_{\beta_s}^{\alpha_o}\frac{C\,d\beta}{\cos^2\beta}\right)^2\right]$$

Comparison of refraction errors for planar and spherical layering

First, one recognises that with spherical layering one has "weighted" integrals over C and C^2 instead of I_1 and I_2, respectively. C depends on r or on β. We switch from $d\beta$ to dr using the relation $(r_o \sin\alpha_o/\cos^2\beta)\, d\beta = -(\mathrm{tg}^2\beta/\cos\beta)\, dr$ and get

$$r_o \sin\alpha_o \int_{\beta_s}^{\alpha_o} \frac{C^n\, d\beta}{\cos^2\beta} = \int_{r_o}^{r_s} \frac{C^n\, \mathrm{tg}^2\beta}{\cos\beta}\, dr = \overline{\frac{\mathrm{tg}^2\beta}{\cos\beta}}^{\alpha_o, C^n} \int_{r_o}^{r_s} C^n\, dr$$

Of course the average for the weighting factor depends both on α_o and on C^n which is indicated by the symbol $\overline{}^{\alpha_o, C^n}$. The dependence is not strong and therefore one can approximate the true average by the value in a "mean ionospheric height", h_i. For lack of information about details of the actual C-profile one assumes a fixed h_i. A good approximation is to identify h_i with the height of the first moment of the height distribution of electron density ("center of gravity" of the ionosphere). A rule of thumb gives $h_i = h_m + 50$ km, h_m being the height of the electron density maximum. Designating $\beta(h_i) = \chi$ gives

$$(s_2)_2 \doteq -\frac{1}{8} \frac{\mathrm{tg}^2\chi}{\cos\chi} \left(I_2 - \frac{\mathrm{tg}^2\chi}{r_o \sin\alpha_o\, (\mathrm{tg}\alpha_o - \mathrm{tg}\beta_s) \cos\chi}\, I_1^2 \right),$$

with $I_1 = \int_{r_o}^{r_s} C\, dr$ and $I_2 = \int_{r_o}^{r_s} C^2\, dr$ as in the case of planar layering. Setting again $C = \frac{A\,N}{f^2}$ which is a sufficient approximation for series expansion up to order 4 in $1/f$ leads to

$$\boxed{(s_2)_2 = -\frac{A^2}{f^4} \frac{\mathrm{tg}^2\chi}{8\cos\chi} (N_1)^2 \left(\frac{\eta}{\tau} - \frac{\xi}{h_s}\right)}$$

In a good approximation we have to exchange the angle of arrival α_o with the zenith angle χ in the "mean ionospheric height" and $1/h_s$ with ξ/h_s to switch from the case of planar layering to the case of spherical layering. Depending on the situation it is often possible to gain a much less involved approximation for the geometric factor

$$\xi \doteq h_s \frac{\mathrm{tg}^2\chi}{r_o \sin\alpha_o\, (\mathrm{tg}\alpha_o - \mathrm{tg}\beta_s) \cos\chi}\,.$$

For "small" values of α_o a good approximation is $\xi = (r_s\, r_o) / r_i^2$ with $r_i = r_o + h_i$. For satellite heights h_s near 1000 km this leads to $\xi = 1$. Model calculations show that in general this approximation can be used up to $\alpha_o \approx 70^o$. For higher satellite altitudes (e.g., for geostationary satellites) usually one can set $\xi/h_s = 0$.

We remark that the derivation of the second order refraction error is

Table 1: Results of model calculations.
Chapman layer with "scale height" H_1 below and "scale height" H_2 above the maximum. Numerical integration with relative accuracy of about 10^{-7}.

1) h_S = 1000 km, h_i = 400 km, h_m = 350 km, H_1 = 50 km, H_2 = 100 km.

α_o	t/	tv	G_1	I_1	I_2	I_3	I_4	I_5
15	228.22	221.34	14.39	14.22	9.57	3.19	6.38	6.38
30	250.55	221.09	71.33	70.27	47.43	15.80	31.63	31.63
45	295.40	220.53	235.58	230.61	156.77	51.82	104.96	104.48
60	378.50	219.40	754.91	730.50	503.93	160.34	343.60	334.80
75	521.55	217.53	2520.72	2411.29	1707.59	426.49	1281.10	1117.93
90	639.53	216.55	5049.20	4871.57	3514.03	0.00	3514.03	2239.30

equivalent slab thickness: 221.42 km.

2) h_S = 1000 km, h_i = 400 km, h_m = 350 km, H_1 = 120 km, H_2 = 120 km.

α_o	t/	tv	G_1	I_1	I_2	I_3	I_4	I_5
15	334.79	324.71	21.11	21.04	14.50	6.98	7.52	7.55
30	367.86	324.61	104.61	104.21	72.03	34.74	37.29	37.43
45	434.60	324.44	345.51	344.36	239.31	115.54	123.77	123.63
60	559.77	324.47	1107.19	1111.37	779.73	371.12	408.61	396.18
75	783.27	326.69	3697.04	3899.26	2754.56	1115.26	1639.29	1322.88
90	983.51	333.03	7405.47	8802.05	6060.88	0.00	6060.88	2649.83

equivalent slab thickness: 324.75 km.

3) h_S = 4000 km, h_i = 400 km, h_m = 350 km, H_1 = 50 km, H_2 = 100 km.

α_o	t/	tv	G_1	I_1	I_2	I_3	I_4	I_5
15	228.63	221.75	14.42	14.25	9.57	1.15	8.42	8.77
30	251.00	221.49	71.46	70.37	47.43	6.11	41.33	43.46
45	295.91	220.91	236.01	230.90	156.78	22.86	133.92	143.55
60	379.11	219.75	756.30	731.23	503.93	87.80	416.13	460.01
75	522.27	217.83	2525.37	2412.82	1707.59	315.87	1391.72	1536.03
90	640.31	216.82	5058.51	4873.68	3514.04	0.00	3514.04	3076.78

equivalent slab thickness: 221.83 km.

4) h_S = 1000 km, h_i = 500 km, h_m = 350 km, H_1 = 50 km, H_2 = 100 km.

α_o	t/	tv	G_1	I_1	I_2	I_3	I_4	I_5
15	228.22	221.55	13.94	14.22	9.57	3.19	6.38	6.18
30	250.55	221.99	68.42	70.27	47.43	15.80	31.63	30.34
45	295.40	223.04	221.11	230.61	156.77	51.82	104.96	98.06
60	378.50	225.58	674.50	730.50	503.93	160.34	343.60	299.14
75	521.55	231.98	2018.52	2411.29	1707.59	426.49	1281.10	895.21
90	639.53	239.49	3624.82	4871.57	3514.03	0.00	3514.03	1607.59

equivalent slab thickness: 221.42 km.

5) h_S = 1000 km, h_i = 300 km, h_m = 400 km, H_1 = 50 km, H_2 = 100 km.

α_o	t/	tv	G_1	I_1	I_2	I_3	I_4	I_5
15	227.84	220.77	14.85	13.98	9.42	3.09	6.33	6.60
30	249.74	219.43	74.35	68.76	46.45	15.13	31.32	33.05
45	293.40	216.39	251.39	223.23	151.83	48.55	103.27	111.76
60	372.90	209.60	851.91	689.82	475.65	142.98	332.68	378.71
75	504.36	194.69	3271.72	2148.60	1517.35	338.63	1178.72	1454.44
90	606.29	179.77	7737.94	4067.83	2921.10	0.00	2921.10	3439.90

equivalent slab thickness: 221.16 km.

$t/ = \int (Ch(r)/\cos\beta)\, dr$; $tv = (t/)\cdot\cos\chi$; $G_1 = \tau\, tg^2\chi/\cos\chi$;
$I_1 = \int (Ch(r)tg^2\beta/\cos\beta)\, dr$; $I_2 = \int (Ch^2(r)tg^2\beta/\cos\beta)\, dr$;
$I_3 = I_1^2/(r_o\sin\alpha_o(tg\alpha_o - tg\beta_S)$; $I_4 = I_2 - I_3$; $I_5 = G_1(\eta - \tau/h_S)$.
$\tau = \int(Ch(r))dr$ for α_o=0 (equiv. slab thickness). All integrals from B to S.

valid for the troposphere, too: in this case we have $n_o \neq 1$ but one can simply put $(n/n_o)^2 = 1 - C(h)$ and all the derivations and results are valid.

We checked the validity of the approximations by means of model calculations. Some of the results are shown in Table 1. For the height profile of electron density a Chapman-layer was used: $N(h) = N_m \cdot Ch(h)$, with $Ch(h) = \exp[1 - z - \exp(-z)]$, $z = (h-h_m)/H$, h_m: height of layer maximum, H: "scale height". It was possible to assume different values of H below and above the layer peak, respectively (H_1 for $h \leq h_m$, H_2 for $h > h_m$). Parameter sets 1, 2, and 3 give examples for a "good" assumption of h_i ($h_i=h_m+50$ km), set 4 assumes $h_i=h_m+150$ km (too high), set 5 assumes $h_i=h_m-100$ km (too low).

3. Discussion of Observables

The formulae derived show that the following four parameters of the height profile of the electron density influence the second order refraction error. (They influence likewise the other partial errors of second order which stem from the expansion of the refractive index - compare Leitinger, 1974, Hartmann and Leitinger, 1984).

1) the (vertical) electron content of the ionosphere, $N_\perp$
2) the equivalent slab thickness, τ
3) the height of the layer, h_m
4) the shape factor, η.

For planar layering the layer height does not appear, for spherical layering the layer height enters in the "mean ionospheric height" and should be taken into account in calculating χ. Layer height influences the geometric factor ξ, too.

In discussing the importance of the influencing parameters one should distinguish at least three different latitude regions:

a) high latitudes,
b) mid-latitudes,
c) low latitudes.

The geographic coordinate system is not really suitable to define the boundaries between these regions in a simple and straightforward way. The so-called magnetic coordinates are more adequate for this purpose. Unfortunately one has to use several different definitions for magnetic latitude. With an accuracy of a few degrees the boundary between high latitudes and mid-latitudes can be given in geomagnetic dipole coordinates. For the boundary between mid-latitudes and low latitudes the best system is the so-

called "dip latitude". The dipole coordinates make use of the dipole term of the geomagnetic field only. (One can include higher terms of the spherical harmonics expansion of the geomagnetic field, too, which leads to the "corrected" magnetic coordinates or to the "invariant" magnetic coordinates, but simple dipole coordinates are good enough for most propagation error estimates.) Dip latitude is calculated from the inclination of the geomagnetic field vector (the tangent of dip latitude is one half of the tangent of inclination). The difference between dipole latitude and dip latitude is significant.

The boundaries between the latitude regions are dynamic and depend on the time of day, on season, on solar activity, on the level of geomagnetic disturbance. The appropriate magnetic latitude is of primary importance for definition of the boundaries but for refined considerations an influence of geographic longitude should be taken into account, too. Except during some severe geomagnetic disturbances one is safely in ionospheric mid-latitudes when the dipole latitude is less than 55 degrees and the dip latitude is higher than 30 degrees. One should be very careful in extrapolating error estimates based on experience from mid-latitudes over these "safety limits".

Unfortunately the amount of collected data is distributed very unevenly over the globe which results in a strong bias for northern hemisphere mid-latitudes in error assessment.

In the vicinity of the latitude boundaries we find prominent features of ionization: the electron content shows a distinct Winter night "trough" near the boundary between mid-latitudes and high latitudes. This depression of ionization is sometimes seen during daytime, too and even in summer the trough has been detected in some cases. The months around the equinoxes behave similar to the Winter months. (Compare Leitinger et al., 1986)

Near the boundary between mid-latitudes and low latitudes we find the "crest" of the "equatorial anomaly" in ionization. The electron content values at the crest are the highest values found in the ionosphere. Around the magnetic dip equator we find often lower ionization levels than at the two crests.

Of all four influencing parameters electron content is the most important: its variability is the strongest and $(s_2)_2$ depends on the square of electron content. For most applications the equivalent slab thickness is next in terms of importance. Layer height plays an important role only when the zenith angle of the satellite is high. The shape factor could be of importance in lower and higher latitudes, in mid-latitudes probably under disturbed conditions only.

Table 2 gives estimates for the variability of the four influencing parameters. Extreme situations were not included. Of course it is possible to restrict the range of variability for a given geographical region or for a given time span or for a given time of the day. For example: the listed minimum of electron content is valid for the minimum of the "trough" in winter nights under conditions of low solar activity. The listed maximum of electron content is valid for the crest of the equatorial anomaly under conditions of high solar activity. The high values of slab thickness and of layer height are representative for low latitudes only.

Table 2: Estimated variablity of parameters which influence $(s_2)_2$

Parameter	Symbol	Range of values	Dimension
Electron content	N_1	$(10 \ldots 2000) \times 10^{15}$	m^{-2}
equivalent slab thickness	τ	200 ... 600	km
Layer height	h_m	250 ... 500	km
Shape factor	η	2/3 ... 1	

Shape factor: we remark that a homogeneous ionosphere (layer of constant electron density) has $\eta = 1$. A triangular layer (linear increase from N=0 to N_m at the bottomside, linear decrease from N_m to N=0 at the topside) has $\eta = 2/3$. A Chapman-layer with uniform "scale height" H for both the bottom and the topside has $\eta = e/4 = 0{,}6796$.

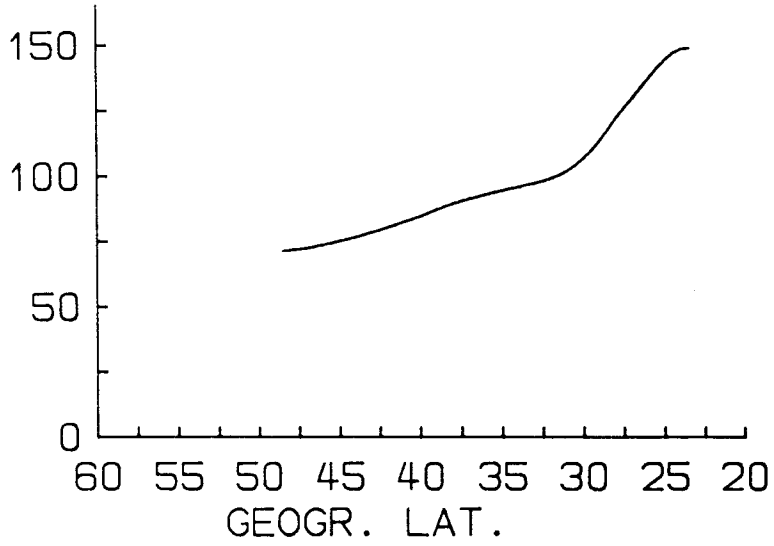

Figure 2: Electron content in units of 10^{16} m^{-2} vs. geogr. latitude in ^{o}N. Longitude of ionospheric points about $28^{o}E$. Data gained at the temporary station Dionysos from Diff. Doppler on the signals of an NNSS satellite on 8 April, 1981 around 11:40 UT. The crest of the equatorial anomaly is indicated near $25^{o}N$.

Previous estimates give an upper limit of 1000×10^{15} m^{-2} for maximal electron content. Table 2 lists twice this value. This is justified by data measured during times of high solar activity near the crest of the equatorial anomaly. Figure 2 shows an example. The peak electron content was $> 1500 \times 10^{15}$ m^{-2}, well above the "usual" limit of 1000×10^{15} m^{-2}.

The ranges of values listed in Table 2 are useful only for planning of measuring systems which are intended for global operation at all times of day and in all seasons and independent of solar activity. Then the ranges of values allow to estimate the worst case errors which are not likely to be exceeded except perhaps under extremely disturbed ionospheric conditions (see Hartmann and Leitinger, 1984). For the calculation of second order propagation error corrections and for estimating remaining errors it is recommended to use measured data. If necessary the measured data could be complemented by data from a good ionospheric model.

3.1 Discussion of models

Models describe the ionosphere in a numerical statistical form in terms of time of the day, season, solar activity, and location. In principle, one can distinguish between empirical and theoretical modelling approaches. The theoretical models are based on the physical processes which are responsible for the formation and variability of the ionosphere. Essentially, they are used for geophysical explanation of experimental observations and not for predictions. Some theoretical models can take into account geomagnetic activity but need input data which are difficult to obtain.

In our context the empirical models are more important. They are based on observations and share the deficiencies and gaps of the data used. One should distinguish between local, regional, and global models. In the following we deal with global models only and remark that for some locations and for some regions model descriptions are available which are more reliable than global descriptions specialised to the appropriate location or region (compare, e.g., Royden and Green, 1986).

All global empirical models apply spatial as well as temporal smoothing: they aim at descriptions with a minimum of parameters and use large scale spatial functions, e.g., spherical harmonics expansions for latitude and longitude dependence of ionospheric parameters. Smaller scale features of the horizontal structure of ionization distribution are smoothed out and do not appear in the reconstructed data. Especially, two important medium scale features are lost, namely the "trough" and details of the equatorial anomaly (see above).

Although there exist several empirical models that are routinely used for predictions of ionospheric parameters we restrict our short discussion to two widely known models, namely the Bent model and the International Reference Ionosphere (IRI - 79).

The Bent model (Llewellyn and Bent, 1973) determines vertical electron content up to 1000 km, the vertical profile of electron density and the electron content along the path between the ground and a satellite. The input parameters of the model are date, Universal Time (UT), location of the user, solar radio flux ($S_{10.7}$), and the sunspot number (R_Z). Output parameters which refer to satellite links need the orbital elements of the satellite and the operation frequencies. In midlatitudes the model predicts average ionization parameters with an accuracy of 75% to 80% provided that the sunspot number is <130 (Royden and Green, 1986). When the model is updated whith observed data from nearby stations the predictability is improved to 90%.

The IRI-79 (Rawer et al., 1978, Lincoln and Conkright, 1981) serves as a standard reference and gives monthly median vertical profiles of electron and ion densities, electron and ion temperatures. The inputs are location, sunspot number, date, and time. The IRI itself provides relative profiles only and relies on other models for peak electron density (foF2). Preference is given to the so-called CCIR model 1967 (CCIR 1967, 1970) for this parameter but other sources or measured values can be used, too. McNamara (1983) tested the ability of the IRI to predict electron content at 15 different locations for which measured data were available. He found that the discrepancies between observed and predicted monthly median values were reasonably small for mid and high latitudes, except during the night. (No comparison was made for the region of the "trough".) For low latitude stations, the discrepancies can be considerable. Model values were found to be too low by a factor of two and showed an incorrect diurnal variation. Use of the Bent model instead of the IRI profile could not improve the results.

It is important to note again that in general the spatial variability of electron content is not fully represented by ionospheric models. The models give smoothed average conditions. In the actual ionosphere strong gradients can exist over comparatively small scales. Examples are given in Figures 3 and 4. Figure 3 shows strong gradients connected to nighttime enhancements in the trough region (the enhancement appears near the location where one expects the trough minimum). Figure 4 shows unusually strong

but confined gradients in mid-latitudes (well equatorwards of the trough which is seen in this Figure, too). The gradients persisted for several hours. Presently it is not known how often such gradients occur.

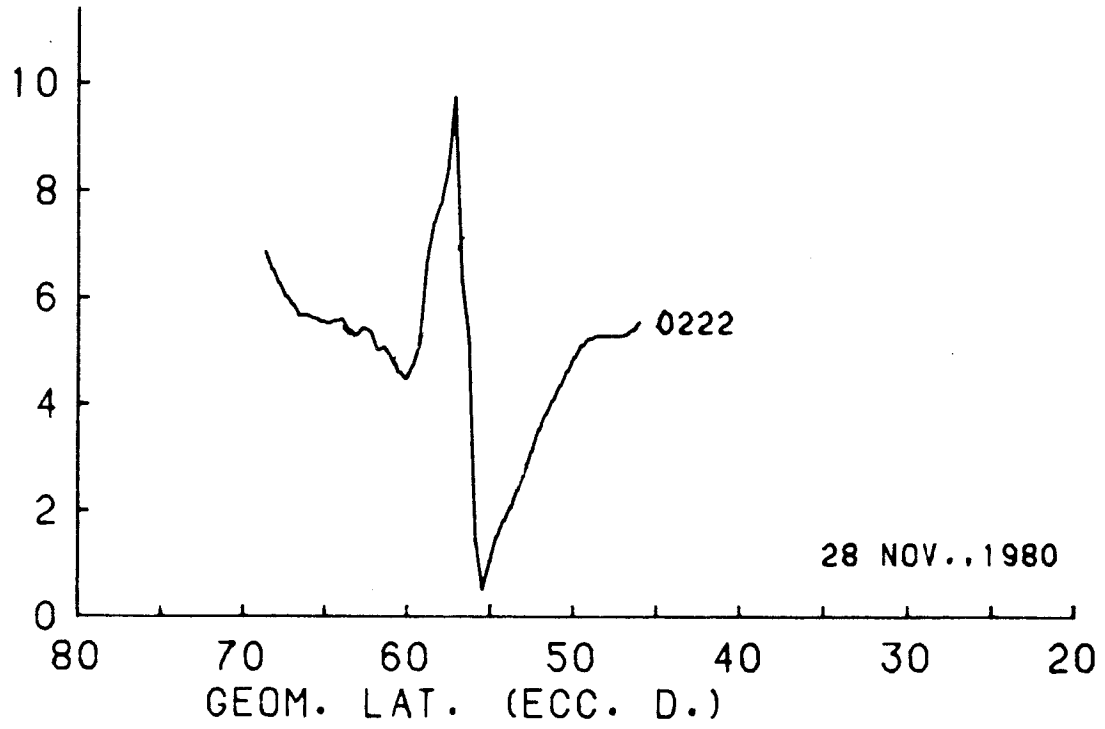

Figure 3: Electron content in units of 10^{16} m^{-2} vs. geomagnetic (eccentric dipole) latitude in ^{o}N. Data gained at the station Uppsala from Diff. Doppler on the signals of an NNSS satellite on 28 November, 1980 around 02 LT. Sharp trough region enhancement (strong gradients).

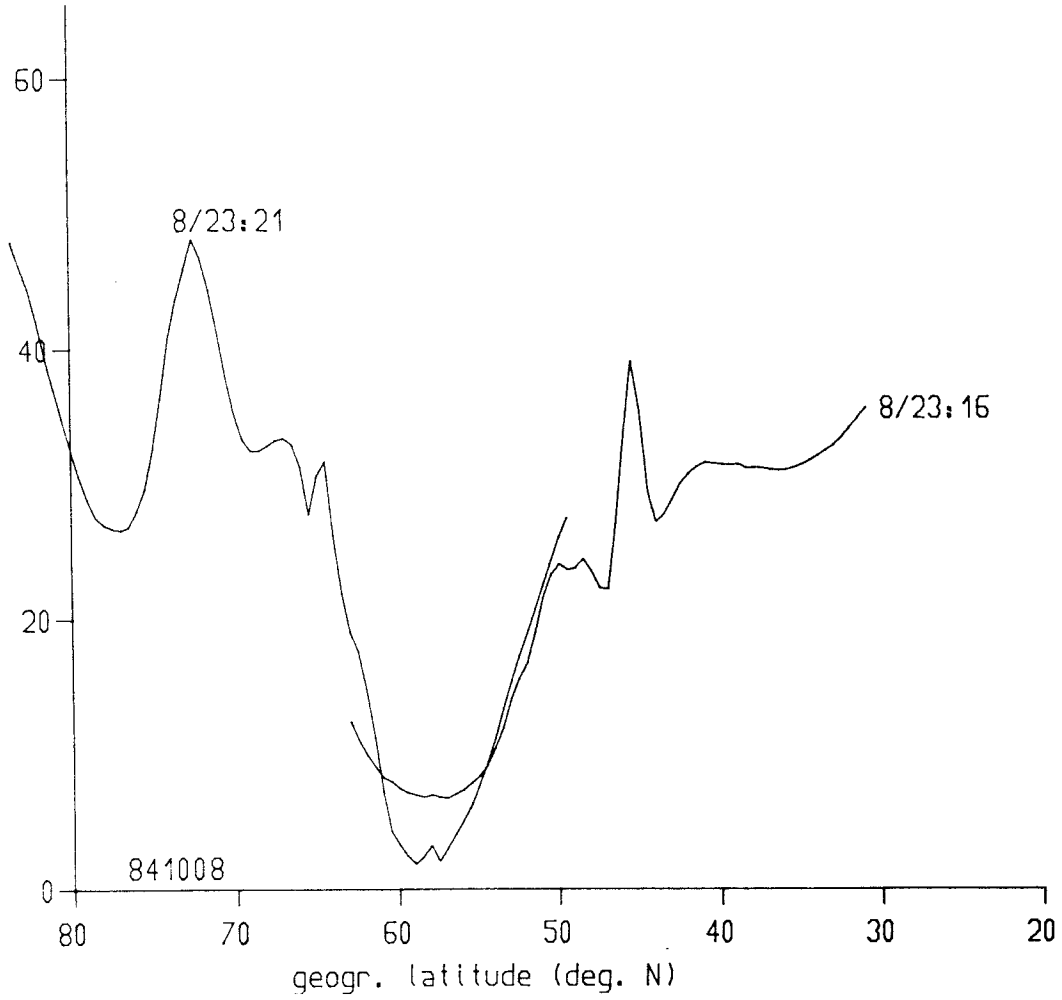

Figure 4: Electron content in units of 10^{16} m^{-2} vs. geogr. latitude in ^{o}N. Data gained at the stations Uppsala (left hand curve) and Graz (right hand curve) from Diff. Doppler on the signals of an NNSS satellite on 8 October, 1980 around 23 LT. Though minimum near 58^{o}N, sharp mid-latitude gradients near 43^{o}N.

An other remark concerns the difference between average and actual ionization conditions. The actual values of electron content could be between about 0.5 times the monthly average and 2.0 times the monthly average (see e.g., Figure 5). This spread should be increased if one wants to include days with severe geomagnetic disturbances (storms).

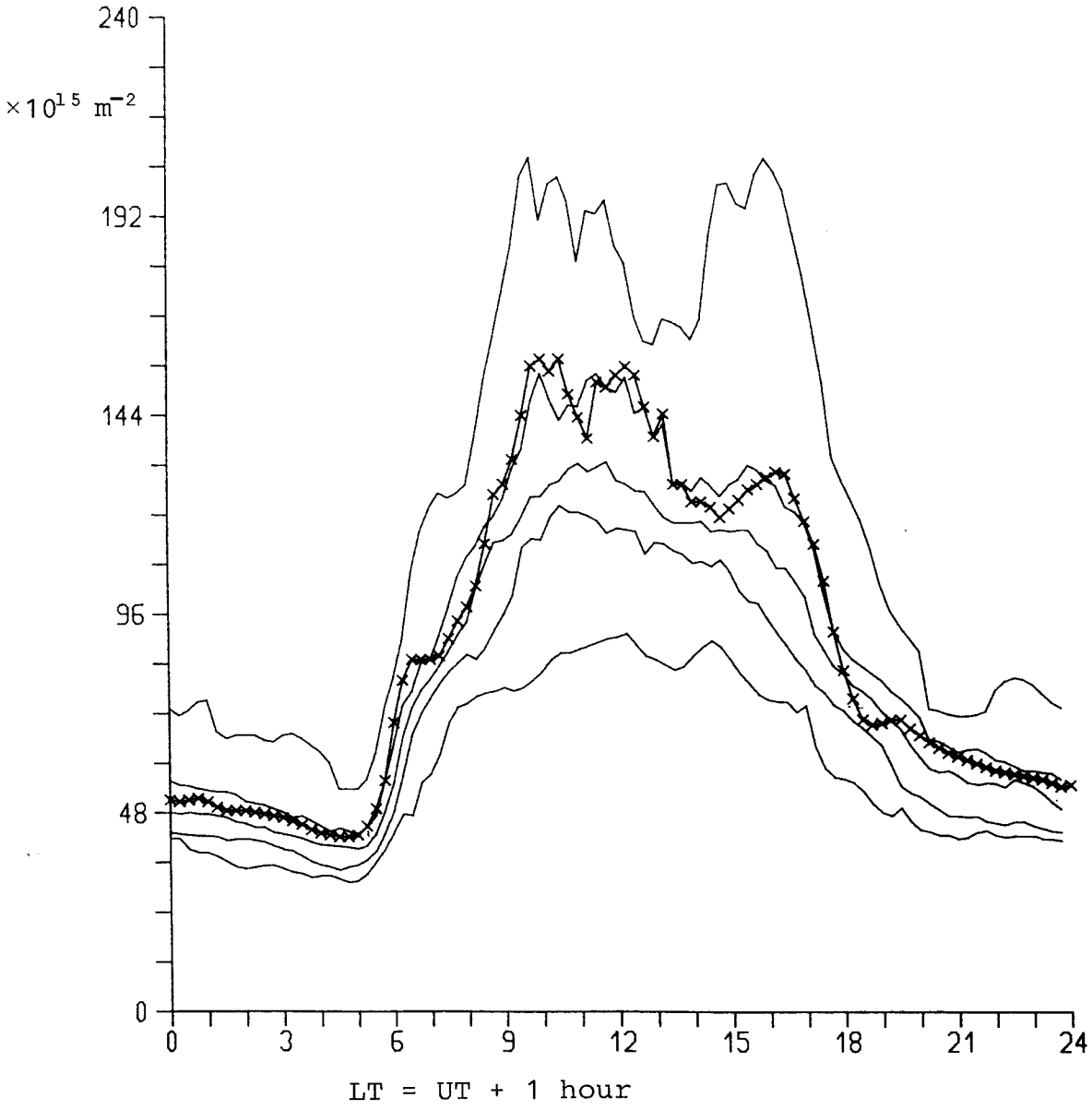

Figure 5: Example for average versus actual data and for the spread of data: diurnal curves of ionospheric electron content in units of 10^{15} m^{-2}. Curve marked with crosses: actual electron content of October 5, 1984. Unmarked curves from bottom to top: minima, lower quartiles, medians, upper quartiles, maxima for October 1984. Receiving station Graz (47.1°N, 15.5°E), vertical electron content derived from Faraday effect on the signals of SIRIO (geostationary at about 65°E). Location of the ionospheric point (in 400 km height on the ray from the station to the satellite): 42.2°N, 25.0°E. Abscissa: zonal time 15°E (UT + 1 hour). On the 5th of October, 1984 there was no appreciable geomagnetic disturbance and this day can be considered as a "typical quiet day". The solar activity was very low throughout October 1984.

3.2 Data from observations

The bulk of data on the morphology and dynamics of the ionosphere stem from groundbased observations made or by means of the "classical" pulse sounder, the ionosonde, or by means of propagation effects on satellite signals. Ionosondes onboard satellites, in-situ measurements, and the incoherent scatter of radio waves are other important sources for ionospheric data. For questions in connection with groundbased HF communications the ionosondes are the most important data sources. The ionospheric models which were constructed for HF communication purposes are therefore primarily based on data derived from ionograms. Information on the F region above the peak is not important in HF communication work. For propagation error assessment the upper F region is more important than the lower F region: there are much more free electrons above the F layer peak than below. In fact all four of the parameters which are needed for the assessment of higher order propagation effects (see Table 2) include information on both the bottom and the topside F region. The data sources which are available to derive these parameters are listed in Table 3 and are described in more detail in the following.

Table 3: Availability of measured data

Parameter	Measurability by means of method no.	Spatial and temporal density	Availability
Electron content	1: very good	good	good
Equiv. slab thickn.	1 + 2a: good	mediocre	mediocre
Layer height	2b: problematic	mediocre	mediocre
	2b + 3: mediocre	rather bad	bad
	4: very good	bad	rather bad
Shape factor	2b + 3: rather bad	bad	bad
	4: very good	bad	rather bad

Measuring methods:
1: Propagation effects on satellite signals (in general Faraday-effect on signals of geostationary satellites, Differential-Doppler-effect on signals of polar orbiting Navigation Satellites)
2: Bottom-Ionosonde;
2a: Determination of maximal electron density only;
2b: Profile of electron density ("true height analysis")
3: Satellite-Ionosonde ("Topside-Sounder"): electron density profile
4: Incoherent Scatter: electron density profile

3.2.1 Propagation effects on satellite signals

From the measuring methods listed in Table 3 the observation of propagation effects on satellite radio signals can provide the best temporal and spatial resolution but it gives one parameter only, namely electron content. With a few exceptions the bulk of data comes or from observation of the Faraday effect on VHF signals of geostationary satellite beacons or from observation of the so-called Differential Doppler effect on coherently emitted VHF/UHF signal pairs of satellites in nearly circular and nearly polar orbits (e.g., the Navy Navigation System - NNSS). Geostationary satellites give the time dependence of ionospheric electron content with very good resolution (one datum every minute is easily achievable; routine readings are usually done to give quarter hourly or hourly values). With receiving stations in low and middle latitudes polar orbiting satellites give the latitude dependence of electron content with a resolution of 0.5^{o} or better. Optimal results can be gained by combining Faraday data from geostationary beacons with Differential Doppler from polar orbiting beacons (for examples see Leitinger and Hartmann, 1977).

The Global Positioning System (GPS) provides a novel opportunity with a different type of orbit. Experience exists which demonstrates the capability of this system to give both well calibrated electron content and eccellent resolution. Presently it is not clear whether measuring systems which try to give calibrated electron content without making use of the precise (long) code will give good results or not. This is an important issue because it seems that access to the precise code will remain restricted. Since VHF beacons aboard geostationary satellites are fading out it is important to investigate closely the future possibilities of the GPS system.

Although in principle electron content can be measured with very good temporal as well as spatial resolution one should be aware that the existing network of receiving stations is far from optimal. Therefore it is recommended to make provisions for accompanying electron content observations if precise error assessment or error corrections are needed. One possibility to improve data coverage is the use of "geodetic" Doppler ranging equipment provided it has the capability to access the phase measurements ("Doppler counts") on both the 150 MHz and the 400 MHz channels (Leitinger et al., 1984).

3.2.2 Ionosondes.

In some regions of the world, e.g., in Europe, in East Asia, in India, in Australia, the ionosonde network is still quite dense but there are important

gaps elsewhere, e.g., in most parts of the Southern hemisphere and in the Pacific sector of the Northern hemisphere. Coverage in high latitudes is improving but recently gained data have not yet been included in model work. In low and especially in equatorial (dip) latitudes the African sector has been nearly neglected.

From "routine" ionosonde operation one can expect hourly values of peak electron density N_m. The N_m values can be calculated from F-layer critical frequency foF2 which is given in the "Bulletins" of the ionosonde stations with usually a delay of several months. With a longer delay foF2 can be got from the World Data Centers, too. Since equivalent slab thickness τ is N_I/N_m, carefully interpolated N_m can be used to provide this quantity for a given location for which electron content data are available. This procedure needs great care if τ is wanted around sunrise or for low latitudes or during a stronger geomagnetic disturbance (storm). The availability of F region parameters from ionosondes can be bad in higher latitudes (in dipole latitudes $>60^o$). This is especially true for times of geomagnetic disturbances. This is due to disturbed conditions or to the "blanketing" of the F-region by the E-region. It should be mentioned that foF2 or N_m can be taken from satellite ionograms, too.

The usability of ionograms for "true height analysis" which provides among others estimates for the layer height as needed for second order error assessment is rather restricted. Usually true height analysis is done with very good quality ionograms only and is never a "routine" service provided by the ionosonde network. Probably a restricted accuracy would do for error assessment purposes. One possibility to gain a (rough) estimate is to use an empirical formula relating the height of the F layer peak to a combination of "routine" F layer parameters (see e.g., Piggott and Rawer, 1972, 1978).

One such formula was published by Shimazaki in 1955 and has found wide application. It relates the estimated height of the peak electron density, hmF2, to the parameter M(3000)F2:

$$\mathrm{hmF2} = \frac{1490}{\mathrm{M(3000)F2}} - 176 \quad \text{(in km)}$$

(M(3000)F2 × foF2 is an estimate for the maximal communication frequency for links over 3000 km)

An improvement was introduced by Bradley and Dudeney in 1973 using an additional parameter, namely the maximal plasma frequency of the E layer, foE:

$$\mathrm{hmF2} = \frac{1490}{\mathrm{M(3000)F2} + \Delta M} - 176 \quad \text{(in km)}, \quad \text{with} \quad \Delta M = \frac{0.18}{x - 1.4}\ , \ x = \frac{\mathrm{foF2}}{\mathrm{foE}}$$

Bottom ionograms give no information about the ionosphere above the F layer peak. Such information is needed if one aims at precise evaluation of layer height and shape factor (first and second moments of the height distribution of electron density). Topside information is provided or by satellite ionosondes ("topside sounders") or in a restricted way by in-situ measurements. Unfortunately a network of satellites would be needed to give spatial resolution comparable to the density of ground based ionosondes and even in the lucky case that a topside sounder took an ionogram around the right time and near an ionosonde station there are serious co-location problems.

3.2.3 Incoherent Scatter

Remain the Incoherent Scatter stations. There is no doubt that incoherent scatter data give the best information about ionospheric electron distribution but the station density is very poor and operation is restricted in time. The following stations are operational: Jicamarca, Peru (12.0°S, 283.1°E), Arecibo, Puerto Rico (18.4°N, 293.3°E), Millstone Hill, USA (42.6°N, 288.5°E), Søndrestrøm Fjord, Greenland (67.0°N, 309.0°E), the European Incoherent Scatter System (EISCAT) with a transmitting/receiving station near Tromsø, Norway (69.6°N, 19.2°E) and two additional receiving stations near Kiruna, Sweden (67.8°N, 20.4°E) and Sodankylä, Finland (67.4°N,26.4°E). Usually these stations gain height profiles of ionospheric electron density for three days per month only. The data are not yet readily available but plans exist for an Incoherent Scatter data base with easy access.

A fair guess is to expect continuation of the present operation scheme in the near future. (Two stations in lower latitudes, one in mid latitudes, two in higher latitudes, N-h-profiles for one to three pre-arranged days a month.) It would be unrealistic to expect improved station density or better operation schedules. Arrangements for adopted operation schedules during major "campaigns" should be possible.

References

BRADLEY, P.A., J.R. DUDENEY 1973 A simple model of the vertical distribution of electron concentration in the ionosphere. J. atmos. terr. Phys. 35, 2131-2146

CCIR 1967 Comité Consultatif International des Radiocommunications (CCIR), Report 340 and 340-2 "CCIR Atlas of Ionospheric Characteristics", Doc. XIth Plenary Ass., International Telecommunications Union (ITU), Geneva, Switzerland.

CCIR 1970 CCIR Report 252-2 "Interim Method for Investigating Sky-Wave Field Strength and Transmission Loss at Frequencies Between the Approximate Limits of 2 and 30 MHz", Doc. XIIth Plenary Ass., ITU, Geneva, Switzerland.

HARTMANN, G.K., R. LEITINGER 1984 Range errors due to ionospheric and tropospheric effects for signal frequencies above 100 MHz. Bull. Géod. 58, 109-136

LLEWELLYN, S.K., R.B. BENT 1973 Documentation and Description of the Bent Ionospheric Model. Rep. AD-772 733, Natl. Tech. Inf. Serv., Springfield, Va., USA

LEITINGER, R. 1974 Der Einfluß ionosphärischer Ausbreitungsfehler bei der geodätischen Anwendung von Navigationssatelliten. Kleinheubacher Berichte 17, 321-332

LEITINGER, R., G.K. HARTMANN 1977 Zeit- und Breitenabhängigkeit von transionosphärischen Ausbreitungsfehlern. Kleinheubacher Berichte 20, 267-276

LEITINGER, R., G.K. HARTMANN, F.-J. LOHMAR, E. PUTZ 1984 Electron content measurements with geodetic Doppler receivers. Radio Sci. 19, 789-897

LEITINGER, R., E. PUTZ, G.K. HARTMANN 1986 Morphology and dynamics of the main trough in electron content. Proceedings Intern. Beacon Satellite Symposium 1986 (Ed.: A. Tauriainen), Univ. Oulu, Finland, 143-152

LEITINGER, R. 1987 Ionosphärische Ausbreitungsfehler und ionosphärische Meßgrößen. Kleinheubacher Berichte 30, 127-136

LINCOLN, J.V., R.O. CONKRIGHT 1981 International Reference Ionosphere - IRI-79. Report UAG-82, World Data Center A for Solar Terrestrial Physics, Boulder, CO, USA

McNAMARA, L.F., P.J. WILKINSON 1983 Prediction of total electron content using the International Reference Ionosphere. J. atmos. terr. Phys. 45, 169-174

PIGGOTT, W.R., K. RAWER (Eds.) 1972 U.R.S.I. Handbook of ionogram interpretation and reduction. Second Edition. Report UAG-23, World Data Center A for Solar-Terrestrial Physics, Washington, D.C., U.S.A.

PIGGOTT, W.R., K. RAWER (Eds.) 1978 U.R.S.I. Handbook ... as above, Revisions of Chapters 1-4, Report UAG-23A, publishers as above.

RAWER, K. D. BILITZA S. RAMAKRISHNAN 1978 Goals and status of the International Reference Ionosphere. Rev. Geophys. Space Phys. 16, 177-181

ROYDEN, H.N., D.W. GREEN 1986 Comparison of two models of total electron content at three midlatitude stations. Proceedings Intern. Beacon Satellite Symposium 1986 (Ed.: A. Tauriainen), Univ. Oulu, Finland, 197-203

SHIMAZAKI, T. 1955 World-wide daily variations in the height of the maximum electron density of the ionospheric F2-layer. J. Radio Res. Labs., Japan 2, 85-97

IONOSPHERE MODELING FOR A VLBI EXPERIMENT

G. Petit

Abstract

The GRIG - 2 experiment was realized in June-July 1985 between five stations in Europe (Nancay, Onsala and DSS63), South America (Atibaia) and Africa (Hart.RAO). Taking advantage of the configuration set up for the VEGA experiment it was carried out at L band (1.66 GHz), allowing two of the stations (Nancay and Atibaia) to be determined for the first time by VLBI with decimeter accuracy.

Due to the relatively low frequency and to the fact that no dual band recording could be used, the results are strongly dependent on the chosen ionosphere model. Three different treatments were applied which are described and discussed. Comparisons of these solutions with other geodetic determinations are attempted.

One of the methods is the use of simultaneous dual frequency Doppler recording of signals from the satellites of the NNSS TRANSIT system. This method is of great interest when the use of a dual frequency VLBI or GPS system is not available.

In Brunner, F.K. (Ed.), 1988, "Atmospheric Effects on Geodetic Space Measurements", *Monograph 12, School of Surveying, University of New South Wales, pp. 103-110.*

1. - INTRODUCTION

Propagation of radio waves from space to Earth is affected by atmospheric effects. For wavelengths of several centimeters to several decimeters which are used in all the systems of space geodesy (the Global Positioning System and Very Long Baseline Interferometry will be considered in this paper), the effect of the ionised upper atmosphere or ionosphere can affect measurements of ranges by many meters or even dozens of meters.

Due to the dispersive nature of the ionosphere, the main part of this effect is inversely proportional to the square of the frequency, and can be eliminated by the simultaneous observation of two frequency bands. Although higher order terms will remain [1], the elimination of first order terms is generally sufficient to achieve decimeter or centimeter level accuracy.

However it is not always possible to use dual frequency calibration to correct the ionospheric effects, either because only one frequency band is emitted, or because only one band can be received. In geodetic VLBI, single band observations are not of common use, but some experiments are still set up [2]. Single band VLBI happens also to be used in spacecraft navigation when the craft has only one frequency, and also in astrometry when the source is very weak at high frequencies (fast pulsars for example).In GPS, single band receivers are widely used because of the lower cost and because only one band is modulated with the C/A code. The main uses are geodesy and synchronization.

It is thus desirable to be able to use single band VLBI and GPS systems, and this requires some external estimation of the ionospheric effect to correct the measurements. One of the methods is the use of dual frequency Doppler measurements on the NNSS satellites of the TRANSIT systeme. It has been described previously by other authors, specially at the Bonn Geodetic Institute ([3], [4]).
We will present a new example where this method has been used to correct the observations of a VLBI single band geodetic experiment. Results will be discussed in part 2 . We will then present in part 3 a new approach for deriving the ionospheric effect from the Doppler measurements.

2. - APPLICATION TO A SINGLE BAND VLBI EXPERIMENT

The participating stations were Atibaia (Brazil), Hartebeesthoeck (S.Africa), Madrid (Spain, Deep Space Station 63), Nancay (France, a quasi meridian antenna of 94m equivalent diameter), and Onsala (Sweden). Some constraints

in the available equipment led to the following set-up : L-band observations (1.66 GHz), with Mark II recording of two channels 18 MHz apart and switched at 1 pps to construct BWS delay. To minimize the ionospheric effect in taking advantage of the common night time at all stations, two 6.5 hour sessions were conducted starting June 29. 1985 at 20h45 UT and July 4, 1985 at 21h00 UT.

The post-correlation processing was done with the JPL software MASTERFIT [5]. It allows to introduce ionosphere models in the form of a list of zenithal TEC values versus time. This value is then mapped to the relevant longitude with an hour angle dependence, and to the direction of the source. Four different models were used to derive the TEC values. They are thereafter represented by the symbols I0 to I3:

I0 is the absence of any model

I1 is the default MASTERFIT model

I2 is the Bent model [6]

I3 is derived from dual band Doppler observations

Application of the ionosphere correction reduce significantly the scatter of the delay residuals (Table I). However the two sophisticated ionosphere models (I2 and I3) do not differ very significantly in this respect.

Solution	I0	I1	I2	I3
RMS (ns)	1.08	1.05	0.86	0.88
	1.68	1.64	0.90	0.95
RMS (ps/s)	1.54	1.54	1.55	1.54
	1.11	1.28	1.13	1.13

Table 1: Statistical analysis of the delay and rate residuals.

It is much more important to compare the geodetic solutions which are derived, although the interpretation is not simple in such a case of very long baselines.It is known that for regional baselines the average global effect of a mismodeling is in the local vertical and the scale (see [4]).

On very long baselines this is not generally the case because the ionosphere behaviours on the different areas are nearly not correlated and neither are the mismodelings. Table 2 lists the coordinate differences between each solution and the I2 one.

solution		I0	I1	I2	I3
ONSALA	X	-0.07	-1.20	3 370 966.16±0.37	-0.02
	Y	0.23	0.00	711 466.01±0.10	0.01
	Z	0.57	-0.27	5 349 663.75±0.08	0.00
NANCAY	X	0.33	-0.48	4 324.165.81±1.15	0.04
	Y	-0.10	0.10	165 927.11±0.71	-0.06
	Z	0.18	-0.13	4 670 132.83±0.19	0.01
ATIBAIA	X	0.00	-0.74	4 034 109.79±0.46	0.04
	Y	-0.75	0.71	-4 259 743.95±0.20	-0.18
	Z	-1.73	0.98	-2 495 904.74±0.13	0.03
HART.RAO	X	-0.73	-1.40	5 085 442.43±0.41	+0.07
	Y	0.24	-0.25	2 668 263.61±0.12	-0.04
	Z	-1.21	0.55	-2 768 697.46±0.08	0.00

Table 2:Coordinates offsets in meters relative to solution I2
DSS63 coordinates fixed X= 4 849 093.15
Y= - 360 180.50
Z= 4 115 108.94

However the main effect of mismodeling can still roughly be assimilated to a scale error as can be seen in table 3 which lists the length differences between each solution and solution I2.

Solution	IO	I1	I2	I3
ATIBAIA-DSS63	1.85	-1.12	7 718 568.19	0.06
ATIBAIA-HART.RAO	0.85	-1.02	7 012 631.82	0.13
DSS63-HART.RAO	1.18	-0.64	7 524 235.86	-0.02
ATIBAIA-ONSALA	2.46	-1.41	9 311 585.95	0.08
DSS63-ONSALA	0.48	0.65	2 203 953.54	0.02
HART.RAO-ONSALA	1.56	-0.88	8 525 038.09	0.01
ATIBAIA-NANCAY	1.98	-1.25	8 427 502.08	0.04
DSS63-NANCAY	-0.13	0.25	927 571.80	-0.05
HART.RAO-NANCAY	1.32	-0.83	7 885 266.40	0.15
ONSALA-NANCAY	0.64	0.42	1 291 497.01	0.07

Table 3 : lenght offsets in meters relative to solution I2.

Finally we have tried to estimate the accuracy of the solutions by comparison with a fiducial solution [7] based on Mark3 S/X experiments for 3 of our stations: DSS63 Onsala and Hartebeesthoeck. After removal of a best fit translation, the RMS of the coordinates differences are computed. They appear in table 3. It is clear that estimations I2 which is a theoretical model, and I3, which is computed from dual band Doppler measurements are very compatible in all respects. Both achieve decimeter accuracy for the solution, thanks probably to the low solar activity at that time and to the choice of night time for the experiment. More challenging conditions would probably give much more different solutions.

Solution		IO	I1	I2	I3
Translation	X	2.15	2.75	1.86	1.85
	Y	-1.39	-1.15	-1.24	-1.22
	Z	0.57	0.27	0.35	0.36
Least Squares Estimalor		0.58	0.60	0.19	0.17
RMS of residuals	X	0.37	0.73	0.14	0.13
	Y	0.18	0.11	0.17	0.15
	Z	0.70	0.41	0.12	0.13

Table 4: Best fit translation between each solution and the fiducial solution.

3. - A NEW APPROACH FO ESTIMATING THE IONOSPHERIC EFFECT

In the process of estimating from the dual band Doppler observations the ionospheric effect on the propagation, one basic concept has to be defined first, the ionospheric point: It is assumed that the intricate structure of the ionosphere can be represented by a thin layer at a given and somewhat arbitrary height HI. If P is a point on this layer, the ionospheric effect for a vertical line of sight crossing the layer in P is IV(P),and the ionospheric effect for any line of sight crossing the layer in P is IE(P)=IV(P)/COS(Z) where Z is the zenith angle of the line of sight at P, i.e.IE(P) is IV(P) mapped to the line of observation.

The Doppler observation allows to determine exactly the difference of ionospheric effect between two measurement times in a given pass,

$$IE\ (tj) = IE\ (ti) + k*Nij \quad (1)$$

where Nij can be expressed simply with the Doppler counts from time ti to time tj (See [4]) but the determination of the absolute value at time ti requires the knowledge of an additive unknown which is characteristic of the pass.

$$IE(ti) = IE0 + k*Noi \quad (2)$$

or, using the ionospheric point formalism

$$\frac{IV(Pi)}{\cos(Zi)} = IE0 * Noi \quad (3)$$

The estimation of this unknown can be attempted by several ways.

a - The simplest, and the one which can be used in all cases, is to assume some kind of simple variation of the vertical ionospheric effect with latitude, thus allowing to solve for the unknown IE0 in a system of equations (3).

b - In the so-called "two station method" [8], it is necessary to collect data from the same satellites in two stations situated on a North-South line so that for each pass at least one data point of each station is related to the same ionospheric point.

In a research program currently undertaken, we propose to use an extension of the two station method, making use not only of observations of two stations with the same ionospheric point, but of all observations which ionospheric points are close in the coordinate system (Local Solar Time, Latitude). Such observations can be taken from two stations on a given pass, from one station on two different passes, or from several stations on several different passes.

It can be described as follows:
We want to determine Vertical Ionospheric Effects on a given part of the space (Local Solar Time, Latitude). The collected data represent N passes (One pass is the recording of one satellite trajectory at one station). The basic equations (3) leave us with the determination of N unknowns. If the whole data set contains Nc couples of close ionospheric points in different passes i and j, we can add Nc conditions like

$$IE(ik)-IE(jl) = a*dLAT(kl)+b*dH(kl) \quad (4)$$

Where the subscripts i and j relate to the passes
the subscripts k and l relate to the points
dLAT(kl) is the latitude difference between the two points
dH(kl) is the local Solar Time difference

The choice of the parameters a and b conditions the solution. They can be

- adopted from an a priori model

- determined from a model with a small number of estimable parameters
- estimated (one couple of parameters for each couple of passes i,j)

This procedure adds n extra parameters (n=o in the first case).A solution can be determined if the number of relations Nc is greater that the number of unknowns N+n.
Then the Vertical Ionospheric Effect must be evaluated at the points of interest (either the ionospheric points of a given experiment or a regular grid) from the data points by a filtering procedure.

4. - CONCLUSIONS

In most applications of space geodesy and astrometry, ionosphere calibration is achieved by using dual band equipment. Several applications still involve single band equipement, whether it be VLBI, GPS or other systems. In this case a good ionosphere model can be achieved with the use of simultaneous recording of dual frequency NNSS Doppler signals.

This method has been used to process an L-band VLBI experiment, and it clearly helped to reach the decimeter level accuracy, with RMS of the delay residuals at about 0.9 nanosecond.

Plans are to use this method routinely on a given area where single band GPS experiments are regularly set up, and single band VLBI occasionally. Ionosphere models will be derived from a global adjustment to the Doppler data.

REFERENCES

[1] J.C. De munck (1982). Ionospheric correction for pseudo-range measurement to satellites. Proc. of the General Meeting of IAGA, Tokyo, Japan.
[2] G.Petit, J-F.Lestrade, C.Boucher, F.Biraud, A.Rius, A.Nothnagel, C.R., Academie des Sciences Paris, t.303, serie II, n°20, 1986,p.1793.
[3] F.J.Lohmar, Dr.-Ing.Thesis, Bonn,1984
[4] J.Campbell, H.Cloppenburg, F-J.Lohmar: Estimating the ionospheric refraction effect on interferometric GPS measurements. Presented at the international Symposium on Space Techniques for Geodynamics Sopron, Hungary,(July 9 to 13, 1984)
[5] J.L.Franselow, O.J.Sovers, JPL Publication, 83-39, 1985, Rev.1
[6] S.K.LLewellyn, R.B.Bent, rep.AD-772-773, Nat. Techn. Inf. Serv., springfieldl, Va. 1973
[7] C.Ma, W.Himwich, A.Mallama, M.Kao, in Annual Report of the 1986, 1987 (in press)
[8] R.Leitinger, G.Schmidt, A.Taurianen, J.Geophys. 41, 201-213,1975

ACKNOWLEDGMENT

The data reduction of part 2 has been made possible thanks to the help of the staff at the Bonn Geodetic Institute under supervision of Dr.J.Campell and to the expertise of F.J.Lohmar.

Publications from

THE SCHOOL OF SURVEYING, THE UNIVERSITY OF NEW SOUTH WALES.

All prices include postage by surface mail. Air mail rates on application. (Effective July 1988)

To order, write to Publications Officer, School of Surveying, The University of New South Wales, P.O. Box 1, Kensington N.S.W., 2033 AUSTRALIA

NOTE: ALL ORDERS MUST BE PREPAID

UNISURV REPORTS - G SERIES

Price (including postage): $3.50

G14. A. Stolz, "The computation of three dimensional Cartesian coordinates of terrestrial networks by the use of local astronomic vector systems", Unisurv Rep. 18, 47 pp.

G16. R.S. Mather et al, "Communications from Australia to Section V, International Association of Geodesy, XV General Assembly, International Union of Geodesy and Geophysics, Moscow 1971", Unisurv Rep. 22, 72 pp.

G17. Papers by R.S. Mather, H.L. Mitchell & A. Stolz on the following topics:- Four-dimensional geodesy, Network adjustment and Sea surface topography, Unisurv G17, 73 pp.

G18. Papers by L. Berlin, G.J.F. Holden, P.V. Angus-Leppan, H.L. Mitchell & A.H. Campbell on the following topics:- Photogrammetry co-ordinate systems for surveying integration, Geopotential networks and Linear measurement, Unisurv G18, 80 pp.

G19. R.S. Mather, P.V. Angus-Leppan, A. Stolz & I. Lloyd, "Aspects of four-dimensional geodesy", Unisurv G19, 100 pp.

G20. Papers by J.S. Allman, R.C. Lister, J.C. Trinder & R.S. Mather on the following topics:- Network adjustments, Photogrammetry, and 4-Dimensional geodesy, Unisurv G20, 133 pp.

G21. Papers by E. Grafarend, R.S. Mather & P.V. Angus-Leppan on the following topics:- Mathematical geodesy, Coastal geodesy and Refraction, Unisurv G21, 100 pp.

G22. Papers by R.S. Mather, J.R. Gilliland, F.K. Brunner, J.C. Trinder, K. Bretreger & G. Halsey on the following topics:- Gravity, Levelling, Refraction, ERTS imagery, Tidal effects on satellite orbits and Photogrammetry, Unisurv G22, 96 pp.

G23. Papers by R.S. Mather, E.G. Anderson, C. Rizos, K. Bretreger, K. Leppert, B.V. Hamon & P.V. Angus-Leppan on the following topics:- Earth tides, Sea surface topography, Atmospheric effects in physical geodesy, Mean sea level and Systematic errors in levelling, Unisurv G23, 96 pp.

G24. Papers by R.C. Patterson, R.S. Mather, R. Coleman, O.L. Colombo, J.C. Trinder, S.U. Nasca, T.L. Duyet & K. Bretreger on the following topics:- Adjustment theory, Sea surface topography determinations, Applications of LANDSAT imagery, Ocean loading of Earth tides, Physical geodesy, Photogrammetry and Oceanographic applications of satellites, Unisurv G24, 151 pp.

G25. Papers by S.M. Nakiboglu, B. Ducarme, P. Melchior, R.S. Mather, B.C. Barlow, C. Rizos, B. Hirsch, K. Bretreger, F.K. Brunner & P.V. Angus-Leppan on the following topics:- Hydrostatic equilibrium figures of the Earth, Earth tides, Gravity anomaly data banks for Australia, Recovery of tidal signals from satellite altimetry, Meteorological parameters for modelling terrestrial refraction and Crustal motion studies in Australia, Unisurv G25, 124 pp.

G26. Papers by R.S. Mather, E.G. Masters, R. Coleman, C. Rizos, B. Hirsch, C.S. Fraser, F.K. Brunner, P.V. Angus-Leppan, A.J. McCarthy & C. Wardrop on the following topics:- Four-dimensional geodesy, GEOS-3 altimetry data analysis, analysis of meteorological measurements for microwave EDM and Meteorological data logging system for geodetic refraction research, Unisurv G26, 113 pp.

G27. Papers by F.K. Brunner, C.S. Fraser, S.U. Nasca, J.C. Trinder, L. Berlin, R.S. Mather, O.L. Colombo & P.V. Angus-Leppan on the following topics:- Micrometeorology in geodetic refraction, LANDSAT imagery in topographic mapping, adjustment of large systems, GEOS-3 data analysis, Kernel functions and EDM reductions over sea, Unisurv G27, 101 pp.

G29. Papers by F.L. Clarke, R.S. Mather, D.R. Larden & J.R. Gilliland on the following topics:- Three dimensional network adjustment incorporating ξ , η and N, Geoid determinations with satellite altimetry, Geodynamic information from secular gravity changes and Height and free-air anomaly correlation, Unisurv G29, 87 pp.

From June 1979 Unisurv G's name was changed to Australian Journal of Geodesy, Photogrammetry and Surveying. These can be ordered from The Managing Editor, Australian Journal of Goedesy, Photogrammetry and Surveying, Institution of Surveyors - Australia , Box 4793 G.P.O., Sydney, N.S.W., 2001, AUSTRALIA.

UNISURV REPORTS - S SERIES

S8 - S19	Price (including postage):		$7.50
S20 onwards	Price (including postage):	Individuals	$18.00
		Institutions	$25.00

S8 A. Stolz, "Three-D Cartesian co-ordinates of part of the Australian geodetic network by the use of local astronomic vector systems", Unisurv Rep. S 8, 182 pp, 1972.

S9 H.L. Mitchell, "Relations between MSL & geodetic levelling in Australia", Unisurv Rep. S 9, 264 pp, 1973.

S10 A.J. Robinson, "Study of zero error & ground swing of the model MRA101 tellurometer", Unisurv Rep. S 10, 200 pp, 1973.

S12. G.J.F. Holden, "An evaluation of orthophotography in an integrated mapping system", Unisurv Rep. S 12, 232 pp, 1974.

S14. Edward G. Anderson, "The Effect of Topography on Solutions of Stokes` Problem", Unisurv Rep. S 14, 252 pp, 1976.

S15. A.H.W. Kearsley, "The Computation of Deflections of the Vertical from Gravity Anomalies", Unisurv Rep. S 15, 181 pp, 1976.

S16. K. Bretreger, "Earth Tide Effects on Geodetic Observations", Unisurv S 16, 173 pp, 1978.

S17. C. Rizos, "The role of the gravity field in sea surface topography studies", Unisurv S 17, 299 pp, 1980.

S18. B.C. Forster, "Some measures of urban residual quality from LANDSAT multi-spectral data", Unisurv S 18, 223 pp, 1981.

S19. Richard Coleman, "A Geodetic Basis for recovering Ocean Dynamic Information from Satellite Altimetry", Unisurv S 19,332 pp, 1981.

S20. Douglas R. Larden, "Monitoring the Earth's Rotation by Lunar Laser Ranging", Unisurv Report S 20, 280 pp, 1982.

S21. R.C. Patterson, "Approximation and Statistical Methods in Physical Geodesy", Unisurv Report S 21, 179 pp, 1982.

S25. Ewan G. Masters, "Applications of Satellite Geodesy to Geodynamics", Unisurv Report S25, 208 pp, 1984.

S26. Andrew Charles Jones, "An Investigation of the Accuracy and repeatability of Satellite Doppler relative positioning techniques", Unisurv Report S26, 222 pp, 1984.

S27. Bruce R. Harvey, "The Combination of VLBI and Ground Data for Geodesy and Geophysics", Unisurv Report S27, 239 pp, 1985.

S28. Rod Eckels, "Surveying with GPS in Australia", Unisurv S28, 220 pp, 1987.

S29. Gary S. Chisholm, "Integration of GPS into hydrographic survey operations", Unisurv S29, 190 pp, 1987.

S30. Gary Alan Jeffress, "An investigation of Doppler satellite positioning multi-station software", Unisurv S30, 118 pp, 1987.

S31. Jahja Soetandi, "A model for a cadastral land information system for Indonesia", Unisurv S31, 168 pp, 1988.

PROCEEDINGS

Prices include postage by surface mail

P1. P.V. Angus-Leppan (Editor), "Proceedings of conference on refraction effects in geodesy & electronic distance measurement", 264 pp. Price: $ 6.50

P2. R.S. Mather & P.V. Angus-Leppan (Eds), "Australian Academy of Science/International Association of Geodesy Symposium on Earth`s Gravitational Field & Secular Variations in Position", 740 pp. Price $12.50

MONOGRAPHS

Prices include postage by surface mail

M1. R.S. Mather, "The theory and geodetic use of some common projections", (2nd edition), 125 pp. Price $ 9.00

M2. R.S. Mather, "The analysis of the earth's gravity field", 172 pp. Price $ 5.50

M3. G.G. Bennett, "Tables for prediction of daylight stars", 24 pp. Price $ 2.00

M4. G.G. Bennett, J.G. Freislich & M. Maughan, "Star prediction tables for the fixing of position", 200 pp. Price $ 5.00

M5. M. Maughan, "Survey computations", 98 pp. Price $ 8.00

M6. M. Maughan, "Adjustment of Observations by Least Squares", 61 pp. Price $ 7.00

M7. J.M. Rueger, "Introduction to Electronic Distance Measurement", (2nd Edition), 140 pp. Price $ 14.00

M8. A.H.W. Kearsley, "Geodetic Surveying". 77pp. Price $ 8.00

M9. ** R.W. King, E.G. Masters, C. Rizos, A. Stolz and J. Collins, "Surveying with GPS", 128 pp.

M10. W. Faig, "Aerial Triangulation and Digital Mapping", 102. pp. Price $ 13.00

M11. W.F. Caspary, "Concepts of Network and Deformation Analysis", 183 pp. Price $ 22.00

M12. F.K. Brunner, "Atmospheric Effects on Geodetic Space Measurements", 110 pp. Price $ 13.00

** No longer for external sale from the School of Surveying. Now published by Ferd. Dümmlers Verlag, Kaiserstrasse 31 - 37, D - 5300 Bonn 1, Federal Republic of Germany